Dynamics of semiconductor nonlinear optical waveguides

Spencer, P. S.

Award date:
1993

Awarding institution:
University of Bath

DYNAMICS OF SEMICONDUCTOR NONLINEAR OPTICAL WAVEGUIDES

Submitted by P. S. Spencer, B.Sc.(Hons)
for the degree of
Doctor of Philosophy
of the University of Bath
1993

ProQuest LLC
789 East Eisenhower Parkway
P.O. Box 1346
Ann Arbor, MI 48106-1346

To my Mother and Father
(Pound-set)

Summary

This thesis analyses the origins of two fast optical nonlinearities observed in semiconductors and investigates the dynamic response of nonlinear waveguides. The mechanisms that induce optical nonlinearities are discussed, and particular attention is paid to those that can induce a large fast nonlinear refraction. Measurements of quantum well intersubband absorption are presented and a model is derived for the linear and nonlinear optical properties of such transitions. This model takes into account the frequency dependence of the intersuband dephasing time. An expression is also derived for the fast nonlinear refraction recently observed in semiconductor optical amplifiers. The types of spectral and temporal distortions a pulse experiences in nonlinear dispersive medium are discussed, and a model for the co-propagation of a strong pump pulse and weak probe pulse in such a medium is developed. Finally a formalism is established to model the pulsed operational characteristics of a nonlinear directional coupler. The results predicted by this model are compared with experimental results recently obtained from a semiconductor optical amplifier based nonlinear directional coupler.

Acknowledgements

I would like to express my deep gratitude to Dr K.A. Shore for his excellent supervision throughout the course of this work.

I also wish to thank Drs Mike Adams, Mike Fisher, Dave Davies and Mike Burt of BTRL at Ipswich, for their help and advice.

I would also like to thank Dr J. Sarma for the many useful comments he has made about this work, and in particular for explaining the real origins of flu. I am also grateful for all the help and assistance, provided by the other members of electronics group at Bath University, who are: Rob Noyes, Ian Middlemast, C.H. Chong, Lloyd Langley, Mac Green and W.M. Yee. I am also indebted to Dr C.S. Chang for explaining the more esoteric features of our computer facility.

Finally, I would like to thank my family for all their support and encouragement.

Contents

List of Figures

List of Tables

Chapter 1

Introduction

1.1 Introduction

The optical properties of materials, familiar to us through our visual sense, are predominately those of linear optics. The relatively low light intensities that normally occur in nature ensure that the optical properties of a material are independent of the intensity of illumination. In linear optics light beams propagate in a medium without interacting with each another. However, if the illumination can be made sufficiently intense, the optical properties of the medium will depend on the intensity and other characteristics of light. In this regime light waves begin to interact with each other as well as with the medium. This is the realm of nonlinear optics.

In recent years the field of nonlinear optics has seen a rapid increase in activity which has been stimulated mainly by the telecommunication industry. In order to fully exploit the large bandwidth of the opto-electronic devices extensively used in today's optical communications and other optical information processing systems, nonlinear components such as all-optical switches need to be developed.

This requirement has motivated the considerable current interest in semiconductor materials that possess large nonlinearities, and has also stimulated the effort to find waveguide structures that can be used in conjunction with these semiconductor materials to produce an all-optical switch. The potential usefulness of all-optical switches will be determined by their pulsed operational characteristics and for telecommunication applications the devices must be able to operate at fast switching rates. Thus there is a need to analysis the transmission characteristics of nonlinear optical devices.

1.2 Optical Nonlinearity

The fact that intense electric and magnetic fields are capable of inducing optical changes in a medium has been known for some time. Faraday observed that the plane of polarization of a optical beam propagating in glass can be rotated by an applied magnetic field. This is now known as the Faraday effect. Kerr discovered, in a complementary experiment, that light propagating in glass suffers double refraction if a strong electric field is applied. This is known as the Kerr effect. From these results it is reasonable to suppose that a sufficiently intense optical beam will alter the medium it is incident upon, thus affecting its own propagation. The intensities necessary to observe nonlinear optical effects only became readily available after the invention of the laser in the 1960's.

At the end of the seventies Gibbs *et al*, [1], and Miller *et al*, [2] observed intensity dependent changes in the absorption and refraction coefficients of semiconductors. Since then intensive experimental and theoretical analysis of semiconductor optical nonlinearities has taken place. Optical nonlinearities are induced

by either resonant or non-resonant mechanisms. In general resonant mechanisms induce large nonlinearities which have slow response time, while the converse is true of non-resonant mechanisms. A large absorption is also associated with resonant nonlinearities. However recently, large fast nonlinearities have been observed in semiconductor optical amplifiers, [3], and quantum well structures, [4]. The first half of this thesis studies two mechanisms that have the potential to induce a fast and a large nonlinearity.

1.3 All-optical Switching

Many of the characteristics of optical waveguides suggest them to be the optimum media for performing efficient nonlinear optical interactions. The strong beam confinement to regions of the order of the wavelength of the light in one (planar waveguides) or two (channel waveguides) dimensions implies that large intensities can be produced with small total powers. Thus to maintain high intensities and make efficient use of any nonlinearity present, guided wave structures need to be employed. In general nonlinear waveguide structures have transmission characteristics that are intensity dependent. Therefore it should be possible to produce an all-optical switch from a suitably configured nonlinear waveguide structure. Probably one of the simplest waveguide structures that can be used to produce an all-optical switch is the nonlinear directional coupler, (NLDC), which was first proposed by Jensen, [5]. Such a coupler consists of two closely separated parallel waveguides whose transmission characteristics are determined by the intensity of the incident optical field.

The optical sources and detectors used in optical communications systems are fabricated from semiconductors. Thus the realisation of a semiconductor all-optical switch would open the possibility of constructing integrated optical processing circuits. In principle such structures should operate at much higher data rates than an equivalent electronic circuit. In order to better assess the potential speed advantages of integrated optical circuits, the dynamic response of individual optical components likely to be used in their construction needs to be known. The pulsed operational characteristics of a particular device are limited by the temporal properties of the materials used in its construction. The second half of this thesis is concerned with pulse propagation in nonlinear dispersive media, and in particular with the dynamic response of a NLDC all-optical switch.

1.4 Structure of the Thesis

The next three chapters of the thesis are concerned with the mechanisms that induce optical nonlinearities in semiconductors. In chapter[2] a model for the optical properties of quantum well intersubband transitions is derived and experimental measurements of intersubband absorption in InGaAs/InAlAs quantum wells are presented. Chapter[3] outlines the mechanisms responsible for inducing nonlinearities in active semiconductors, and in chapter[4] a model is derived for the fast component of the nonlinearity observed in optical amplifiers.

The last three chapters are concerned with pulse propagation in nonlinear medium. Chapter[5] outlines the effects that can occur when a pulse propagates in a nonlinear dispersive media. Chapter[6] analyses pump and probe pulse propagation in a medium that has a Kerr-type nonlinearity. In the last chapter

a model is derived that can describe pulse propagation in a nonlinear directional coupler formed from coupled semiconductor optical amplifiers.

References

[1] H.M.Gibbs *et al*, Appl. Phys. Lett., 35, 451, (1979).

[2] D.A.B.Miller *et al*, Appl. Phys. Lett., 35, 658, (1979).

[3] R.S.Grant and W.Sibbett, Appl. Phys. Lett., 58, 1119, (1991).

[4] D.Walrod *et al*, Appl. Phys. Lett., 59, 2932, (1991).

[5] S.M.Jensen , IEEE J. Quantum Electron., QE-18, 1580, (1982).

Chapter 2

Intersubband Transitions in InGaAs/InAlAs Quantum Wells.

2.1 Introduction.

2.1.1 Quantum Wells

Recent advances in crystal growth techniques have made it possible to accurately grow thin layers of different semiconductors in complex sequences. If an alternating system consisting of two semiconductors with different band-gaps, E_g, is grown, a quantum wells structure will be formed, provided the thickness of the smaller E_g material, or well layer, is of the order of the electron wavelength, (typically $< 100\mathring{A}$). The layers either side of the well material are usually referred to as the barrier layers and are generally made from the same semiconductor, figure(2.1). If the barrier layer thickness is also of the order of the electron de Broglie wavelength then a superlattice structure is formed.

Band-gap discontinuities are induced in the conduction, ΔE_c, and valence, ΔE_v, bands, because the well and barrier semiconductors have different band-gaps, figure(2.1). This energy mismatch is not split evenly between conduction and valence bands. ΔE_c is always larger than ΔE_v, because the effective mass of the conduction band is always less than that of the valence band.

The reduced dimensionality in the growth direction leads to the formation of one dimensional potential wells, which restrict the motion of the carriers in one direction. From quantum mechanics it is known that the energy levels within a potential well are discrete. The separation between these discrete energy levels is determined by the depth of the well, (i.e the band-gap discontinuity), the thickness of the well layer, L_z, and the effective masses of the carriers. The increased carrier confinement in quantum wells also results in stronger optical interactions.

2.1.2 Optical Transitions in Quantum Wells

As well as the usual interband transitions between the valence and conduction bands allowed in bulk semiconductors, additional intersubband transitions are possible in quantum well structures, figure(2.1).Intersubband transitions can occur between the discrete energy levels within either of the potential wells. As the energy levels are discrete only certain wavelengths will be resonant with the quantum well system. The energy of the photons of the incident light must be equal to the energy difference between two of the discrete energy levels, to induce intersubband transitions. Intersubband transition can occur within the potential wells of either the valence or the conduction bands. Conduction band intersub-

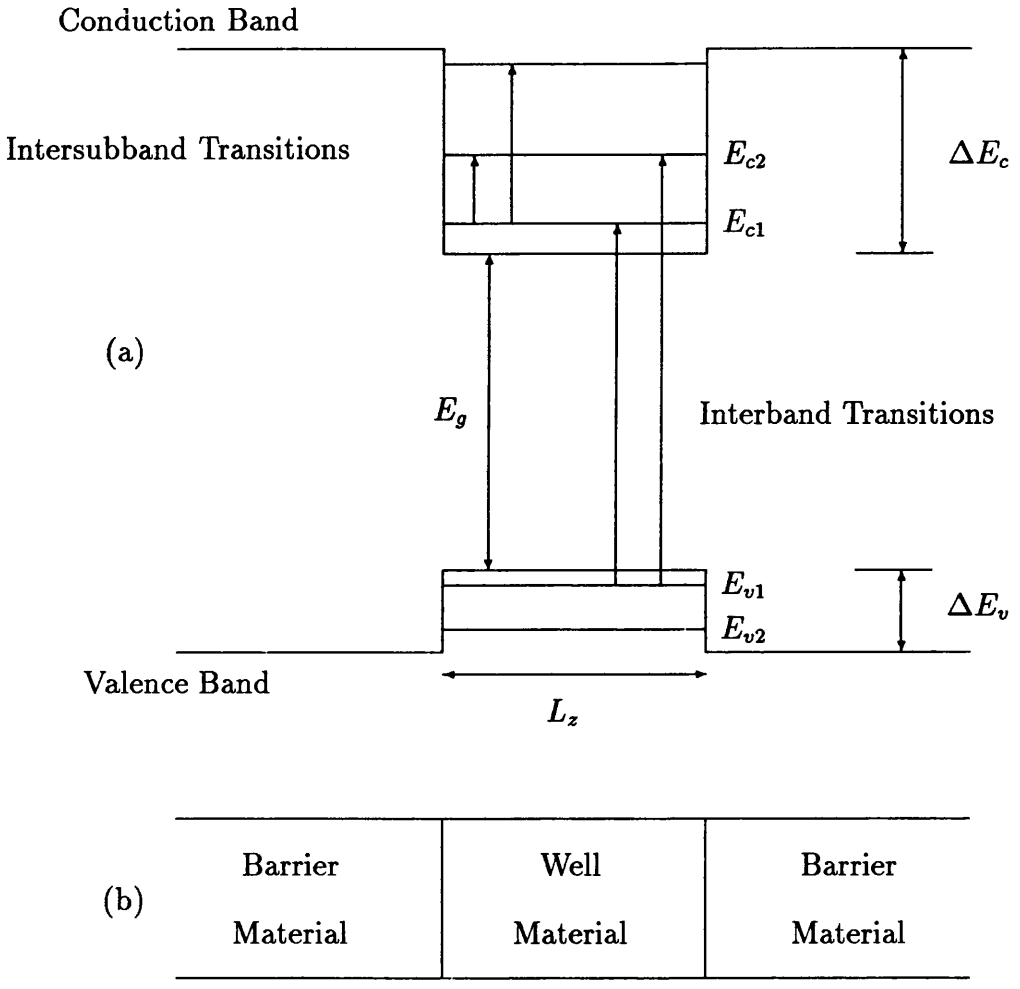

Figure 2.1: Intersubband and Interband transition in quantum wells are shown diagrammatically in (a), and a schematic of the layer structure used to produce a quantum well is shown in (b).

band transitions can be induced using wavelengths of the order $10\mu m$ and only these will be considered.

The separation between the conduction band energy levels in the potential wells is considerably less than the band-gap of either the well or the barrier materials, and thus intersubband transitions are responsive to much longer wavelengths than the bulk materials. Thus wavelengths that would be transparent in the bulk material, will suffer intersubband absorption (ISBA) if they match one of the resonant wavelengths of the quantum well. This has been one of the prime motivating factors for investigating such systems, because intersubband absorption, has potential for use in long wavelength photodetectors. Photodetectors that utilize ISBA have the added advantage of having a fast response time, because the relaxation times associated with intersubband transitions are very short, ($\sim 1ps$).

The increased carrier confinement in quantum wells causes the dipole moment of intersubband transitions to be larger than that of interband transitions and thus there is a higher probability that a photon in resonance with a particular intersubband transition will be absorbed. The discrete nature of the allowed transitions in quantum well structures means that the optical properties are significantly different from those of a bulk semiconductor, and recently such structures have received a great deal of attention.

The possible use of quantum wells in novel optical switching devices has also acted as a spur to recent investigation of the properties of intersubband transitions because these transitions have been shown to possess large dipole moments, [1-4], strong nonlinearities, [5, 22], and fast relaxation times, [7, 8, 9]. The fact that

the dipole moments are large, gives rise to the possibility of significant changes in the absorption and refractive index near the resonant frequency. Interestingly these transitions have also been found to have a large fast transient nonlinear refractive index.

The first observations of intersubband transitions were reported in a GaAs/AlGaAs material system, [1], with an intersubband transition resonant wavelength of approximately 8-10 microns. Obviously from a technological viewpoint, it would be advantageous if the resonant wavelength was shorter, (i.e around 0.8-1.55 microns), as this would then open up the possibility of utilising intersubband transitions in switching components and photodetectors of optical communication systems.

Several methods have been suggested for shifting the energy levels, in order to reduce the resonant wavelength. The available methods can be classified into three different groups:

- Change of the material structure
- Change of the layer structure
- The application of an electric field perpendicular to the layers

Probably the simplest way to achieve an appreciable reduction in the resonant wavelength, is to increase the depth of the quantum well by means of a change in the material. This can be achieved if a material composition system with a larger band-gap discontinuity than that of the GaAs/AlGaAs system, is used. Consequently other material systems, with larger band-gap discontinuities, are being actively sought. One such system which has been investigated recently,

consists of alternating layers of InGaAs, for the wells, and InAlAs, for the barriers, [3, 4]. The InGaAs/InAlAs system has a band-gap discontinuity of 500meV, which brings the resonant wavelength, for the $E_{c1} \rightarrow E_{c2}$ transition, figure(2.1), down to around 4-5 microns.

The following sections of this Chapter are separated into two main components. The first describes the experimental techniques used, and the results obtained, when the optical absorption properties of a number of InGaAs/InAlAs quantum well samples, were investigated. The second main section gives the development of a theory that models both the linear and nonlinear optical properties of quantum well intersubband transitions.

2.2 Optical Transmission Measurements Of InGaAs/InAlAs Quantum wells

2.2.1 Introduction

The quantum well samples tested were kindly supplied by BT Laboratories, who also provided all the necessary equipment needed to measure the transmission spectra of the samples. The samples were grown using MOCVD technology, and had different well widths and doping levels. The infra-red transmission spectra obtained have subsequently been used to calculate several physical parameters. On the basis of the experimental results estimates of the momentum matrix element, dephasing time, and intersubband absorption coefficient, and the effects of different well widths, and doping levels on them, have been obtained.

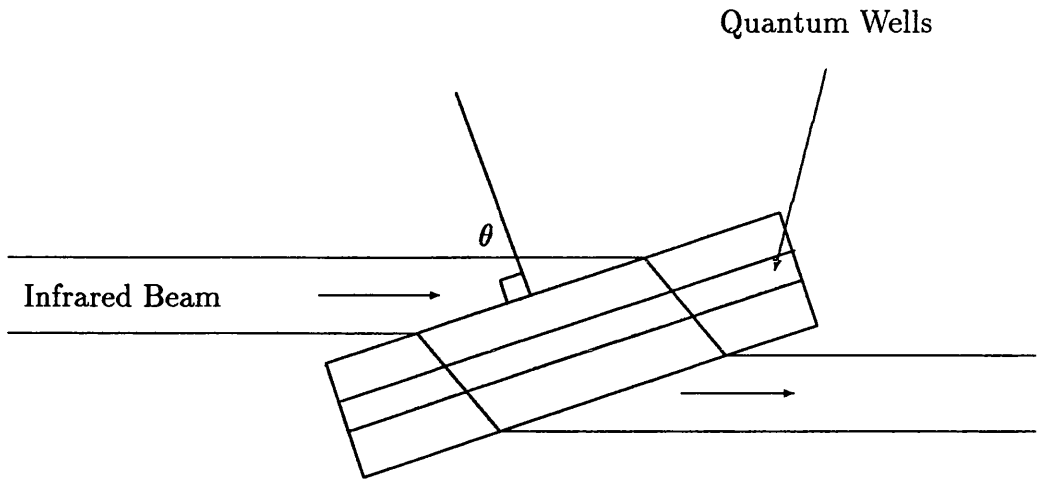

Figure 2.2: The experimental setup used, showing the orientation between the the sample and the incident infrared beam.

2.2.2 Experimental Procedure.

The InGaAs/InAlAs quantum well wafers investigated were fabricated on Fe-doped InP substrates. The InGaAs wells were S-doped and all but one of the samples also had a S-doped InP capping layer. The wafers were grown to produce a system of 50 quantum wells, consisting of 100$\AA$ InAlAs barriers and either 50$\AA$ or 45$\AA$ InGaAs wells. Both sides of the wafers were polished.

An absorption spectrum of each sample was measured on a BRUKER IFS 66 Fourier Transform Infra-Red spectrometer. The spectrometer sweeps the frequency of the CW beam incident on the sample and records the strength of the optical beam at the rear of the sample. Measurements were made with the beam incident on the sample at various angles, figure(2.2). The peak intersubband

absorption occurred at Brewster's angle, which in this case was found to be 72°. The data obtained was presented in the form of a transmission spectrum. A transmission spectrum is produced by measuring, over a range of wavelength, the percentage of the input power which passes straight through the sample.

Before measurements were performed the sample chamber was purged with N_2 gas for 15 minutes. This was done to reduce the amount of CO_2 and water vapour present, since both gases have significant absorption bands within the wavelength range scanned. The samples were referenced against the spectrum of a Fe-doped InP wafer, thereby removing the substrate absorption, and 200 scans were taken to produce each transmission trace. After each set of measurements the reference sample was tested again to ascertain whether any inadvertent changes in the experimental conditions had occurred.

The referenced transmission spectrum was subsequently baseline corrected and then converted into an Absorbance spectrum (Absorbance = - Log (Transmission)). The baseline correction involves splitting the trace into 32 sections, to give a set of reference points. The new baseline is obtained by drawing the shortest line, which does not 'cut' the spectrum, through the reference points. This procedure does not shift the resonant wavelength or alter the absolute magnitude of the absorption peak.

Table(2.1) sets out the doping levels, well widths, and barrier widths of the seven wafers tested. Three of the samples have had their well widths verified by TEM analysis.

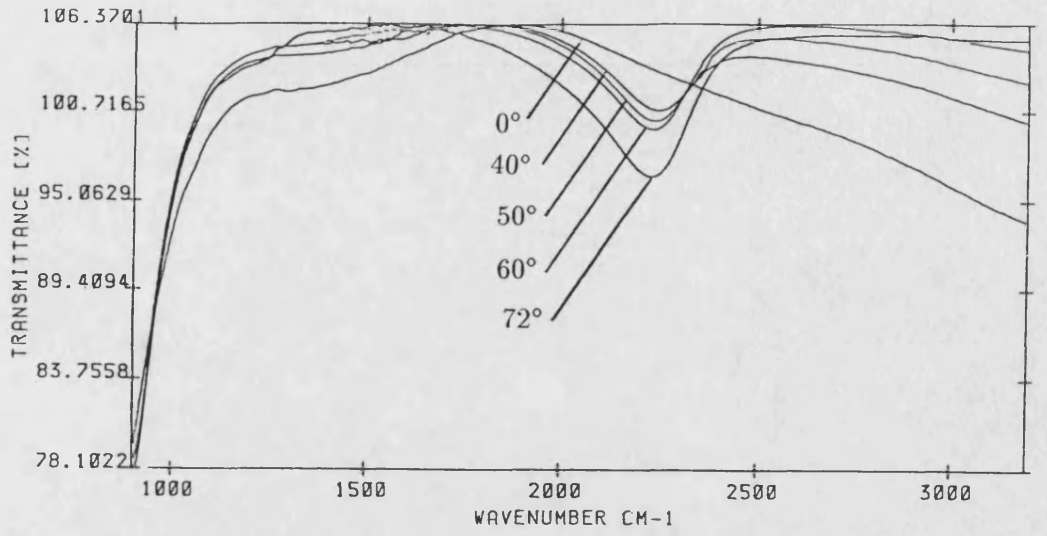

Figure 2.3: Uncorrected Transmission scan for the sample with the strongest intersubband absorption, AX514.

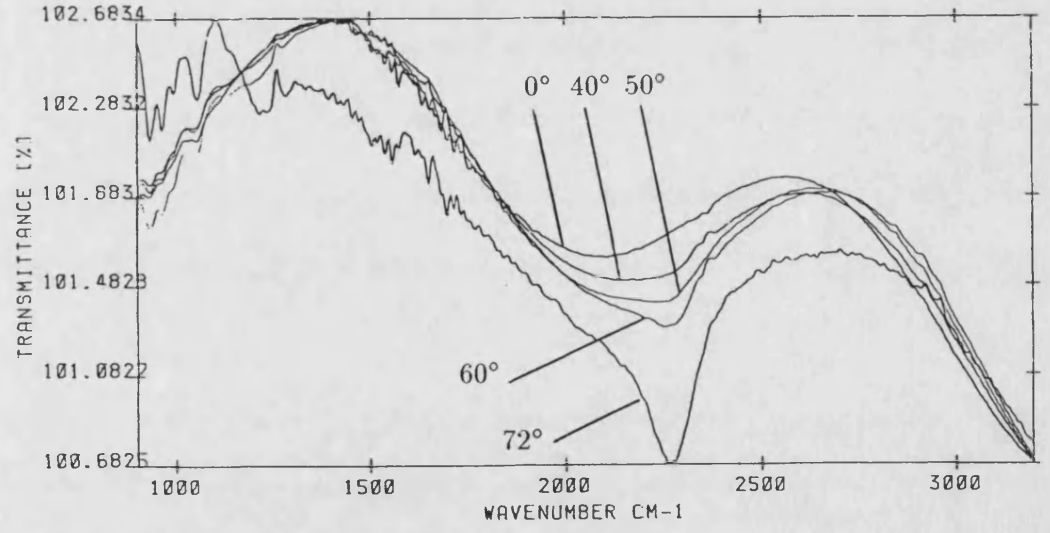

Figure 2.4: Uncorrected Transmission scan for the sample with the weakest intersubband absorption, AX538. (Note the difference in ordinate scale)

Sample No.	Well width Å	Barrier width Å	Well Dopant $10^{18}\ cm^{-3}$	Capping Dopant $10^{18}\ cm^{-3}$
AX556	50	100	5.0	0.5
AX514	49 ±5	93 ±6	1.0	1.0
AX538	50	100	0.5	1.0
AX555	50	100	0.2	0.5
AX528	45	100	1.0	1.5
AX480	42 ±5	72 ±5	1.0	—
AX482	57 ±5	93 ±5	1.0	1.0

Table 2.1: Well and Barrier widths and doping levels of the samples.

2.2.3 Results.

Transmission Spectra.

The quality of the conduction band intersubband absorption, (ISBA), spectra obtained varied significantly. Three wafers, AX480, AX482, and especially AX514, gave strong absorption with very little noise. In all the other samples it was possible to discern intersubband absorption, but some traces showed substantially weaker absorption and more noise. The sample AX538 was particularly poor with very weak ISBA. As the same procedures were used to reduce the effects of CO_2, water vapour and the InP substrate, the additional noise observed in some of the samples must emanate from the epitaxial layers.

Figures(2.3, 2.4) show the best, (AX514) and worst, (AX538), uncorrected referenced transmission scans, at various angles. Both traces show the characteristic variation of the absorption with the angle of incidence of the CW beam indicative of ISBA. The selection rules for intersubband transitions dictate that only the component of the electric field normal to the plane of the quantum well can induce transitions. Therefore the peak absorption will occur when the sam-

Sample No.	Well width Å	λ_{expt} μm	λ_{theo} μm	E_0 meV	E_1 meV
AX556	50	4.68	4.43	126.9	406.7
AX514	49 ±5	4.47	4.43	129.9	413.9
AX538	50	4.42	4.43	126.9	406.7
AX555	50	4.34	4.43	126.9	406.7
AX528	45	4.19	4.13	143.0	443.3
AX480	42 ±5	4.70	3.99	154.2	464.9
AX482	57 ±5	4.92	4.94	108.5	359.2

Table 2.2: Experimental and Theoretical resonant wavelengths for the samples.

ple is oriented at Brewster's angle, figure(2.2). At this angle minimum reflection from the surface, and maximum coupling of the electric field into the wells, will occur.

Resonant Wavelength

Calculations of the energy levels were performed assuming both infinite and finite potential wells. The resultant energy levels predicted by these two simple models were, however, inconsistent with the experimental data, indicating that account needed to be taken both of the nonparabolicity of the bands, and of the finite well depth. The resonant wavelengths measured experimentally and the theoretically predicted value, (obtained using the empirical nonparabolic model outlined in Appendix(1)), are shown in Table(2.2). The nonparabolicity factor used in the calculation was $9 \times 10^{-19}\ m^{-2}$. This compares favourably with the value of $\gamma = 11 \times 10^{-19}\ m^{-2}$ used by Levine, [4]. In figure(2.5) the theoretically predicted variation of the resonant wavelength with the well width is shown. The resonant wavelength changes considerably as the well width is increased. As the well width increases so does the number of allowed energy states, which causes a reduction in the separation between adjacent energy levels and hence increases the resonant

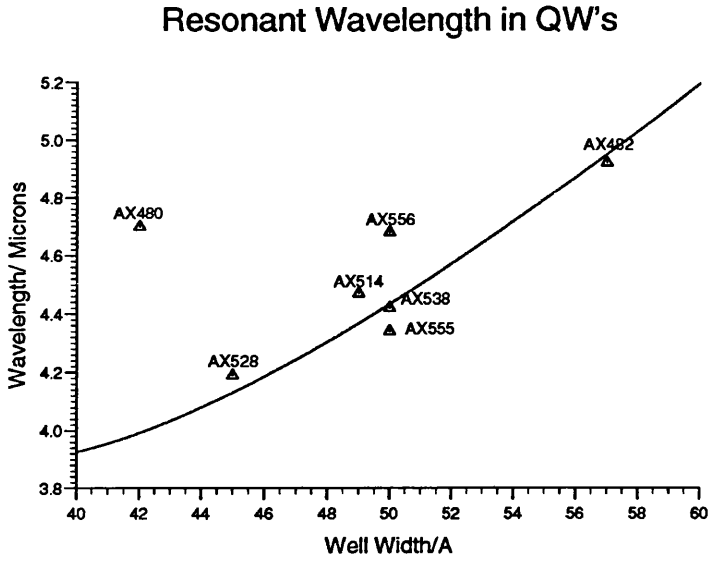

Figure 2.5: Theoretical variation of the resonant wavelength with well width, assuming a Nonparabolicity factor of $9 \times 10^{-19}\ m^{-2}$, (solid line), and the experimental measured wavelengths.

wavelength. Further calculations have also been undertaken to check that there is no appreciable coupling between adjacent wells, because such coupling would have meant that another model would have had to have been used to calculate the energy levels. These showed that the barriers were indeed thick enough to ensure that there is no evanescent coupling between the wells.

Good agreement between the theoretical and experimental values for the resonant wavelength has been achieved, figure(2.5), with one exception, AX480. The anomalous value of AX480 can be attributed to the fact that it was grown without a doped capping layer. This results in more band bending, and increased nonparabolicity. By increasing the nonparabolicity factor, used in the theoretical calculations, to $20 \times 10^{-19} m^{-2}$, good agreement between the experimental and theoretical values was again obtained for this sample.

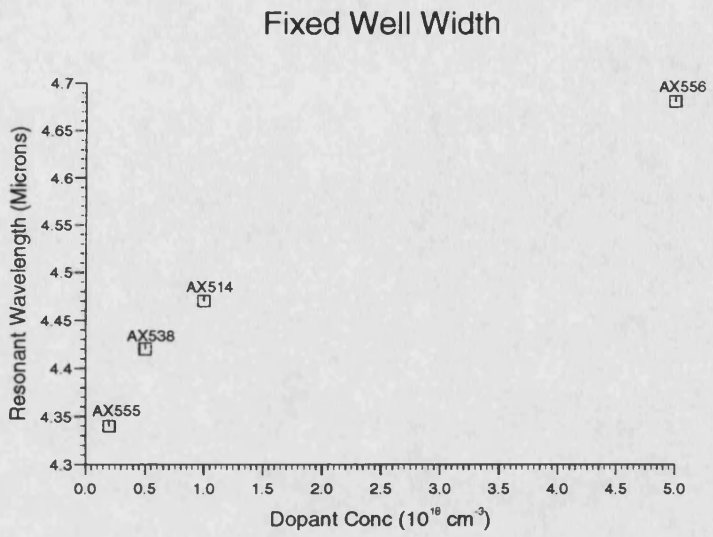

Figure 2.6: Experimental variation of the resonant wavelength with doping, for $50\mathring{A}$ wells.

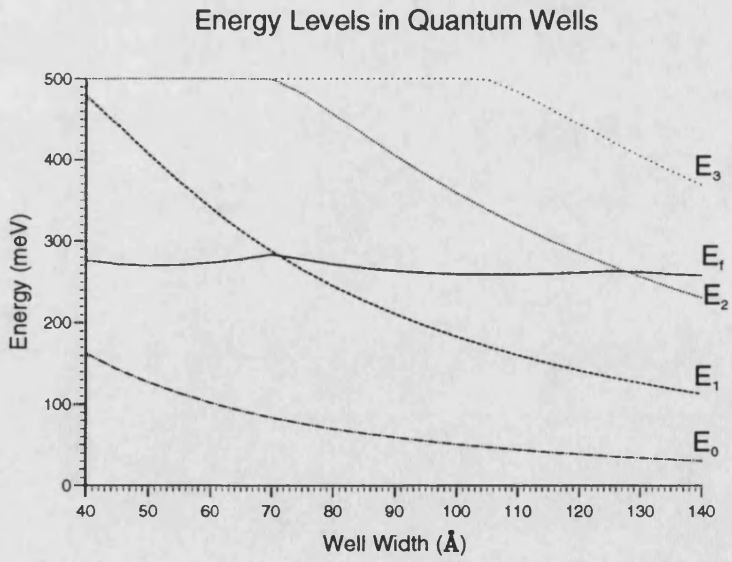

Figure 2.7: Theoretical variation of the energy levels and fermi level with well width, assuming a Nonparabolicity factor of $9 \times 10^{-19}\ m^{-2}$.

The results shown in figure(2.6) indicate the variation of the resonance wavelength with carrier concentration, for a fixed well width of $50\mathring{A}$. The reason for this variation is unclear, but it has been proposed, [3], that it is caused by resonant screening of the infra-red radiation by the electrons in the well. The strength of this effect increases with the carrier concentration. This appears not to be borne out by figure(2.6), which shows the resonant wavelength increasing with the doping, instead of decreasing with the wavelength, as would be expected if screening was occurring.

In figure(2.7) the variation of the conduction band energy levels, and quasi-Fermi level, with well width is shown. As the well width increases the energy levels all drop, with the first excited state falling at the greatest rate. At larger well widths the Fermi level moves further away from the ground state and closer to the upper energy level.

Allowing for the fact that the well widths of four of the samples have not been verified by TEM measurements, (and thus they could vary significantly from the value aimed for), the experimental and theoretical values of the resonant wavelength are in good agreement.

Calculation of Matrix Element.

The integrated absorbance, I_a, (absorbance=-LOG(transmission)), can be shown to be related to the matrix element, $< Z_{21} >$, and oscillator strength, f, of the

Sample No.	α_{ISB} cm^{-1}	Peak Magn. Arb. Units	τ fs	FWHM cm^{-1}	I_a meV	f	$< z >$ Å
AX556	1243	0.0135	58.6	181	0.70	0.10	5.95
AX514	3768	0.0401	38.7	274	3.13	2.36	27.8
AX555	1096	0.0119	55.5	191	0.65	2.40	27.6
AX528	665	0.0065	68.8	154	0.29	0.23	8.48
AX480	3509	0.0320	51.0	208	2.01	1.77	24.7
AX482	2682	0.0332	52.8	201	2.14	1.39	22.4

Table 2.3: Gives the Peak absorption coefficient, α_{ISB}, Peak absorbance, FWHM, relaxation time, τ, integrated absorption, oscillator strength,f, and the matrix element of all the samples.

intersubband transition by, [2],

$$I_a = \frac{N L_z W e^2 h}{4\epsilon_0 c m^*} \frac{f}{n_0^2(n_0^2+1)^{1/2}} \tag{2.1}$$

where,

$$f = \frac{4\pi c m^*}{\hbar \lambda_0} < Z_{21} >^2 \tag{2.2}$$

Here λ_0 is the resonant wavelength, W is the number of wells, n_0 is the refractive index, N is the carrier density, L_z is the well width and m^* is the carrier effective mass in the wells.

The integrated absorbance, I_a, has been estimated by multiplying the peak absorbance by the FWHM of the scan, [2]. This approximation leads to a slight, underestimate, ($\sim$ 5%), of I_a. The oscillator strengths and matrix elements, shown in Table(2.3), were calculated with the aid of the following experimental data, $m^* = 0.042 m_0$ (InGaAs), W=50, $n_0 = 3.6$ and $N = 1.0 \times 10^{18} cm^{-3}$.

The values calculated for the matrix element for all but two of the samples are within the range $22 - 28 \mathring{A}$. The two samples with anomalously low matrix elements, also had the weakest intersubband absorption and largest noise levels. In the published literature, the matrix element for this material system has been

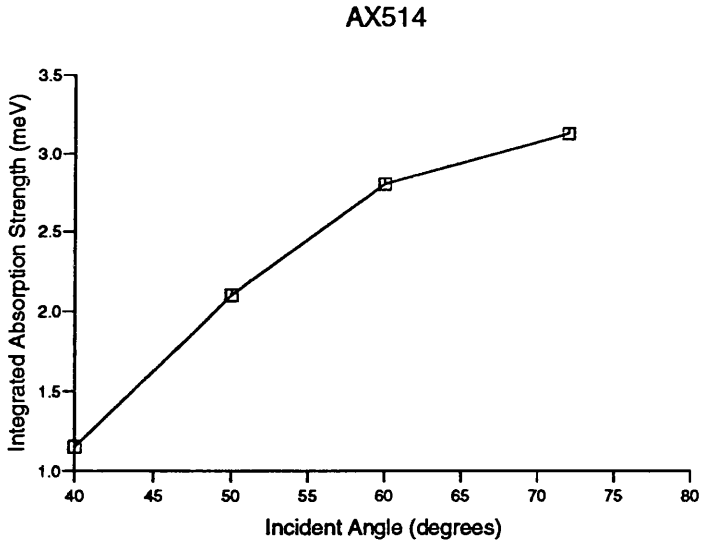

Figure 2.8: Variation of the integrated absorption strength with incident angle of the IR beam, for sample AX514.

reported to be $\sim 15\mathring{A}$, [3, 4] for a $50\mathring{A}$ well, considerably smaller than the value obtained for four of the samples reported here. Matrix elements as large as those shown in Table(2.3), have been reported in the more extensively studied GaAs/AlGaAs system, [1, 2], where values of $20\mathring{A}$ have been observed. It would appear that the matrix elements of the transitions tested here are much larger than those previously observed.

In figure(2.8) the change in the integrated absorption strength as the angle of incidence between the wafer and the IR beam is varied is shown. As expected the absorption strength decreases as the sample is moved away from its optimum position. When the beam is perpendicular to the sample none of the beam couples into the well and so no ISBA is observed.

Absorption coefficient and Dephasing Relaxation Time.

The intersubband absorption coefficient, α_{ISB}, can be obtained from the peak absorbance, using, α_{ISB} = - 2.303 Absorbance/l, where l is the number of wells $\times$ thickness of the wells. As the absorption is proportional to the number of carriers in the well, the sample with the greatest doping, (AX556), should have the largest absorption coefficient and conversely the least doped wafer, (AX555), should have the lowest α_{ISB}.

If the four samples, (AX480, AX482, AX514, AX555), which gave approximately the same matrix element are considered in isolation, then the lightly doped sample, AX555, $N = 0.2 \times 10^{18}\ cm^{-3}$, does indeed have a smaller absorption coefficient than the three samples doped to $N = 1.0 \times 10^{18}\ cm^{-3}$, Table(2.3). Also, if the two other samples, which had matrix elements less than $10\mathring{A}$, (AX528, AX556), are considered together, it is again evident that the more heavily doped sample, AX556, has the larger absorption coefficient. However, if all the samples are considered together, then the most lightly doped and the most heavily doped samples do not have the smallest and largest α_{ISB}, respectively; the reason for this is unclear. The most heavily doped sample, AX556, also gave an anomalously low matrix element, suggesting that perhaps this sample has some growth defects.

The full width half maximum, $\Delta\nu$, of the absorbance can be used to estimate the dephasing relaxation time, T_2, using $T_2 = 1/(\pi\Delta\nu)$, [10]. The values obtained, shown in Table(2.3), are all in the range of 50-60 femtoseconds, with one exception, AX514, which has an exceedingly fast relaxation time. The relaxation

time for InGaAs/InAlAs system shown here are very fast, but are in agreement with the values which can be inferred from Asai's, [3], (58 fs), and Levine's, [4], (55 fs), work. It is worth noting that the reported values for the relaxation time of the GaAs/InGaAs system are twice as long, ($\sim$ 100 fs).

2.2.4 Summary

The intersubband matrix elements of several InGaAs/InAlAs quantum wells were measured experimentally and the values obtained were found to be larger than those previously reported, at $\sim 25\mathring{A}$, for $50\mathring{A}$ wells. Matrix elements as large as $25\mathring{A}$ have been measured in GaAs/AlGaAs quantum wells. The absorption coefficient showed the expected variation with doping level, provided the samples were separated into two groups, determined by the matrix element of each sample. The dephasing time for the InGaAs/InAlAs system was estimated to be about half that of the GaAs/AlGaAs system, at $\sim$ 55 fs. The value of $\sim$ 55 fs obtained for the InGaAs/InAlAs system is, however, consistent with dephasing time that can be inferred from other published work. The variation of the resonant wavelength with well width, indicated a nonparabolicity factor, ($\gamma = 9 \times 10^{-19}\ m^{-2}$), in good agreement with previously reported values, and the variation of wavelength with doping and incident beam angle also showed the anticipated relationships.

2.3 Theoretical model for Intersubband Transitions.

2.3.1 Introduction.

As well as the large body of experimental work on intersubband transitions, a considerable amount of theoretical analysis has been published, and several authors have proposed models for the linear and nonlinear susceptibilities of intersubband transitions, [11, 12]. From a basic physics viewpoint intersubband transitions provide a ideal vehicle to test quantum mechanical predictions, because the subbands in quantum wells can be thought of as a simple two level system. Thus the optical properties of these subband transitions have been modelled using the idea of an ensemble of two level systems.

Experimental work on semiconductor lasers, [13, 14, 15], and more general theoretical work on interband transitions, [16-19], has indicated that the dephasing time associated with such two level systems is frequency dependent. The exact nature of this dispersion is subject to debate, but some general features of the frequency dependence of the reciprocal of the dephasing time, Γ_2, are accepted. Specifically, it is clear that there is a rapid change in Γ_2 for frequencies below the resonant frequency, ω_0, whilst only a relatively slow change in Γ_2 for frequencies above ω_0.

The following sections outline the effects that are induced in the optical properties of intersubband transitions, when dispersion of the dephasing time is taken into account. The linear and nonlinear refractive index and absorption coefficients

are calculated assuming both a frequency dependent and a constant dephasing time. The differences obtained are discussed and a comparison with published work is also given.

2.3.2 Theory.

The response of any dielectric to light becomes nonlinear if the electromagnetic field is of sufficient intensity. The origin of this nonlinear response is related to anharmonic electron motion induced when a strong field is applied. As a result the induced polarization, P, from the electronic dipoles is not linear in the electric field, E, but satisfies the more general relationship,

$$P = \epsilon_0 [\chi^{(1)} E + \chi^{(2)} E \cdot E + \chi^{(3)} E \cdot E \cdot E + \ldots] \tag{2.3}$$

where ϵ_0 is the permittivity of free space, and $\chi^{(j)}$ $(j = 1, 2, \ldots)$ is the j^{th} order susceptibility. The susceptibilities, $\chi^{(j)}$ are in general tensors of rank $j + 1$ but fortunately the crystal symmetry of most solids is such that only a limited number of elements of each tensor are utilised.

The expressions for the first and third-order susceptibilities, used in this section, were taken from reference[11], having been derived using the density matrix formalism. This model for the susceptibility assumes that a passive semiconductor can be modelled as a two level system. In effect it assumes that the conduction and valence bands of a semiconductor can be modelled as a set of independent energy systems, each of which consists of only two energy levels. Each of these systems has a different energy separation. The generalised expressions for the susceptibility, given in [11], are capable of dealing with pulses as well as CW

beams.

$$\chi^{(1)}(\omega) = \frac{N}{\epsilon_0}\left(\frac{e|P_{12}|}{m\omega}\right)^2 \frac{(\omega_0-\omega)+i\Gamma_2(\omega)}{\hbar(\omega_0-\omega)^2+\Gamma_2^2(\omega)} \tag{2.4}$$

$$\chi^{(3)}(\omega) = \frac{N}{8\epsilon_0\hbar^3}\left(\frac{e|P_{12}|}{m\omega}\right)^4 \frac{4(\Gamma_2(\omega)+\gamma)}{\Gamma_1+2\gamma}\Omega(\omega,\omega_0,\gamma) \tag{2.5}$$

and

$$\Omega(\omega,\omega_0,\gamma) = \frac{(\omega-\omega_0)-i(\Gamma_2(\omega)+3\gamma)}{[(\omega-\omega_0)^2+(\Gamma_2(\omega)+3\gamma)^2]}\frac{1}{[(\omega-\omega_0)^2+(\gamma+\Gamma_2(\omega))^2]} \tag{2.6}$$

Here Γ_1 is the reciprocal of the recombination time, N is the carrier density, m is the electrons mass, γ is the inverse risetime of the pulse and P_{12} is the momentum expectation value, which is related to the matrix element measured in the previous section.

The above model for the third-order susceptibility incorporates the one - electron mechanisms of the band-filling and the Optical Stark effects. The band-filling effect is the name given to the change in the polarization that occurs when sufficient optically excited carriers have been promoted to the higher energy level to inhibit further upward transitions; this is a real process. A real process is one in which there is a change in the total energy of the carriers - energy is removed from the optical field. Some carriers remain in higher excited state after the optical field has been turned off, (non-adiabatic transitions).

The other mechanism included in this model is the Optical Stark effect, which is a shift in the absorption edge due to an applied electric field. This is a virtual process, and thus is one in which carriers only remain in a higher energy state, while the pulse is present. No carriers are left in an excited state after the optical field has been turned off, (adiabatic transitions). The applied field causes a

temporary modification of the band structure of the material, while it is present in the medium. A considerable body of work has been reported on these and the various other one-electron mechanisms that can induce a nonlinear response, [20-23].

The effects of a frequency dependent dephasing time on the optical properties of intersubband transitions can be investigated, by incorporating a model for the dispersion of the dephasing time, into eqns(2.4, 2.5) for the complex triply resonant first and third order susceptibility. The general features of the dispersion of Γ_2 can be modelled, [11,13-19], by combining a Lorentzian, for frequencies above, and a Gaussian function, for frequencies below ω_0. The Gaussian provides the required rapid fall of Γ_2 from its maximum value at ω_0, while the Lorentzian reproduces the relatively slow fall of Γ_2 above resonance. The model for the dispersion of Γ_2 thus consist of a Gaussian below the band-gap, and a Lorentzian above.

The susceptibilities calculated assuming a frequency dependent dephasing time, can be shown to be related to the linear refractive index, n_L, linear absorption, α_{ISB}, nonlinear index, n_2, and nonlinear absorption,α_{NL} by the following expressions,

$$n_L = \frac{\Re[\chi^{(1)}]}{2n_0} \tag{2.7}$$

$$\alpha_{ISB} = \frac{\omega\Im[\chi^{(1)}]}{cn_0} \tag{2.8}$$

$$n_2 = \frac{3\Re[\chi^{(3)}]}{4\epsilon_0 cn_0^2} \tag{2.9}$$

$$\alpha_{NL} = \frac{2\omega\Im[\chi^{(3)}]}{\epsilon_0 c^2 n_0^2} \tag{2.10}$$

The total refractive index and absorption due to intersubband transitions are given by $n = n_L + n_2 I$ and $\alpha = \alpha_{ISB} + \alpha_{NL} I$, respectively. Where I is the optical intensity, c is the velocity of light in vacuo, n_0 is the background refractive index and ϵ_0 is the permittivity of free space. Here $\Re[]$ and $\Im[]$ signify the real and imaginary part, respectively, of the complex function.

2.3.3 Results.

Adding a frequency dependence to Γ_2 considerably changes the linear and nonlinear optical properties induced by intersubband transitions. The results given here were obtained by using the following parameters, appropriate for the GaAs/InGaAs material system $n_0 = 3.3$, $T_{2max} = 1/\Gamma_{2max} = 100$fsec, $T_1 = 1/\Gamma_1 = 2$psec, N=1.5×10^{18} cm^{-3}, $\lambda_0 = 10.6\mu m$ and the matrix element was taken to be $15\mathring{A}$. The momentum matrix element has been assumed to be frequency independent and the following relationship between the momentum expectation value and the matrix element has been used $P_{12} = m\omega_0 < z >$.

The calculations were undertaken assuming that the risetime of the perturbing pulse is much longer than the dephasing time and thus $(3\gamma + \Gamma_2)$ & $(\gamma + \Gamma_2) \rightarrow \Gamma_2$, essentially a CW perturbing beam has been assumed.

The frequency dependence of Γ_2 used in the calculations of the first and third order susceptibilities is shown in figure(2.9) for two different values of the Gaussian half width. The corresponding values of the linear refractive index and nonlinear index are shown in figures(2.10-2.11), together with the values for a constant dephasing time curve.

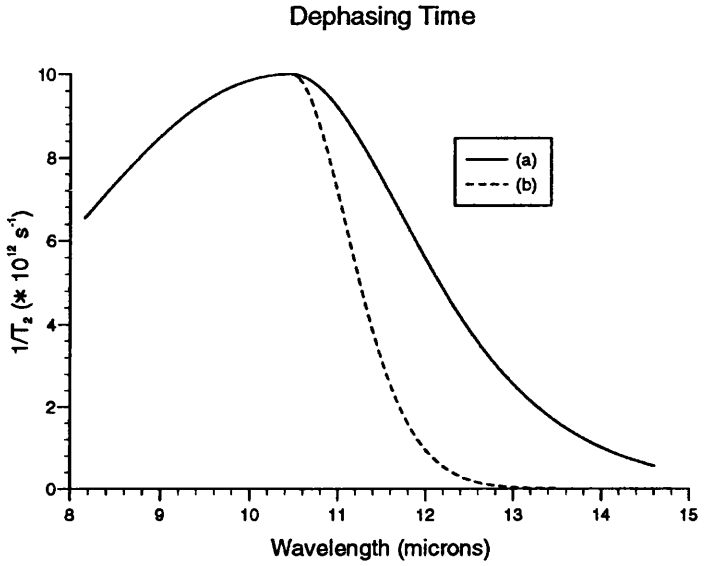

Figure 2.9: Frequency Dependence of Γ_2 with Gaussian half widths of (a) $1.1 \times 10^{13}s^{-1}$, (b) $1.5 \times 10^{13}s^{-1}$.

Initial work on the implications of a frequency dependent dephasing time have been presented at the OSA Topical Conference on Nonlinear Optics '92, in Hawaii, USA, [24].

Linear Intersubband Refractive Index

The magnitude of the linear index, figure(2.10), is very slightly decreased, below resonance, but significantly increased, above resonance, in comparison with results calculated with a frequency independent dephasing time. The fall of $\Gamma_2(\omega)$ from its peak value at resonance results in the denominator of eqn(2.4) always being less than when Γ_2 is assumed to be constant, hence the increased maxima and minima of figures(2.10b-2.10c).

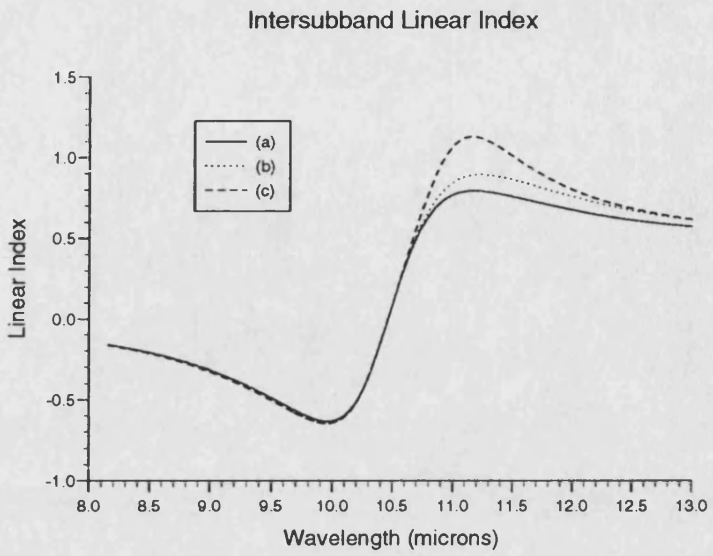

Figure 2.10: Linear Index, n_{ISB}, for a constant dephasing time, (a) $\Gamma_2 = 1.10^{13}s^{-1}$, and a frequency dependent dephasing time with Gaussian half widths of (b) $1.1 \times 10^{13}s^{-1}$, (c) $1.5 \times 10^{13}s^{-1}$.

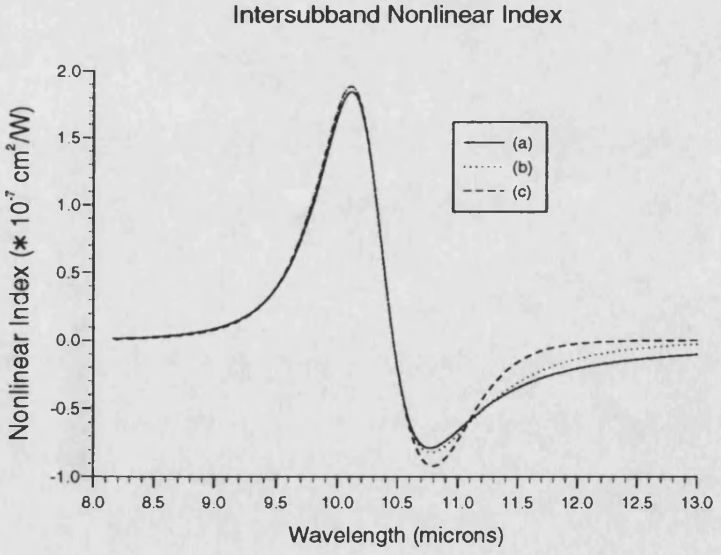

Figure 2.11: Nonlinear Index, n_2, for a constant dephasing time, (a) $\Gamma_2 = 1.10^{13}s^{-1}$, and a frequency dependent dephasing time with Gaussian half widths of (b) $1.1 \times 10^{13}s^{-1}$, (c) $1.5 \times 10^{13}s^{-1}$.

The maximum and minimum of figures(2.10b-2.10c) are also shifted in frequency. The extrema points move towards the frequency values they would attain if $\Gamma_2 = 0$. Since this small shift is dependent on the difference between $\Gamma_2(\omega)$ and Γ_{2max}, it is only visible when $\Gamma_2(\omega)$ is falling rapidly, i.e, below resonance.

Nonlinear Intersubband Refractive Index

Adding a frequency dependence to Γ_2 causes the intensity dependent refractive index, n_2, to vary in an analogous manner to that of the linear index, figure(2.11).

The nonlinear refractive index extrema occur in the opposite sequence to those of the linear index, because band-filling effects cause a reduction in the absorption and hence a reduction in the contribution to the index, resulting in a sign change. The maximum value of n_2 calculated in the present work compares favourably with measurements made using wavelengths near $10\mu m$ where a n_2 of the order of $10^{-7}\ cm^2/W$ was obtained, [5, 22].

Linear Intersubband Absorption

The frequency dependence of the dephasing time results in an asymmetric linear absorption spectrum, figure(2.12), with a reduced bandwidth. A slight hump also appears caused by the interplay between the dispersion of Γ_2 and the non-coincidence between the absorption peak frequency and the resonance of the two level system.

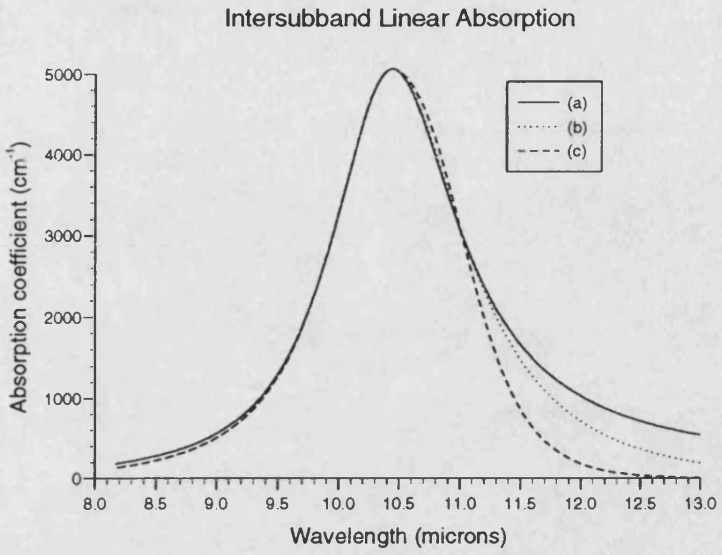

Figure 2.12: Linear absorption, α_{ISB}, for a constant dephasing time, (a) $\Gamma_2 = 1.10^{13}s^{-1}$, and a frequency dependent dephasing time with Gaussian half widths of (b) $1.1 \times 10^{13}s^{-1}$, (c) $1.5 \times 10^{13}s^{-1}$.

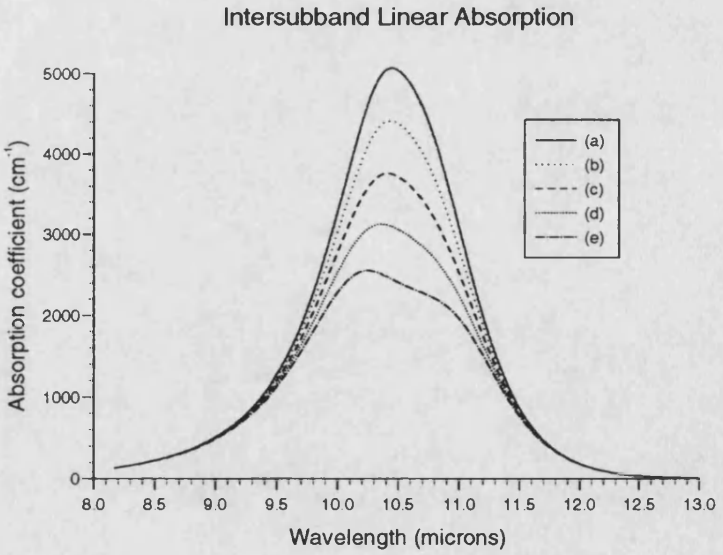

Figure 2.13: The total absorption for intensities of (a) low intensity limit, (b) 0.25 MW/cm^2, (c) 0.5 MW/cm^2, (d) 0.75 MW/cm^2, and (e) 1.0 MW/cm^2.

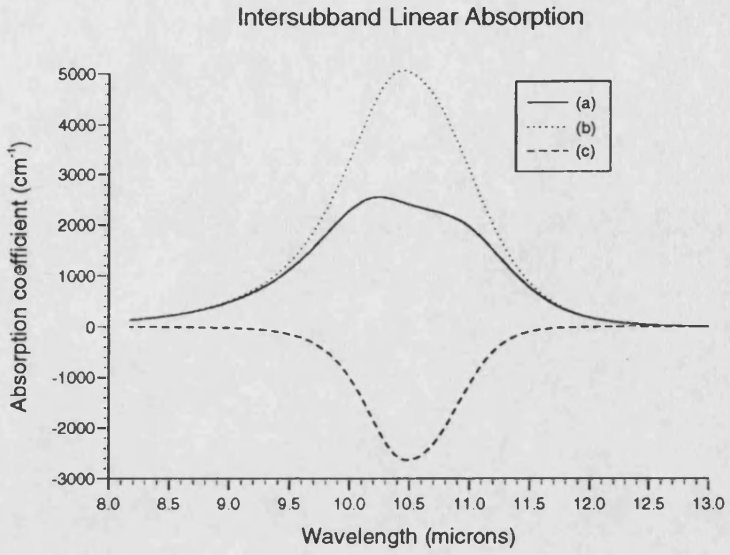

Figure 2.14: The components of the total absorption, for an intensity of $1.0MW/cm^2$ and Gaussian half widths of $1.5 \times 10^{13}s^{-1}$, (a) linear absorption, (b) total absorption and (c) nonlinear absorption.

Nonlinear Intersubband Absorption

Significant bleaching of the absorption, caused by band-filling, can occur if sufficiently high intensities are used. Figure(2.13) shows the total absorption for the case of a frequency dependent Γ_2, for various optical intensities. The extrema of the linear and nonlinear absorption occur at slightly different frequencies, and have marginal different bandwidths, resulting in a asymmetric total absorption spectrum, figure(2.14).

The effect of making the reciprocal of the dephasing time frequency dependent reduces the bandwidth of both the linear and the nonlinear contributions to the total absorption and also increases the asymmetry of the nonlinear and linear absorption coefficient.

The results obtained here show the same general features as those recently reported by several authors, [11,20-22]. The absorption also begins to saturate for intensities of $\sim 0.25\ MW/cm^2$, again in agreement with published experimentally work, [26, 27]

2.3.4 Summary

The inclusion of a frequency dependent dephasing time into a model for the optical properties of intersubband transitions, results in increased asymmetry in the spectra of the linear and nonlinear index and absorption. The FWHM of the linear and nonlinear absorption are also reduced. The peak magnitude of the nonlinear index and the linear absorption coefficient, plus the saturation intensity, all agree with published results.

The intersubband transitions of InGaAs/InAlAs quantum wells were investigated, and values obtained for the matrix element, ($\sim 25\mathring{A}$ for $50\mathring{A}$ wells), and dephasing time, (55 fs).

Several groups are working on ways of utilizing intersuband transition in far infra-red photodetectors, while others are investigating the possibility of using the large nonlinear refraction associated with intersubband transitions in all-optical switching devices.

The next chapter looks at another possible effect that could be used in an all-optical switching device. This effect was discovered in semiconductor optical amplifiers when their ultra-fast gain dynamics were being studied.

References

[1] L.C.West and S.J.Eglash, Appl. Phys. Lett., 46, 1156, (1985)

[2] B.F.Levine *et al*, Appl. Phys. Lett., 50, 273, (1987)

[3] H.Asai and Y.Kawamura, Phys. Rev B., 43, 4748, (1991)

[4] B.F.Levine *et al*, Appl. Phys. Lett., 52, 1481, (1988)

[5] D.Walrod *et al*, Appl. Phys. Lett., 59, 2932, (1991)

[6] M.Segev, I.Grave, and A.Yariv, Appl. Phys. Lett., 61, 2403, (1992)

[7] M.C.Tatham, J.F.Fyan, and C.T.Ryan, Phys. Rev. Lett., 63, 1637, (1989)

[8] J.Feldmann, E.Gobel, and K.Ploog, Appl. Phys. Lett., 57, 1520, (1990)

[9] P.Sotirelis, P.von Allmen, and K.Hess, Phys. Rev. B., 47, 12744, (1993)

[10] B.F.Levine *et al*, Appl. Phys. Lett., 50, 1092, (1987).

[11] M.G.Burt, Semicond. Sci. Technol., 5, 1215, (1990)

[12] K.J.Kuhn *et al*, J. Appl. Phys., 70, 5010, (1991)

[13] A.Tomita and A.Suzuki, IEEE J. Quantum Electron., QE-27, 1630, (1991)

[14] A.I.Kucharska and D.J.Robbins, IEEE J. Quantum Electron., QE-26, 443, (1990)

[15] M.Yamanishi and Y.Lee, IEEE J.Quantum Electron., QE-23, 367, (1987)

[16] T.Ohtoshi and M.Yamanishi, IEEE J.Quantum Electron., QE-27, 46, (1991).

[17] M.Asada, IEEE J. Quantum Electron., QE-25, 2019, (1989)

[18] P.C.Becker *et al*, Phys. Rev. Lett., 61, 1647, (1988)

[19] Y.Hamano and F.Shibata, J. Phys. Soc. Japan., 51, 2728, (1982)

[20] B.S.Wherrett Proc. R. Soc. Lond. A, 390, 373, (1983)

[21] B.S.Wherrett Phil. Trans. R. Soc. A, 313, 213, (1994)

[22] S.Y.Auyang and P.A.Wolff, J. Opt. Soc. Am. B, 6, 595, (1989)

[23] A.C.Walker, Opt. Comput. Process, 1, 91, (1991)

[24] P.S.Spencer and K.A.Shore, OSA Nonlinear Optics Topical Meeting, Hawaii, MD6, (1992).

[25] D.Ahn and S.L.Chuang, J. Appl. Phys., 62, 3052, (1987)

[26] F.H.Julien *et al*, Appl. Phys. Lett., 52, 116, (1988)

[27] Da-fu Cui *et al*, Phys. Rev. B, 47, 6755, (1993)

Chapter 3

Nonlinearities in Active Semiconductors

3.1 Introduction

The recent drive by telecommunication companies to replace copper cables by optical fibres has facilitated a drastic increase in the rate at which information can be transmitted. This push for ever increasing data rates has meant that sources and detectors with ever increasing responsiveness, and all-optical switching components are being sought. It is therefore important to know what physical phenomena will limit the future performance of such devices.

This concern has lead to the recent studies of the ultra-fast gain dynamics of semiconductor optical amplifiers, [1-9]. These investigations have uncovered some unexpected features. The most interesting and potentially the most useful of these, has been the discovery that semiconductor optical amplifiers possess a large ultra-fast nonlinear refraction. A number of groups are at present actively

engaged in studying this fast nonlinear refraction, with a view to exploiting this effect to implement an all optical switch, [10, 11, 12].

The first section of this Chapter reviews the experimental results that have been reported, and indicates which mechanisms are thought to have been responsible for the observed effects. The second section examines the physical origins of these mechanisms and reviews the theoretical work which has been undertaken to unify, and model, these mechanisms.

3.2 Experimental investigation of Optical Amplifiers

3.2.1 Introduction

The discovery of a fast nonlinear refraction in semiconductor optical amplifiers, by groups working on the ultra-fast gain dynamics of such devices, has resulted in a flurry of activity to investigate this newly observed nonlinear refraction. The experimental work has concentrated on two types of optical amplifier, those based on InGaAsP and those on AlGaAs, and both show the same qualitative features, but quantitatively there are some slight differences.

Two main experimental techniques have been used to investigate the nonlinear index and gain of semiconductor optical amplifiers:

- The Pump-Probe Technique: In this approach an intense pump pulse is used to perturb the sample, and the effects induced on a short weak probe pulse are monitored. The time delay between the pump and the probe pulse is varied, so that the recovery time of the device can be studied.

- Frequency Domain Analysis: In this case a single pulse is launched into the device, and the output spectrum recorded. The nonlinear index induces a change in the phase of the pulse proportional to the intensity profile of the pulse and hence self phase modulation, (SPM), occurs. For this reason these results are commonly referred to as SPM measurements.

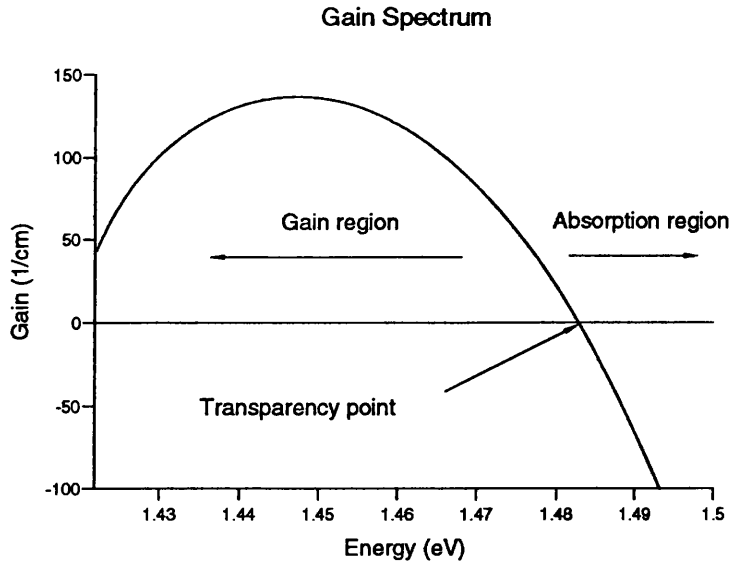

Figure 3.1: Gain spectrum illustrating the three possible operating condition of Gain, Absorption and Transparency.

Unlike the passive devices studied in Chapter 2, the optical amplifiers considered in this chapter are either optically or electrically pumped so that a carrier population inversion is obtained, and they are thus active devices.

Using photon energies above the band-gap active devices can be investigated in three different regimes; gain, transparency, or absorption, figure(3.1). In the gain region the input pulse experiences a net gain in energy, while in the absorption region the pulse suffers a net loss in energy. The transparency point occurs at the boundary between these two regions, and is where no net change in pulse energy occurs. At the transparency point the number of upward carrier transitions exactly equals the number of downward transition; there is no net change in the carrier population.

Two approaches can be used to experimentally switch the device from one region to the next; either, changing the current and keeping the wavelength constant, or conversely by changing the wavelength and keeping the bias current constant. The experiments reported in the literature have used both techniques, [2], and have shown that the same effects are observed regardless of whether the current or the wavelength is swept.

The experimental data has also indicated that the response of semiconductor optical amplifiers is significantly different for sub-picosecond optical pulses than for optical pulses of a few picoseconds duration.

The following sub-sections outline both the effects observed experimentally, and the mechanisms thought to induce them, for pulses of sub-picosecond and picosecond pulsewidths.

3.2.2 Gain Dynamics

Sub-Picosecond Pulses

The pump-probe pulses used to investigate the gain dynamics typically use optical pulse widths of between 100-400fs, and pulse energies of a few pico-joules for the pump and fractions of a pico-joule for the probe. Both the InGaAsP and AlGaAs devices showed similar features in their transmission versus time-delay scans, but the recovery times associated with each of the discernible components of the scans were found to be material dependent.

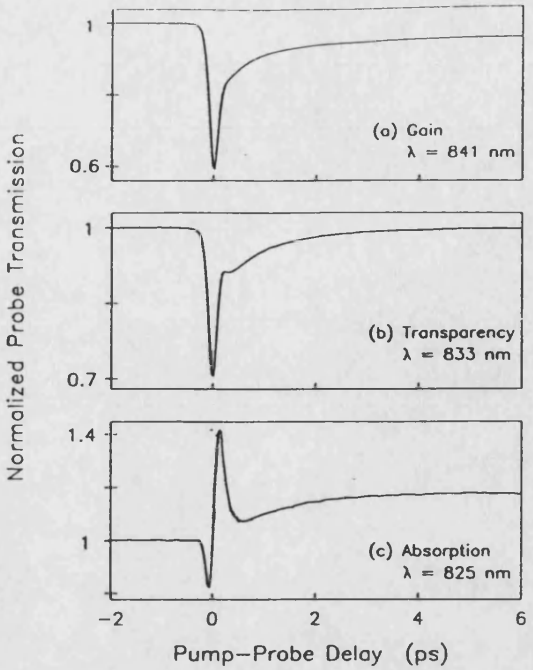

Figure 3.2: Above-band gain dynamics. This shows the probe transmission through the AlGaAs optical amplifier as a function of pump-probe time-delay. The pump-probe wavelength was tuned to access the (a) gain, (b) transparency, and (c) absorption regimes.

Figure(3.2) is taken from [7] and shows probe transmission dynamics in a AlGaAs optical amplifier. The wavelength was swept so that the dynamics in the gain, transparency, and absorption regions could be studied.

A long-lived step change in the gain and absorption regions caused by carrier density variations, stimulated by the pump, can be seen. In the gain region the pump induces gain compression, by reducing the number of carriers. Conversely in the absorption region the carrier concentration increases, resulting in reduced absorption. The recovery time of this component is of the order of the carrier recombination time, ($\sim ns$).

In all three regions two fast gain compression components are observed, fig(3.2). The slower of the two, has been attributed to dynamic carrier heating, caused

by free carrier absorption and stimulated emission. The resultant heating of the carrier distribution causes a decrease in the gain, that relaxes on a picosecond time scale, as the carriers cool back to the lattice temperature.

A detailed analysis of fig(3.2) by Hultgren and co-workers showed that there was a delay in the heating of the carriers, ($\sim 120fs$), [7]. Physically this suggests that it takes a finite time before the free carriers, that have absorbed pump photons, start to lose energy to the cooler free carriers at the bottom of the conduction band. This delay in the carrier heating has not as yet been observed in InGaAsP devices. The other negative gain component appears to have an instantaneous response and is thus thought to be induced by a virtual process. Hence, this instantaneous component has been attributed to two-photon absorption.

Hultgren and co-workers also showed that a further fast component, that had previously only been seen in InGaAsP devices, was also present in transmission dynamics of AlGaAs optical amplifiers, fig(3.2). This component has been attributed to spectral-hole burning. The spectral-hole burning component has the same sign as that of the long-lived stimulated carrier change, and is thus negative in the gain region, positive in the absorption region, and zero at the transparency point. The recovery time is very fast and has been estimated to be $\sim 120fs$.

The fast recovery times of the spectral-hole burning, carrier heating and two-photon absorptions effects ensure that a partial recovery of the gain is observed.

Picosecond Pulses

The transmission-time delay data for picosecond pulses have not shown the partial recovery of the gain seen in the experimental results of shorter sub-picosecond pulses. Hence dynamic carrier heating and spectral-hole burning effects would appear not to be an important effect for pulses of this time scale. The experimental results have indicated that saturation of the gain/absorption, caused by band-filling, is the most significant phenomenon in this regime, [10, 13].

Sufficiently intense pulses can promote enough electrons from the valence band to the conduction band, to begin to block further upward interband transitions, ie. there are not enough free states in the conduction band to accept all the carriers that could be excited.

Summary

The experimental work on the gain dynamics of optical amplifiers has shown that, for sub-picosecond pulses partial gain recovery can occur, caused by spectral-hole burning, two-photon absorption, and dynamic carrier heating. For longer pulses no such gain recovery is observed, and the dominant effect for picosecond pulses was found to be gain saturation, caused by band-filling effects.

3.2.3 Nonlinear Index

Sub-Picosecond Pulses

Time-Division interferometry can be used, in conjunction with standard pump-probe techniques, to measure pump-induced refractive changes. The pump-induced refractive changes cause a probe pulse phase shift, which can be measured by interfering the probe pulse with a reference pulse. The refractive index dynamics associated with the transmission dynamics of figure(3.2) are shown in figure(3.3), and again are taken from [7].

Figure(3.3) shows a long-lived step change in the refractive index, in the gain and absorption regions, caused by pump stimulated carrier density changes. In the gain region the reduction in the number of carriers causes an increase in the index, while in the absorption region the increased number of carrier causes a reduction in the index. There is no long-lived component observed at the transparency point, because the effect is caused by changes in the carrier population, which cannot occur at the transparency point.

A negative refractive index transient is observed in all three regions, fig(3.3). This index change appears to be instantaneous, indicating that it is probably a virtual effect, and measurements below the band-gap have indicated that it is resonantly enhanced. These two observations suggest that the most likely mechanism is the Optical Stark effect.

Time-Division interferometry has also indicated that there is a positive refractive index transient with a recovery time of the order of a picosecond in these

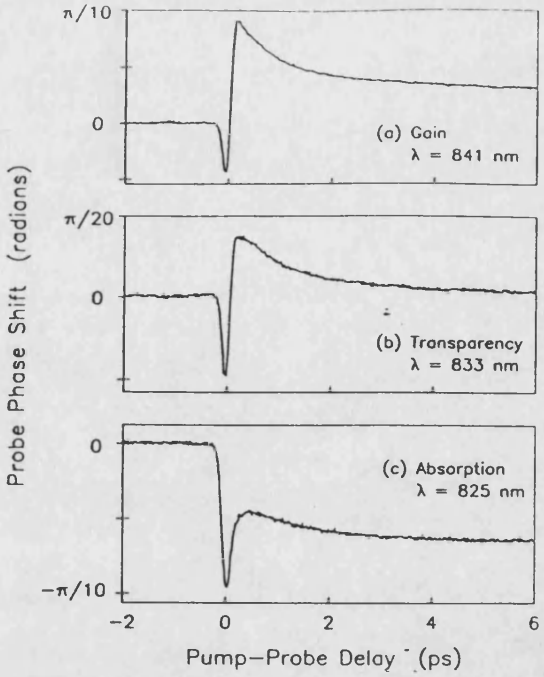

Figure 3.3: Above-band index dynamics. This shows the probe phase shift through the AlGaAs optical amplifier as a function of pump-probe time-delay. The pump-probe wavelength was tuned to access the (a) gain, (b) transparency, and (c) absorption regimes.

devices, fig(3.3). This index change has been attributed to the carrier heating effect, (observed in the gain dynamics studies). The Kramer-Kronig relation predicts that a change in the gain will also cause a corresponding change in the index. This effect is observed in all three regions, since carrier heating only causes a redistribution of the carriers and not a net change in their number. Using this time domain technique the instantaneous nonlinear index has been estimated to be $\sim -5.0 \times 10^{-12} cm^2/W$, [5].

The Self Phase Modulation, (SPM), frequency domain technique has been used to measure the refractive index changes in semiconductor optical amplifiers. The devices tested have all been biased so that they are operated in the gain region, [4]. The measurements have shown that at high average powers, ($\sim 5mW$), the spectra obtained are pulsewidth dependent, with more distortion evident in the

spectrum of the short pulses, ($< 0.5ps$). The gain compression, and its subsequent partial recovery, induce a time dependent increase in the refractive index, which in turn causes the instantaneous frequency shift that distorts the output pulse spectrum. The initial gain depletion causes a red-shift of the central frequency of the pulse, but the subsequent carrier thermalization partially replenishes the gain resulting in a reduction in the index, which in turn causes a blue-shift of the central frequency of the pulse.

Picosecond Pulses

The SPM measurement of picosecond pulses , [4], have reinforced the conclusion drawn from gain dynamic results discussed earlier, that the effects of carrier heating and spectral-hole burning need not be considered in this regime. The picosecond pulses results only show the effects of gain compression, which causes a red-shift in the central carrier frequency of the pulse. The magnitude of the red-shift was also found to be proportional to the pulse intensity profile. SPM measurements using picosecond pulses have also been carried out using devices biased to the transparency point, [10], and an estimate of the magnitude and sign of the nonlinear index has been obtained, $n_2 = -2.0 \times 10^{-11} cm^2/W$.

3.2.4 Summary

Both time and frequency domain measurements of optical amplifiers have indicated the presence of a nonlinear refraction. In the case of sub-picosecond pulses it was found that several components contribute to the index change, one of

which was found to respond instantaneously and was attributed to the Optical Stark effect. In both the picosecond and the sub-picosecond regimes the nonlinear index was found to be negative and to have a magnitude of the order of $n_2 \sim 10^{-11} cm^2/W$.

The next section looks at the models derived to explain the physical origin of the mechanisms mentioned above.

3.3 One-Electron Theories of Nonlinear Susceptibility

3.3.1 Introduction

A considerable amount of theoretical work on the nonlinear refractive index and absorption of passive semiconductors has been reported, [14-20]. Expressions for the complex nonlinear susceptibility, (from which the index and absorption can be calculated), have been derived using one-electron theory. This approach neglects many-body effects and assumes that the material can be modelled by an ensemble of independent two-level systems.

The expressions obtained using one-electron theory, have provided a good insight into the physical origins of the mechanisms that determine the susceptibility of passive semiconductors, under strong optical field conditions. These results are also applicable to active semiconductors, provided that account is taken of the different carrier distributions of active and passive semiconductors.

The mechanisms that induce a susceptibility can be separated into two groups: those caused by virtual transitions and those caused by real transitions. A virtual transition takes place when the frequency of the optical field does not correspond to a transition frequency of the medium. An adiabatic excitation occurs, which only lasts while the optical field is present. A real transition occurs when the frequency of the optical field matches a transition frequency of the medium. Energy is removed from the optical field and the effect takes some time to decay after the optical field has been turned off.

The next sections outlines the physical origins of the mechanisms that affect the susceptibility and their inter-relationships. The regime under which each mechanism provides the dominant contribution to the susceptibility will also be highlighted.

3.3.2 One-Electron Theory of Nonlinear Refraction

Several theoretical models have been used to interpret specific experimental results, but only recently has a theory that unifies some of these mechanisms been proposed by Burt, [15, 16].

Before considering the one-electron mechanisms in detail it is worthwhile considering a quasi-dimensional analysis of the problem, as this provides the simplest first assessment of the nonlinear susceptibility, $\chi^{(3)}$. By performing such an analysis, Wherrett, [14], has shown that the nonlinear susceptibility is proportional to the following parameters,

$$\chi^{(3)} \propto \frac{e^4 P}{E_g} F(\hbar\omega/E_g) \tag{3.1}$$

where e is the charge of an electron, E_g is the band-gap, P is the momentum matrix element for the interband transition, ($P = (\hbar/m) \mid p_{cv} \mid$), and F is a dimensionless function which contains resonant enhancement factors. It is clear from this that the band-gap of the material plays an important part in determining the magnitude of $\chi^{(3)}$. The one-electron mechanisms that will now be discussed are responsible for inducing the resonant enhancement factors present in F.

Wherrett, [14], pointed out that the low frequency contribution to the non-linear susceptibility, caused by free carriers moving in non-parabolic bands, can be viewed as a virtual process. To see how the non-parabolicity phenomena can be related to a virtual process this low frequency effect must be viewed in quantum mechanical terms. As the electron changes its wavevector, in response to a perturbing optical field, its wavefunction changes adiabatically. The resultant harmonic variation of the wavefunction causes a constant average shift in the energy levels. All the electron states experience such a shift, and since the effective mass is dependent on the energy levels of the electron states, a change in the effective mass is induced.

As the frequency of the applied optical field increases, the Optical Stark effect starts to become dominant. The nonlinear susceptibility is caused by a shifting of the energy levels, however in this case, the adiabatic oscillation of the wavefunctions results in a blue-shift of the band-gap. In other words an intensity dependent (Optical Stark) shift of the absorption line is induced. Unlike the low-frequency non-parabolicity effect this is a triply resonant process, i.e photons with the same energy are required, and hence the effect is enhanced as the frequency

approaches the band-gap. Both the Optical Stark effect and the non-parabolicity cause no change in the carrier population of the valence and conduction bands

Finally as the optical frequency approaches the interband transition frequency, absorption starts to become the dominant mechanism. The optical field now perturbs the material non-adiabatically - a real process takes place. Blocking of upward transitions by carriers produced by previous interband transitions starts to occur, and it is this saturation effect which provides the dominant contribution to $\chi^{(3)}$. Unlike the Optical Stark effect and the non-parabolicity effects a change in the carrier populations of the valence and conduction bands is induced. Burt, [15], showed that the band-filling can be further sub-divided into two regimes, the transient and steady state. The transient effect dominates when the pulsewidth is shorter than the recombination time, while the steady state effect dominates when the pulse is longer than the recombination time.

It has been know for sometime, [14], that the nonlinear susceptibility induced by real processes is enhanced by a factor of $2T_2/T_1$, (T_1 is the recombination time and T_2 is the dephasing time.), over those induced by virtual effects. A physical basis for this factor and a general relationship between real and virtual excitation has recently been proposed, [16]. The central idea is that of generalised state-filling, i.e the change in the susceptibility does not depend on whether the excitation is real or virtual, but only on the change induced in the occupational probabilities by the optical field. The factor of $2T_2/T_1$ is a measure of the non-adiabaticity and indicates the extent to which the effect persists after the cause has been removed. $2T_2/T_1$ is the ratio of the time electron-hole pair lasts, (T_1), to the time it takes for the interband transition to produce them, ($T_2/2$), since the

relaxation of the electrons to other conduction band states has not been included.

3.3.3 One-Electron Theory of the Nonlinear Gain

Mark and Mork have recently proposed a theoretical model for the gain nonlinearities observed in optical amplifiers, [21, 22, 23].

The model they have derived is based on the semi-classical density matrix equations, [24]. These equations essentially treat the semiconductor as an inhomogeneously broadened set of two-level systems. Their model includes carrier heating, spectral-hole burning and two-photon absorption effects. Spectral-hole burning is the local deviation of the carrier distribution, at the optical transition energy, from that of a Fermi distribution. Two-photon absorption is a physical manifestation of the fact that a strong optical field can excite an electron from the valence band to the conduction band, in two steps, via a virtual intermediate state.

The Mark and Mork theory, phenomenologically models interband and intraband relaxtion, using relaxation times. This avoids the need to follow a many-body analysis of the problem, [25], and is justified provided the carrier distribution does not deviate too far from that of a Fermi distribution, [26]. Their calculations indicated that the contribution from spectral-hole burning and carrier heating were comparable, whereas that from two-photon absorption was more than an order of magnitude smaller.

3.4 Summary

The investigation of the ultra-fast gain dynamics of semiconductor optical amplifiers has revealed gain compression mechanisms that recover on a sub-picosecond time scale. Three mechanisms have been identified, spectral-hole burning, two-photon absorption, and dynamic carrier heating. These effects were found to be unimportant if picosecond pulses are being considered. The main gain compression effect in the picosecond regime was found to be saturation, induced by band-filling.

The reported experimental work has indicated that semiconductor optical amplifiers possess a large defocussing nonlinear refraction. The nonlinearity was found to have several components, one of which is large and appears to respond instantaneously. This component is thought to be induced by the Optical Stark effect. The other components; dynamic carrier heating, and long-lived carrier effects, are all real processes. They all have different recovery times which are also material dependent. If the optical amplifier is operated at the transparency point, only the Optical Stark component contributes to the nonlinear index, and hence optical amplifiers have an instantaneous nonlinear refraction which could possibly be used in an all-optical switch. The one-electron mechanisms that induce a nonlinear refraction in passive semiconductors have also been outlined and there inter-relationships discussed.

In the next Chapter a model is developed for the nonlinear susceptibility of active semiconductors, and this incorporates several of the mechanisms discussed in this chapter.

References

[1] M.P.Kesler and E.P.Ippen, Appl. Phys. Lett., 51, 1765, (1987).

[2] K.L.Hall *et al*, Appl. Phys. Lett., 56, 1740, (1990).

[3] Y.Lai *al*, IEEE Photon. Technol. Lett., 2, 711, (1990).

[4] P.J.Delfyett, Y.Silberberg and G.A.Alphonese, Appl. Phys. Lett., 59, 10, (1991).

[5] C.T.Hultgren and E.P.Ippen, Appl. Phys. Lett., 59, 635, (1991).

[6] K.L.Hall *et al*, Optic Lett., 17, 874, (1992).

[7] C.T.Hultgren, D.J.Dougherty and E.P.Ippen, Appl. Phys. Lett., 61, 2726, (1992).

[8] K.L.Hall *et al*, Appl. Phys. Lett., 62, 1320, (1993).

[9] C.K.Sun *et al*, Appl. Phys. Lett., 63, 96, (1993)

[10] R.S.Grant and W.Sibbett, Appl. Phys. Lett., 58, 1119, (1991).

[11] M.A.Fisher *et al*, Electron. Lett., 29, 1185, (1993).

[12] D.A.O.Davies, *et al*, Electron. Lett., 29, 1710, (1993).

[13] A.Dienes *et al*, Opt. Lett., 17, 1602, (1992).

[14] B.S.Wherrett, Phil. Trans. R. Soc. Lond. A, 313, 213, (1984).

[15] M.Burt, Semicond. Sci. technol., 5, 1215, (1990).

[16] M.Burt, Semicond. Sci. technol., 8, 1393, (1993).

[17] D.A.Austin *et al*, Appl. Opt., 26, 211, (1987).

[18] P.A.Wolff and G.A Pearson, Phys. Rev. Lett., 17, 1015, (1966).

[19] S.Y.Yuen and P.A.Wolff, Appl. Phys. Lett., 40, 457, (1982).

[20] P.N.Butcher and T.P.McLean, Proc. R. Soc., 81, 219, (1963).

[21] M.Willatzen *et al*, IEEE Photon. Technol. Lett., 3, 606, (1991).

[22] A.Uskov, J.Mork, and J.Mark, IEEE Photon. Technol. Lett., 4, 443, (1992).

[23] J.Mark and J.Mork, Appl. Phys. Lett., 61, 2181, (1992).

[24] N.Ogasawara and R.Ito, Jpn. J. Appl. Phys. 27, 615 (1988).

[25] H.Haug and S.W.Koch, "*Quantum Theory of the Optical and Electronic Properties of Semiconductors*", (World Scientific, Singapore, 1990).

[26] K.Henneberger *et al*, Phys. Rev. A, 45, 1853, (1992).

Chapter 4

Nonlinear index of a Semiconductor Optical Amplifier.

4.1 Introduction

As discussed in the previous chapter, there have been several reported experimental observations of a large defocussing nonlinear refraction, near transparency, in semiconductor travelling wave optical amplifiers. This nonlinear refraction was found to have a very fast transient component with a recovery time of $< 100fs$, [1-6]. A virtual process - the Optical Stark effect - has been proposed as the most likely mechanism for this ultra-fast component. The longer-lived components of the nonlinear index also observed, have been attributed to carrier heating and steady-state band-filling effects. These real processes have much longer recovery times of $\sim 1ps$ and $\sim 1ns$, respectively. The fact that the nonlinearity at transparency is both large and fast has aroused much interest, because of potential application in all optical switching components.

Despite the experimental activity on this topic very little theoretical work on these effects has been reported. Recently, by expanding on the work they had previously undertaken on the nonlinear index of passive semiconductor material, [8], Sheik-Bahae and co-workers presented some preliminary calculations of the nonlinear index, [7]. Work has also been published, by several authors, [9, 10, 11], on the changes induced in the refractive index by gain saturation. Mark and Mork have considered the pulse transmission properties of optical amplifiers, but they have not specifically addressed the changes induced in the refractive index, having instead concentrated on the transient properties of the gain, [12].

In this thesis a model for the ultra-fast component of the nonlinear refraction of semiconductor optical amplifiers, at transparency, has been derived, by incorporating a description of the carrier distribution, within an active medium, into the real part of the complex third order susceptibility, $\chi^{(3)}(\omega)$, of a passive semiconductor. In contrast to [8, 9], this approach calculates the nonlinear index directly from the real part of $\chi^{(3)}(\omega)$ and thus does not have to utilize a nonlinear Kramers-Kronig relationship. The latter has been the subject of some recent debate.

Of course the idea of using the complex polarisation of a passive semiconductor as the starting point for a model of the polarisation of an active semiconductor is not new. Such an approach has previously been used to calculate the linear gain of semiconductor lasers, by incorporating a description of the carrier distribution into the imaginary part of the first order susceptibility of a passive semiconductor, [13].

A model for the nonlinear refraction of an active medium is derived in the following sections by utilizing the expression, previously used in Chapter[2], for the complex third order susceptibility of a passive semiconductor. The nonlinear absorption of the active medium has also been calculated and the results compared with published work. An explanation is also given as to why the expression derived for nonlinear absorption cannot be used, in conjunction with the Kramers-Kronig relationship, to obtain the nonlinear index.

4.2 Third Order Susceptibility of a Passive Semiconductor.

For convenience the expressions for the third order susceptibility, [15], are expressed below, but in a slightly different form to that of Chapter(2). The frequency dependence of the dephasing time has been neglected, and thus the expressions for the third order susceptibility simplify to,

$$Re[\chi^{(3)}(\omega)] = \frac{N}{\epsilon_0}\left(\frac{e\,|p_{12}|}{m_0\omega}\right)^4 \frac{1}{8\hbar^3}\frac{4(\Gamma_2+\gamma)}{2\gamma+\Gamma_1}(\omega-\omega_{21})\,\Omega \tag{4.1}$$

$$Im[\chi^{(3)}(\omega)] = -\frac{N}{\epsilon_0}\left(\frac{e\,|p_{12}|}{m_0\omega}\right)^4 \frac{1}{8\hbar^3}\frac{4(\Gamma_2+\gamma)}{2\gamma+\Gamma_1}(3\gamma+\Gamma_2)\,\Omega \tag{4.2}$$

where,

$$\Omega = \frac{1}{(\omega-\omega_{21})^2+(3\gamma+\Gamma_2)^2}\frac{1}{(\omega-\omega_{21})^2+(\gamma+\Gamma_2)^2} \tag{4.3}$$

Here Γ_1 and Γ_2 are the reciprocals of the recombination and dephasing times, respectively. γ is the reciprocal of the pulse risetime. ω_{21} is the resonant frequency of the two level system, m_0 is the electron mass, and $\mid p_{21} \mid$ is the momentum matrix element.

4.3 Description of Carrier Distribution in an Active Semiconductor

In order to obtain an expression for the nonlinear index in an active semiconductor, equation(4.1) has to be modified to take into account the carrier distribution in the conduction and valence bands. The number of oscillators, N, found in the expression for $\chi^{(3)}$ of a passive material, has to be replaced by the appropriate carrier distribution in the medium. The required carrier distribution can be expressed in terms of the joint density of states and the occupational probabilities of each band, (obtained from Fermi-Dirac statistics).

To determine the carrier densities in the conduction and valence bands, the same technique as that outlined in, [14], has been used. This standard procedure assumes that Fermi-Dirac statistics can be applied.

The joint density of states of the conduction and valence bands per unit energy range per unit volume is given by,

$$\rho(E_{21})dE_{21} = \frac{1}{2\pi^2}\left(\frac{2m_r^*}{\hbar^2}\right)^{3/2}(E_{21}-E_g)^{1/2}dE_{21} \tag{4.4}$$

where E_{21} is the transition energy, E_g is the band-gap and m_r is the reduced mass, which is defined as $m_r^{-1} = m_c^{-1} + m_v^{-1}$. The above equation assumes that both the valence and conduction bands are parabolic.

The changes in the polarisation are induced by carriers being promoted from the valence band to the conduction band, and thus the probability of finding an occupied initial and empty final state, at a transition energy, E_{21}, is given by,

$$f_v(E_{21}) - f_c(E_{21}) \tag{4.5}$$

where

$$f_c = \left(1 + exp\left[\frac{(\hbar\omega_0 - E_g)m_v}{(m_c + m_v)kT} - (\phi_c - E_G)/KT\right]\right)^{-1} \tag{4.6}$$

and

$$f_v = \left(1 + exp\left[\frac{-(\hbar\omega_0 - E_g)m_c}{(m_c + m_v)kT} - \phi_v/KT\right]\right)^{-1} \tag{4.7}$$

Here ϕ_c and ϕ_v are conduction and valence band Quasi-Fermi levels, respectively. K is Boltzmann constant and T is the temperature. All the energies are measured from the top of the valence band, and the Quasi-Fermi levels evaluated using the charge neutrality condition.

Combining the equation for the joint density of states, with the expression for the probability of transition, gives the following equation for the carrier density per unit energy,

$$dN = \frac{1}{2\pi^2}\left(\frac{2m_r^*}{\hbar^2}\right)^{3/2}(E_{21} - E_g)^{1/2}[f_v(E_{21}) - f_c(E_{21})]dE_{21} \tag{4.8}$$

Quasi-Fermi Levels in active media

Taking the top of the valence band as the reference point, (E=0), and assuming that the valence and conduction bands are parabolic, then, the energy of a carrier in the conduction band, $E_c(k)$, is given by the equation,

$$E_c(k) = \frac{\hbar^2 k^2}{2m_c} + E_g \tag{4.9}$$

and for a carrier in the valence band, $E_v(k)$, by,

$$E_v(k) = -\frac{\hbar^2 k^2}{2m_v} \tag{4.10}$$

where k denotes the momentum. The quasi equilibrium in each band is described by separate Fermi-Dirac distributions,

$$\rho(k,\phi_c) = \frac{1}{1+exp([E_c(k)-\phi_c]/KT)} \tag{4.11}$$

and

$$\rho(k,\phi_v) = \frac{1}{1+exp([E_v(k)-\phi_v]/KT)} \tag{4.12}$$

The quasi-Fermi levels, $\phi_c \& \phi_v$, can be found from the integral equations for the number of free carriers in each band. The free carrier density in the conduction band, (electrons), is given by,

$$N_e = 1/\pi^2 \int_0^\infty \rho(k,\phi_c) k^2 \, dk \tag{4.13}$$

and the free carrier density in the valence band, (holes) is given by,

$$N_h = 1/\pi^2 \int_0^\infty [1-\rho(k,\phi_v)] k^2 \, dk \tag{4.14}$$

Substituting eqn(4.9) and eqn(4.11) into eqn(4.13) gives,

$$N_e = \frac{1}{2\pi^2}\left(\frac{2m_c}{\hbar^2}\right)^{3/2} \int_0^\infty \frac{\sqrt{E}\, dE}{1+exp[(E-\phi_c)/kT]} \tag{4.15}$$

Substituting eqn(4.10) and eqn(4.12) into eqn(4.14) and defining $E_v = -\tilde{E}$ gives,

$$N_h = \frac{1}{2\pi^2}\left(\frac{2m_v}{\hbar^2}\right)^{3/2} \int_0^\infty \frac{\sqrt{\tilde{E}}\, d\tilde{E}}{1+exp[(\tilde{E}-E_{fv})/kT]} \tag{4.16}$$

where $E_{fv} = -\phi_v$.

The equations for the number of carriers, in either band, are now written in a form amenable to solution by Joyce and Dixon approximation, [16]. Applying the Joyce and Dixon approximation to eqn(4.16) gives E_{fv} from which ϕ_v is easily obtained,

$$\int_0^\infty k^2[\rho_c(k,\phi_c) + \rho_v(k,\phi_v) - 1] \, dk = 0 \tag{4.17}$$

The neutrality condition can now be used to obtain improved estimates of the two quasi-Fermi levels by solving the above equation iteratively, using the quasi-Fermi levels calculated from Joyce and Dixon approximation as initial values [16]. For high carrier concentration Unger's approximation can be used, [17].

4.4 Nonlinear index.

The nonlinear index is related to the susceptibility by, [18],

$$n_2(\omega) = \frac{3Re[\chi^{(3)}(\omega)]}{4\epsilon_0 c n_0^2} \tag{4.18}$$

where c is velocity of light in vacuum and n_0 is the linear refractive index of the material.

The nonlinear index of an active semiconductor can be obtained from eqn(4.18) if N is replaced by eqn(4.8) and the resultant expression is integrated from E_g to infinity, hence the nonlinear index in an active medium is given by,

$$n_2(\omega) = \frac{3}{32\epsilon_0^2 n_0^2 c}\left(\frac{e \mid p_{12} \mid}{m_0\omega}\right)^4 \frac{1}{2\pi^2}\left(\frac{2m_r^*}{\hbar^2}\right)^{3/2} \frac{4(\Gamma_2+\gamma)}{2\gamma+\Gamma_1} I(\omega) \tag{4.19}$$

where

$$I(\omega) = \int_{E_g}^{\infty} \frac{(E_{21}-E_g)^{1/2}(\hbar\omega - E_{21})}{(\hbar\omega - E_{21})^2 + \hbar^2(3\gamma+\Gamma_2)^2} \frac{[f_c(E_{21}) - f_v(E_{21})]}{(\hbar\omega - E_{21})^2 + \hbar^2(\gamma+\Gamma_2)^2}\, dE_{21} \tag{4.20}$$

The expression derived above is capable of describing the fast component of the observed nonlinear index in semiconductor optical amplifiers. The nonlinear index has been modelled using one-electron mechanisms, appropriate to a two-level one-electron system. Eqn(4.19) includes the steady state and transient

band-filling effects and the Optical Stark effect. The relative magnitudes of the dephasing time, recombination time and pulse risetime, determines which of the mechanisms provide the dominant contribution to the nonlinear index.

- Steady State Band-filling dominates when $\gamma \ll \Gamma_1 \ll \Gamma_2$
- Transient State Band-filling dominates when $\Gamma_1 \ll \gamma \ll \Gamma_2$
- Optical Stark effect dominates when $\gamma \gg \Gamma_1 \gg \Gamma_2$

The slower components, that have also been observed, are thought to be caused by carrier heating effects, and have been previously modelled, [19].

The risetime of the pulse determines which mechanism provides the dominant contribution to n_2, and for present purposes the perturbing pulse will be taken to be Gaussian. The risetime is defined here as the time that elapses as the intensity increases from 10% to 90% of its peak value,

$$1/\gamma = ln(9)\frac{T_0}{2} \sim T_0 \tag{4.21}$$

Thus the risetime is approximately equal to the pulsewidth, T_0.

The spectrum of the nonlinear index has been evaluated using material parameters appropriate to the AlGaAs system and pulse risetimes short enough to allow a comparison to be made with experimental results, [1, 3]. The nonlinear index spectra, calculated assuming risetimes of 150fs and 500fs, for various carrier concentrations are shown in figures(4.1, 4.2). The other values used were, $1/\Gamma_2 = 500fs$, $1/\Gamma_1 = 1ns$, $m_c = 0.08m_0$, $m_v = 0.5m_0$, and $E_g = 1.5eV$. The Kane approximation has been used to calculate the momentum matrix element,

$| p_{21} |^2 = (mE_p/2)$. The parameter E_p is essentially material independent and has a value of $\sim 21eV$, for most direct band-gap semiconductors.

From figures(4.1, 4.2) it is clear that as the carrier concentration increases, so the initial sharp negative spike, seen at low injection currents, reduces in magnitude, until finally, when population inversion has been achieved, it changes sign. The increase of carriers in the conduction band destroys the resonant enhancement that occurs in the passive limits.

At transition energies further away from the band-edge the nonlinear index is always negative, with a secondary minimum that shifts to higher energies as the carrier concentration increases. Also, the recovery time of the initial negative spike is faster and its magnitude is greater for longer pulses, while the converse is true for the other minimum, it's magnitude decreases with increased pulse risetime and it's recovery time is slower for longer pulses.

The spectral profiles shown in figure(4.2), are in good agreement with those calculated by Sheik-Bahae, [7]. There is however one important difference. The passive limit in figure(4.2), has a peak magnitude which is greater than the minimum seen in the high carrier concentration spectra. This is in direct contrast to the situation in [7]. The magnitude of the nonlinear index is also slightly greater than that of [7]. The differences between the results may possibly be attributed to the inclusion of more mechanisms, (two-photon absorption, electronic Raman), in the Sheik-Bahae model. However, it is pointed out that Sheik-Bahae's results are obtained using a nonlinear Kramers-Kronig transform, whose validity has recently been questioned. The Sheik-Bahae results should therefore be viewed with some caution.

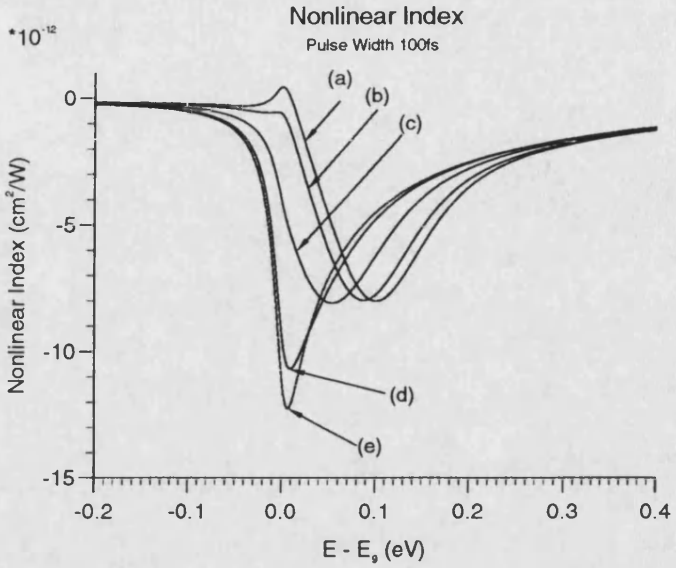

Figure 4.1: Spectrum of the nonlinear index for a 100fs pulse assuming carrier concentrations of (a) $2.5 \times 10^{18}\ cm^{-3}$ (b) $2.0 \times 10^{18}\ cm^{-3}$ (c) $1.0 \times 10^{18}\ cm^{-3}$ (d) $2.0 \times 10^{17}\ cm^{-3}$ (e) Passive Limit

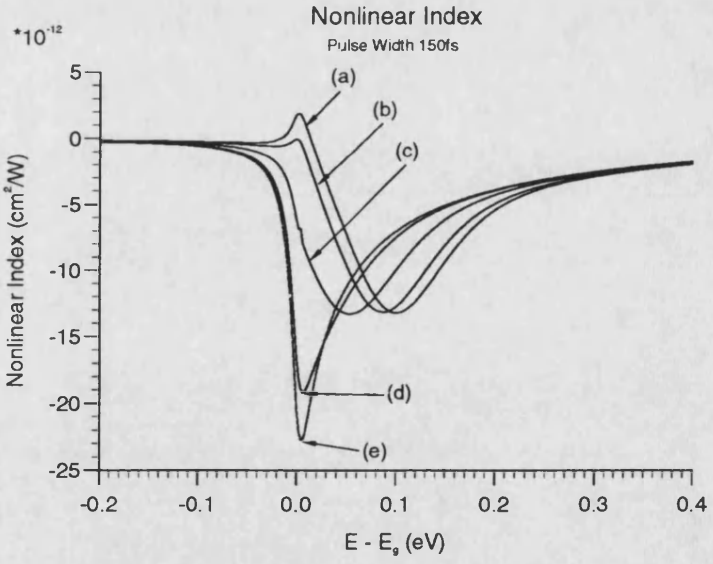

Figure 4.2: Spectrum of the nonlinear index for a 150fs pulse assuming carrier concentrations of (a) $2.5 \times 10^{18}\ cm^{-3}$ (b) $2.0 \times 10^{18}\ cm^{-3}$ (c) $1.0 \times 10^{18}\ cm^{-3}$ (d) $2.0 \times 10^{17}\ cm^{-3}$ (e) Passive Limit

A similar approach to the one outlined above has previously been used to calculate the change in the linear index, [9], but this model only considered saturation effects induced by a CW beam. The expression derived used a detailed model for the saturation that allowed for the possibility of carrier relaxations within the conduction band. The results obtained in [9] agree with experimental results, and support the validity of the theoretical model derived in this Chapter.

The theoretical model used in this thesis predicts a value for the nonlinear index that is in good agreement with that experimentally measured, by various groups, in optical amplifiers, [1-8]. The ultra-short risetimes assumed in generating figures(4.1, 4.2) ensure that the dominant contribution to the nonlinear index comes from the virtual process, the Optical Stark effect.

4.4.1 Passive Limit

The risetime of the pulse dictates which mechanism provides the dominant contribution to the nonlinear index, and consequently has a profound effect on the nonlinear index. The relationship between the risetime and n_2 is most easily highlighted if the passive limit is considered.

It is clear from figure(4.3), that as the risetime becomes slower, so the index drastically increases. As seen from eqn(4.19) this occurs because additional resonant enhancement is provided in the Transient and Steady State band-filling regimes. This enhancement is proportional to $2\Gamma_2/\gamma$ and $2\Gamma_2/\Gamma_1$, respectively. These terms emanate from the fact that both band-filling effects are caused by real transitions, and thus excited carriers, which must eventually relax back to

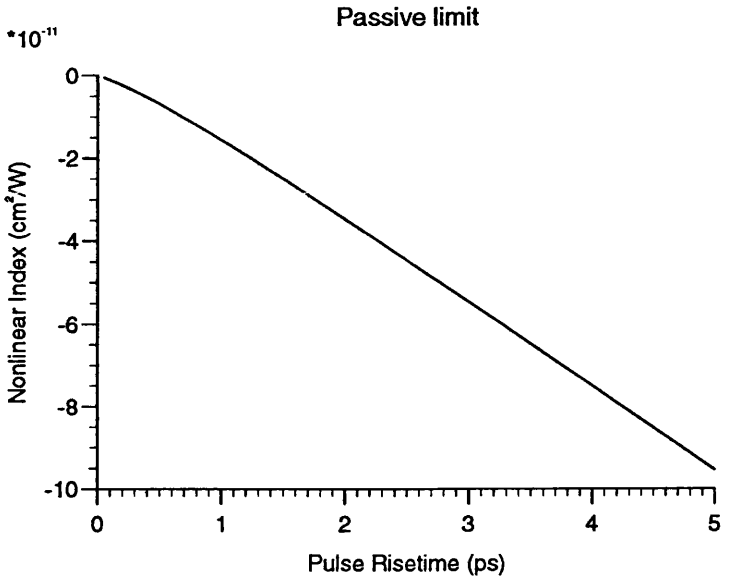

Figure 4.3: Variation of the magnitude of the negative spike, observed in the passive limit, with pulse risetime.

their unperturbed states, have been produced. The terms $2\Gamma_2/\gamma$ and $2\Gamma_2/\Gamma_1$ also give a measure of the extent to which the effects induced by the perturbation, (ie. the pulse), persist after their cause, (the optical pulse in this case), has been removed. When the incident pulse is short enough to induce virtual transitions, the excitation response of a virtual process is essentially instantaneous and simply follows the rise and fall of the intensity profile of the pulse. The perturbation only lasts while the pulse is present, ie. there is no persistent effect, and so $2\Gamma_2/\gamma \rightarrow 1$.

Although the real processes induce far larger nonlinearities, the fact that some carriers have been moved means that these nonlinearities have much longer recovery times. The above discussion implicitly assumes that virtual processes are just as effective as real processes at producing a change in the refractive index. The validity of this assumption has recently been confirmed theoretically, [20].

The ultra-short pulses used by several groups, [1-6], to investigate the gain dynamics of optical amplifiers, are so short that the Optical Stark effect should provide the dominant contribution to the ultra fast transient component of the nonlinear index. The good agreement between the experimentally measured value, and that predicted theoretically from the above model, would seem to indicate the Optical Stark effect is indeed the mechanism that is inducing the observed nonlinearity.

4.5 Nonlinear Absorption.

The procedure of incorporating a description of the carrier distribution into the equation for a passive medium, can also be used to calculate the nonlinear absorption of an active medium. An expression for the imaginary part of the third order susceptibility can be obtained if eqn(4.8) is substituted into eqn(4.2) and the subsequent expression integrated from E_g to infinity. If use is then made of the following expression, relating the susceptibility to the nonlinear absorption,

$$\alpha_{NL}(\omega) = \frac{2\omega}{\epsilon c n_0^2} Im[\chi^{(3)}(\omega)] \tag{4.22}$$

it can be seen that,

$$\alpha_{NL}(\omega) = \frac{1}{4\,\epsilon_0^2\, n_0^2\, c^2\, \omega^3} \left(\frac{e \mid p_{12} \mid}{m_r^*}\right)^4 \frac{1}{2\pi^2} \left(\frac{2m_r^*}{\hbar^2}\right)^{3/2} \frac{4(\Gamma_2+\gamma)}{2\gamma+\Gamma_1} J(\omega) \tag{4.23}$$

where

$$J(\omega) = \int_{E_g}^{\infty} \frac{-(3\gamma+\Gamma_2)(E_{21}-E_g)^{1/2}}{(\hbar\omega-E_{21})^2+\hbar^2(3\gamma+\Gamma_2)^2} \frac{[f_v(E_{21})-f_c(E_{21})]}{(\hbar\omega-E_{21})^2+\hbar^2(\gamma+\Gamma_2)^2}\, dE_{21} \tag{4.24}$$

The same parameter values as those used to calculate the nonlinear index, have been used to calculate the nonlinear absorption, at various carrier concentrations,

for a pulse risetimes of 100fs. The spectrum, with carrier concentrations of 2.5, 2.0, 1.5, 1.0, 0.5, 0.2 $\times$ $10^{18}cm^{-3}$, and the passive limit, is shown in figure(4.4). When sufficient carriers are present to induce a population inversion, it can be seen that the nonlinear absorption changes sign, over a small range of frequencies just above the band-edge. Further away from the band-edge the nonlinear absorption is always negative, with a minimum which moves away from the band-gap as the carrier concentration increases.

As in the case of the nonlinear index, the nonlinear absorption also increases as the pulsewidth increases, and again if the passive limit is considered, a large increase in the nonlinear absorption is observed as the dominant mechanism responsible changes from the Optical Stark effect to the transient band-filling effect, figure(4.5). Additional resonant enhancement is caused by terms other than the Lorentzian in eqn(4.22).

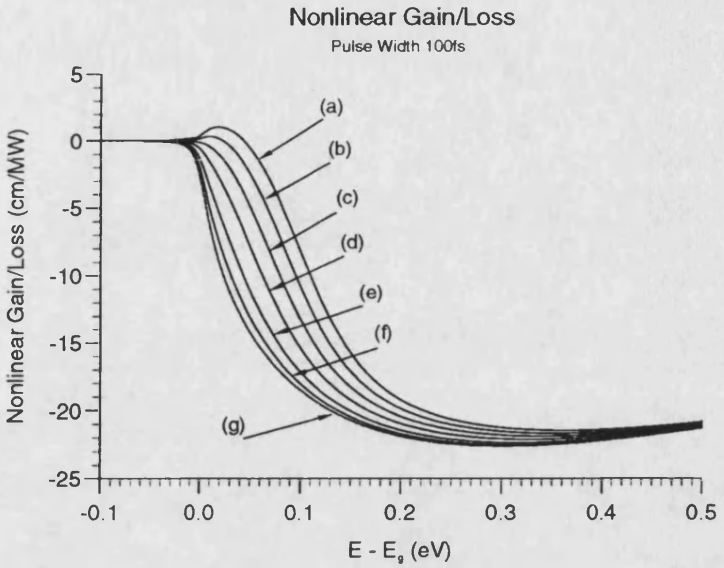

Figure 4.4: Spectrum of the nonlinear absorption for a 100fs pulse assuming carrier concentrations of (a) $2.5\times10^{18}\ cm^{-3}$ (b) $2.0\times10^{18}\ cm^{-3}$ (c) $1.5\times10^{18}\ cm^{-3}$ (d) $1.0\times10^{18}\ cm^{-3}$(e) $2.0\times10^{17}\ cm^{-3}$ (f) $2.0\times10^{16}\ cm^{-3}$(g) Passive Limit

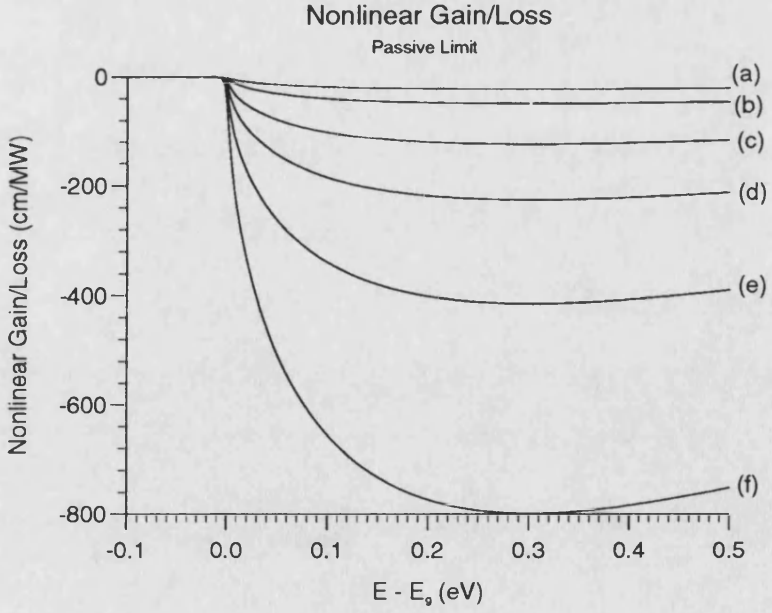

Figure 4.5: The passive limit nonlinear absorption spectra for risetimes of: (a) 100fs, (b) 150fs, (c) 250fs, (d) 350fs (e) 500fs, and (f) 750fs.

4.5.1 Kramers-Kronig relationship

The Kramer-Kronig relationship in the nonlinear case is given by,

$$n_2(\Omega,\xi) = \frac{c}{\pi}\int_0^\infty \frac{\alpha_{NL}(\omega,\xi)}{\omega^2-\Omega^2}\,d\omega \tag{4.25}$$

Here ξ is a parameter (or parameters) denoting the cause of the change in the absorption.

At first sight it would seem possible to use the results obtained from eqn(4.23) in the Kramer-Kronig relationship, to obtain the nonlinear index. However, for this approach to be valid, the perturbation causing the nonlinear effect must remain constant over the frequency integral in eqn(4.25), [21]. This condition is not satisfied by eqn(4.23). The nonlinear Kramers-Kronig relation only applies to situations of the pump-probe type. The pump induces some nonlinear effect, which the probe samples. The probe does not itself perturb the medium. Thus the imaginary part of the complex third-order susceptibility, used in obtaining eqn(4.23), cannot subsequently be used to obtain the nonlinear index by invoking the Kramers-Kronig relationship.

To use the Kramers-Kronig relationship the nonlinear absorption must be written in such a way, that the Kramer-Kronig integration is performed on a system, that consists of the material plus a pump optical field. This new system is then constant over the Kramers-Kronig integration. In reference(8), the nondegenerate absorption at frequency ω_s, when a pump field at frequency Ω_p is applied, is used to calculate the degenerate nonlinear index, ie, $n_2(\omega_s,\Omega_p)$ when $\omega_s = \Omega_p$.

4.5.2 Summary

The results obtained for the fast component of the nonlinear index agree well with experimentally measured values. The dominant mechanism identified was the virtual process the Optical Stark effect.

The expression derived for the nonlinear absorption cannot be used to obtain the nonlinear index, because it invalidates the nonlinear Kramers-Kronig relation. The perturbation which causes the nonlinearity most remain constant over the Kramers-Kronig integral if this approach is to be used.

4.6 Comparison of the Nonlinearities of Active and Passive Semiconductors

4.6.1 Introduction

The nonlinear refraction induced in semiconductor optical amplifiers and in passive quantum wells, by intersubband transitions, have both been studied with a view to being used in phase interference type all-optical switches.

Unfortunately both mechanisms have their advantages and disadvantages and the following sub-sections discuss these and highlight possible future applications.

4.6.2 Passive Quantum Well Devices

Very large values for the nonlinear refractive index of intersubband transitions have been reported, [22], and several schemes for enhancing the nonlinear index even further have been suggested.

Several authors have proposed methods that basically use the Quantum Confined Stark Effect, (QCSE). A voltage is applied across the quantum wells to distort the well potential. This results in a red-shift of the absorption edge, which has a doubly beneficial effect; it both reduces the absorption and, (because of the Kramer-Kronig relation between the index and absorption), induces an enhancement of the index. A number of methods have been proposed to maximize the QCSE by: introducing several steps into the potential, [23, 24]; coupling wells; [26]; or using a graded-gap, [25]. Unfortunately all these approaches suffer from very high absorption, and are limited in response to the intersubband relaxation time, ($\sim$ 1ps).

Another method has been proposed that overcomes the inherent high loss and response limitation of the above approach, [27]. Khurgin predicted that a fast large nonlinear index could be obtained from intersubband two-photon absorption. The disadvantage of this approach is that the wavelength of the optical field is from the telecommunications viewpoint in a less interesting region of the far infra-red. Recently Khurgin has proposed a way of overcoming this problem, [28], by suggesting that two-photon absorption between confined states and continuum states, can occur in appropriately engineered structures.

The wavelength ranges of all the techniques mentioned above are all well away from the 0.8-1.55 micron range that today's optical telecommunication devices use. However, future optical telecommunication systems have been proposed that work at longer wavelength, and thus these effects could possibly be used in such systems.

4.6.3 Semiconductor Optical Amplifiers

The nonlinear index observed in semiconductor optical amplifiers has been found to be large and made up of several components, one of which was found to respond instantaneously. These devices do not suffer from the problem of large inherent absorption, in fact they can be operated such that the optical signal is amplified and these devices also operate in the important 0.8-1.55 micron wavelength range. However, it may prove difficult to isolate the effects of the slower components, thus limiting the speed of the device.

Ideally if these devices are to be used as all-optical switches they would need to be operated in the transparency regime, since then the long-lived component due to net change carrier in the population, would be eliminated.

4.7 Summary

In the next Chapter the effects induced on the temporal and spectral properties of a pulse, by a nonlinear refraction, are investigated. The emphasis of the thesis changes from mechanisms that induce a nonlinear refraction, (as outlined in Chapters[2-4]), to the effects that the nonlinear refraction itself induces.

References

[1] M.J.LaGasse *et al*, Appl. Phys. Lett, 56, 417, (1990)

[2] R.S.Grant and W.Sibbett, Appl. Phys. Lett., 58, 1119, (1991).

[3] C.T.Hultgren and E.P.Ippen, Appl. Phys. Lett., 59, 635, (1991).

[4] C.T.Hultgren, D.J.Dougherty, and E.P.Ippen, Appl. Phys. Lett., 61, 2767, (1992).

[5] K.L.Hall *et al*, Appl. Phys. Lett., 62, 1320, (1992).

[6] M.A.Fisher *et al*, Electron. Lett., 29, 1185, (1993).

[7] M.Sheik-Bahae, E.W.Van Stryland, QELS'92, QThD19, (1992).

[8] M Sheik-Bahae *et al*, IEEE J. Quant. Elect., QE-27, 1296, (1991).

[9] F.de Rougemont and R.Frey, Phys. Rev. B, 37, 1237, (1988).

[10] W.W.Chow, G.C.Dente, and D.Depatie, Optics Lett., 12, 25, (1987).

[11] W.W.Chow, G.C.Dente, and D.Depatie, IEEE J. Quant. Electron., QE-23, 1314,(1987).

[12] J.Mark and J.Mork, Appl. Phys. Lett., 61, 2281, (1992).

[13] K.Vahala, *et al*, Appl. Phys. Lett., 42, 631, (1983).

[14] A.Yariv, "*Quantum Electronics 3rd Ed.*", (Wiley: New York), (1989).

[15] M.G.Burt, Semicond. Sci. Technol., 5, 1215, (1990).

[16] W.B.Joyce and R.W.Dixon, Appl. Phys. Lett, 31, 354,(1977).

[17] K.Unger, Z.Phys, 207, 322,(1967).

[18] P.N.Butcher and D.Cotter, "*The Elements of Nonlinear Optics*", (Cambridge Uni. Press: Cambridge), (1990).

[19] S.Y.Auyang and P.A.Wolff, J. Opt. Soc. Am. B, 6, 595, (1989).

[20] M.G.Burt, Semicond. Sci. Technol., 8, 1393, (1993).

[21] D.C.Hutchings, M.Sheik-Bahae, D.J.Hagan, and E.W.Van Stryland, Opt. and Quant. Electron., 24, 1,(1992).

[22] M.Segev *et al*, Appl. Phys. Lett., 61, 2403, (1992).

[23] Y.J.Mii *et al*, Appl. Phys. Lett., 56, 1986, (1990).

[24] N.Susa and T.Nakahara, Appl. Phys. Lett., 60, 2457, (1992).

[25] T.Hiroshima and K.Nishi, J. Appl. Phys., 62, 3360, (1987).

[26] M.N.Islam *et al*, Appl. Phys. Lett., 50, 1098, (1987).

[27] J.B.Khurgin and S.Li, Appl. Phys. Lett., 62, 126, (1993).

[28] S.Li and J.B.Khurgin, J. Appl. Phys., 73, 4367, (1993).

Chapter 5

Pulse Propagation in Semiconductors

5.1 Introduction

For many important applications, eg, communication systems, material analysis, the processing of short optical pulses is of great interest. Such optical pulses are composed of a spread of frequencies, or equivalently, wavelengths, about some central, or carrier frequency, ω_0. It is this spread of frequencies that leads to many of the pulse propagation effects observed in dispersive nonlinear materials, such as semiconductors.

A dispersive medium is one whose refractive index is frequency dependent. When a pulse propagates in a dispersive nonlinear medium its temporal and spectral properties are distorted. Due to the material dispersion each spectral component of the pulse propagates at a different speed. This can lead to either pulse narrowing or broadening. Using short pulses high peak optical powers can

be achieved, and so the nonlinear response of the medium needs to be taken into account. In this case the different frequency components of the pulse may interact with one another. One spectral component at one frequency may change its own phase velocity or that of an another spectral component at a different frequency. Due to the nonlinearity the pulse cannot be viewed as a simple superposition of waves of different frequencies. Nonlinearities can cause harmonic generation, ie. a new electromagnetic field oscillating at frequency that is a multiple of the perturbing fields may be generated, if certain phase criteria are satisfied. However, in this thesis harmonic generation is not considered.

The theoretical approaches that have been developed to study pulse propagation, fall into two main categories: Time Domain and Frequency Domain analysis. Sub-picosecond pulses are more easily tackled in the frequency domain, while longer pulses can usually be studied in the time domain.

The phenomena that can cause distortion during pulse propagation in a dispersive nonlinear media are discussed in the next section. The theoretical techniques that have been developed to study pulse propagation are outlined in section[5.3].

5.2 Pulse Effects in Dispersive Nonlinear Media

5.2.1 Introduction

When a pulse propagates in a dispersive medium the frequency dependence of the refractive index induces a phase modulation, which in turn induces an instantaneous variation of the frequency, or chirp, across the pulse. Dispersion not only causes, different frequencies to propagate at different velocities, but also pulses at different carrier frequencies to propagate at different velocities.

The nonlinear effects that are considered in this, and the subsequent Chapters, are assumed to arise due either to an instantaneous Kerr-type nonlinearity and/or by saturation effects. These nonlinear effects also induce chirp, and distort the spectral and temporal profiles of the pulse.

The changes induced in the spectral and temporal properties of a pulse, by dispersive and nonlinear effects are discussed in the next sub-sections. Firstly the two effects are considered separately. The effects induced when both are present are addressed in the sub-section(5.2.4).

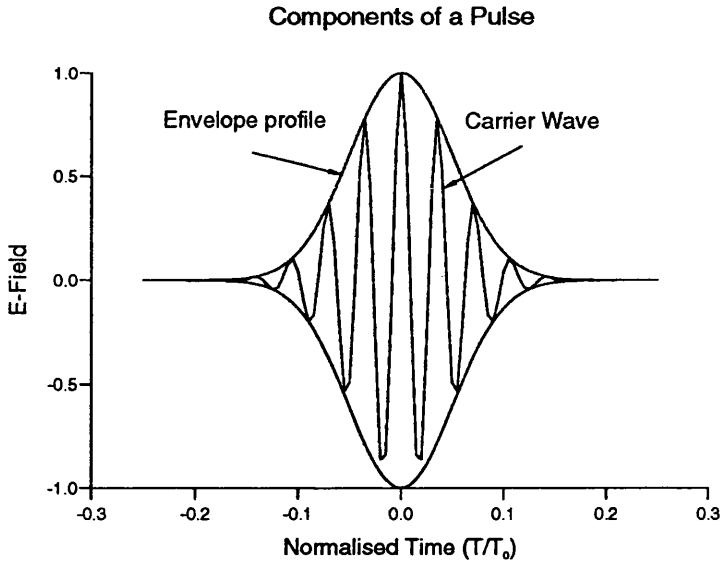

Figure 5.1: A schematic of the slowly varying envelope function and the high frequency carrier wave of a pulse

5.2.2 Chromatic Dispersion

Group Velocity and Phase Velocity

A pulse may be represented by two elements, a slowly varying envelope and a rapidly varying carrier, figure(5.1). It is the speed of the envelope rather than that of the carrier wave which is of primary interest. The pulse envelope propagates at the group velocity, v_g, while the individual cycles within the pulse move forward at the phase velocity, v_p. The energy of the pulse generally moves at the group velocity, and thus the group velocity also represents the speed at which information can be transmitted.

In order to see the difference between v_g and v_p more clearly consider a modulated signal that consists of two amplitude tones at frequencies $\omega_0 \pm \Delta\omega$, these

can be represented at z=0 as,

$$\begin{aligned} f(t) &= Re[e^{\imath(\omega_0+\Delta\omega)t} + e^{\imath(\omega_0-\Delta\omega)t}] \\ &= 2cos(\omega_0 t)cos(\Delta\omega t) \end{aligned} \tag{5.1}$$

Eqn(5.1) shows that the signal consists of a carrier at frequency ω_0 modulated by a slowly varying envelope with frequency, $\Delta\omega$. Now if the signal is assumed to propagate in the z direction with an associated propagation constant $\beta(\omega)$, then by superposition, the signal at some distance z is,

$$f(t,z) = Re[e^{\imath(\omega_0+\Delta\omega)t}e^{-\imath\beta(\omega_0+\Delta\omega)z} + e^{\imath(\omega_0-\Delta\omega)t}e^{-\imath\beta(\omega_0-\Delta\omega)z}] \tag{5.2}$$

Assuming that $\Delta\omega \ll \omega_0$, then $\beta(\omega_0 + \Delta\omega)$ can be approximated by a Taylor series expansion,

$$\beta(\omega_0 \pm \Delta\omega) \cong \beta(\omega_0) \pm \Delta\omega\beta^{(1)}(\omega_0) \pm \frac{\Delta\omega^2}{2}\beta^{(2)}(\omega_0) + ... \tag{5.3}$$

where,

$$\beta^{(m)}(\omega_0) = \left[\frac{d^m\beta(\omega)}{d\omega^m}\right]_{\omega=\omega_0} \tag{5.4}$$

If only the first two terms of the expansion are considered, then by substituting eqn(5.3) into eqn(5.2) it is found that,

$$f(t,z) = 2cos[\omega_0(t-\tau_p)]cos[\Delta\omega(t-\tau_g)] \tag{5.5}$$

where

$$\begin{aligned} \tau_p &= \frac{\beta(\omega_0)}{\omega_0}z \\ \tau_g &= \beta^{(1)}(\omega_0)\,z \end{aligned} \tag{5.6}$$

τ_p and τ_g are the phase and group delays, respectively, and are related to phase and group velocities by,

$$\begin{aligned} v_p &= \frac{z}{\tau_p} = \frac{\omega_0}{\beta(\omega_0)} \\ v_g &= \frac{z}{\tau_g} = \frac{d\omega}{d\beta(\omega)} \end{aligned} \tag{5.7}$$

It can be seen from eqn(5.5) that the phase velocity, v_p represents the speed at which the carrier travels in the medium and that the group velocity, v_g, represents the speed at which the envelope travels in the medium.

Group Velocity Dispersion

Higher order terms from the Taylor expansion give rise to higher order dispersion effects. The first of these is Group Velocity Dispersion, (GVD).

$$\beta^{(2)}(\omega_0) = \left[\frac{d\beta^{(1)}}{d\omega}\right]_{\omega=\omega_0} \tag{5.8}$$

The sign of this term is important as it indicates whether the pulse experiences normal, $\beta^{(2)} > 0$, or anomalous, $\beta^{(2)} < 0$ dispersion. In the normal-dispersion regime, the higher frequency components of the pulse travel slower than the lower frequency components, while the converse is true in the anomalous-dispersion regime.

The presence of GVD also induces a time-dependent phase. This implies that the instantaneous frequency across the pulse differs from the central frequency ω_0. This effect is known as chirp, and it can induce considerable changes in the phase of a pulse, as can be seen by considering a Gaussian pulse,

$$f(z,t) = Re[e^{-(t/t_0)^2} e^{-\imath(\omega_0 t + \phi(z,t))}] \tag{5.9}$$

where $\phi(z,t)$ is the time dependent phase induced by the GVD, which can be shown, [1], to be equal to,

$$\phi(z,t) = -\frac{\beta^{(2)}(z/L_D)}{1+(z/L_D)^2}\frac{t^2}{t_0^2} + tan^{-1}(z/L_D) \tag{5.10}$$

where $L_D = t_0^2/ \mid \beta^{(2)} \mid$. The induced chirp $\delta\omega$, is given by,

$$\delta\omega = -\frac{\partial\phi}{\partial t} = \frac{2\beta^{(2)}(z/L_D)}{1+(z/L_D)^2}\frac{t}{t_0^2} \tag{5.11}$$

Equation(5.11) shows that the frequency changes linearly across the pulse. This is referred to as linear frequency chirp, and it can be seen that the GVD determines the sign of the chirp. Eqn(5.11) also indicates that an initially unchirped pulse is temporally broadened in both of the dispersive regions. However, it can be shown, [1], that for an initially chirped pulse the sign of the GVD determines whether the pulse is broadened, ($\beta^{(2)} > 0$), or compressed, ($\beta^{(2)} < 0$). The temporal distortion increases the further the pulse propagates.

Walk-Off

Another important effect of dispersion is that pulses at different wavelengths propagate at different speeds, because of group velocity mismatch. This feature leads to a walk-off effect. If two pulses are initially coincident then as they propagate through a dispersive medium the faster pulse moves through the slower pulse, and at some point they will cease to be temporally overlapped. If the faster pulse is initially time delayed behind the slower pulse, then as they propagate the faster pulse will start to approach the slower pulse. This effect has important consequences if the medium is also nonlinear, because the strength of the interaction between the pulses will vary depending on the amount of temporal overlap.

Summary

A pulse propagates in a dispersive medium at the group velocity, and the frequency dependence of the refractive index results in pulses of different wavelengths travelling at different spends. Higher-order dispersion terms cause the pulse to become chirped, and either temporally broaden or narrow the pulse, depending on whether the initial chirped pulse is in the normal or anomalous dispersion region.

5.2.3 Nonlinear Effects

Self and Cross Phase Modulation

Two types of nonlinearity will be considered in this section, the first, a Kerr-type intensity dependent refractive index which induces such effects as Self Phase modulation, (SPM), and Cross Phase Modulation, (XPM). The second, gain saturation, as well as inducing phase modulation, also has a direct effect on the temporal profile of the pulse.

Instantaneous nonlinear refractive index effects have been observed in both active and passive semiconductors, and two example have been previously outlined in this thesis. Chapter[2] looked at intersubband induced nonlinearities, and Chapter[4] looked at nonlinearities induced in semiconductor optical amplifiers. The nonlinear refractive index causes a phase change that is proportional to the intensity profile of the perturbing pulse, and the maximum effect occurs at the pulse peak intensity. The phase is thus time dependent, and hence the pulse

becomes chirped. The chirp increases in magnitude as the pulse propagates, and the pulse is spectrally broadened by these changes in the phase. In short, SPM results in new frequency components being continuously generated as the pulse moves through the medium, thus causing spectral broadening.

If two pulses overlap in time in a nonlinear medium, then as well as experiencing SPM, the pulses will also be affected by Cross Phase modulation, (XPM). The phase of each pulse is changed by an amount which is dependent on the intensity profile of the other pulse. In this case the maximum phase may not necessarily occur at the pulse peak intensity. The relative magnitudes of the pulses determines whether XPM or SPM dominates. In a pump-probe situation the high intensity of the pump ensures that the phase of the pump pulse is dominated by its own SPM term, but the SPM of the probe is dominated by the XPM term induced by the pump.

The chirp induced by SPM or XPM shifts the instantaneous frequency at the leading edge of the pulse in an opposite direction to that at the trailing edge. In other words if the phase modulation induces a red-shift (negative chirp) at the front of the pulse then a blue-shift (positive chirp) will be induced at the back. The magnitude of the chirp is dependent on the derivative of the intensity profile, and so the steeper the pulse edges, the larger the chirp. In general a linear chirp is not induced, i.e the chirp is not linearly dependent on the time.

Linewidth Enhancement Factor

In active devices another mechanism can induce a nonlinear refractive index change. Large net changes in the carrier population can occur when an optical signal passes through a semiconductor optical amplifier. Stimulated emission adds photons to the optical field and reduces the number density of electrons in the conduction band. These carrier number changes cause an alteration in the material refractive index.

Due to saturation effects the gain experienced by an intense optical pulse varies as the pulse is being amplified. The leading edge of the pulse sees the full gain, while trailing parts of the pulse may see a much reduced value. The amplification process results in a decrease in the conduction band carrier density. The magnitude of this carrier density reduction is proportional to the intensity of the pulse, and since gain is also proportional to the carrier density, the magnitude of the gain reduces as the pulse is being amplified. Gain recovery will occur if the pulsewidth is longer than the carrier recombination time of the semiconductor.

The induced carrier density changes have been linked to refractive index variations through the Linewidth Enhancement Factor, (LEF), or alpha parameter, α, which is defined as, [2],

$$\alpha = -\frac{d[Re(\chi(n))]/dn}{d[Im(\chi(n))]/dn} \tag{5.12}$$

The α parameter describes the coupling between the carrier-induced variation of the real and imaginary parts of the permittivity. In all practical cases both the carrier induced contribution to the index and imaginary part of the susceptibility are much smaller than the background refractive index, thus eqn(5.12) may be

rewritten as,

$$\alpha = -2k\frac{d\eta/dn}{dg/dn} \tag{5.13}$$

where k is the wavenumber, η is the refractive index, g is the gain per unit length, n is the carrier density and the following relationship has been assumed $\epsilon = (1 + \chi^{(1)}) = (\eta + \imath gc/2\omega)^2$. For small changes in the carrier concentration it is possible to replace the derivatives, such that eqn(5.13), [3], may be written as,

$$\alpha = -2k\frac{\Delta\eta(t)}{\Delta g(t)} \tag{5.14}$$

From the above expression it is clear that a change in the gain, Δg, results in a change in the index, given by,

$$\Delta\eta(t) = -\frac{\alpha\Delta g(t)}{2k} \tag{5.15}$$

The index change expressed above gives rise to phase modulation and spectral broadening. The saturation effects that induce the chirp, also cause temporal distortion, because the magnitude of the gain experienced by the pulse is not constant in time.

The magnitude of the chirp is influenced by the LEF, and much work has been undertaken to investigate the factors which determine the magnitude of the LEF and its limitations. Recently Agrawal and Bowden, [4], have investigated the validity of the Linewidth Enhancement Factor concept, and have suggested that the LEF is not valid for sub-picosecond pulses, because α varies considerably over the pulse duration.

The power spectrum of a pulse, $S(\omega)$, is obtained as the modulus squared of the Fourier Transform of the time domain description of the pulse.

$$S(\omega) = \left| \int_{-\infty}^{\infty} U(z,t) exp[\ \imath(\phi(z,t) + (\omega - \omega_0)t)\ ]\ dt \right|^2 \tag{5.16}$$

U(z,t) is the envelope function of the pulse, $\phi(z,t)$ is the phase, and ω_0 is the carrier frequency. In general the spectrum depends not only on the pulse shape but also on the initial chirp imposed on the pulse. If the pulse is assumed to be a linearly chirped Gaussian, then

$$U(0,t) = exp\left(-\frac{(1+\imath C)}{2}\frac{t^2}{t_0^2}\right) \tag{5.17}$$

where C is the chirp parameter. If $C > 0$ then the pulse is said to be positively chirped, and the instantaneous frequency increases from the leading edge to the trailing edge, and the opposite is true for negatively chirped pulses, $(C < 0)$.

By taking the Fourier transform of eqn(5.17) the spectral half width, (1/e intensity point) can be obtained,

$$\Delta\omega = \frac{(1+C^2)^{1/2}}{t_0} \tag{5.18}$$

In the absence of any initial chirp the spectral width is said to be Transform-limited, (and for a Gaussian pulse $\Delta\omega t_0 = 1$). This indicates that the pulse has no chirp or other internal structure, and is minimum time-bandwidth product, $\Delta\omega t_0$, of the pulse.

Summary

In a nonlinear medium spectral broadening can be induced by linewidth enhancement factor effects, self and cross phase modulation. The phase modulations so induced in general results in non-linear chirp. Saturation of the gain results in temporal distortion which is dependent on the total energy and the width of the pulse.

5.2.4 Combined Dispersion and Nonlinear Effects

In dispersive nonlinear medium interesting new effects arise due to the interplay between GVD and nonlinear phase modulation, (SPM, XPM). In the anomalous dispersion regime the two phenomena can, under certain circumstances, cooperate to produce optical solitons, i.e. pulses that propagate without changing their shape, [5, 6]. The combined effects of dispersion and phase modulation can also be used to produce very intense ultra-short pulses, and pulse compression can be achieved in both dispersion regimes, [1, 7, 8].

If the pulses are very short, ($< 100fs$), then higher-order dispersion effects become important, and self-steepening of the pulse can occur. The spectra of such short pulses are significantly broadened, [9, 10]. Self-steepening of an optical pulse is induced by an intensity dependent group velocity and results in asymmetric spectral and temporal profiles.

In pump-probe situations the dispersion induced walk-off reduces the amount of XPM that can be induced, because at some point the pulses will no longer be temporally co-incident.

5.2.5 Summary

A pulse propagating in a dispersive medium can either be temporally broadened, in the normal dispersion regime, or narrowed, in the anomalous dispersion regime. The frequency dependence of the refractive index also linearly chirps the pulse.

A pulse propagating in a nonlinear regime is spectrally broadened, by nonlinear chirp. Gain saturation results in both spectral and temporal distortion. The spectral effects are usually phenomenologically represented via the Linewidth Enhancement Factor, however for sub-picosecond pulse the LEF concept is considered to be inappropriate.

The interplay between the dispersive and the nonlinear phenomena results in other effects only seen when both phenomena are present. In the anomalous dispersion regime solitons can be supported, while in both the normal and anomalous dispersion regions pulse compression can be induced.

In the next section the theoretical techniques that have been developed to model these effects will be outlined.

5.3 Models of Pulse Propagation

5.3.1 Introduction

Time domain analysis has proved to be very successful at modelling the propagation of picosecond pulses. However, sub-picosecond pulse are more easily analysed in the frequency domain. The greater spectral width of these latter pulses results in higher order dispersion terms becoming important and these terms are more readily handled in the frequency domain.

Electric Field Wave Equation

The starting point for both the time and frequency domain analysis techniques is Maxwell's equations. By manipulating those equations the following vector wave equation can be obtained,

$$\underline{\nabla} \wedge \underline{\nabla} \wedge \underline{E}(\underline{r},t) = -\frac{1}{c^2}\frac{\partial^2}{\partial t^2}\underline{E}(\underline{r},t) - \mu_0 \frac{\partial^2}{\partial t^2}\underline{P}(\underline{r},t) \tag{5.19}$$

where $\underline{E}(\underline{r},t)$ is the electric field vector, $\underline{P}(\underline{r},t)$ is the polarization field vector, c is the speed of light in free space, and μ_0 is the permeability of free space. In obtaining eqn(5.19) it was assumed that $\underline{\nabla} \cdot (\epsilon \underline{E}) = \epsilon \underline{\nabla} \cdot \underline{E} = 0$

By expressing $\underline{E}(\underline{r},t)$ and $\underline{P}(\underline{r},t)$ in terms of their Fourier transforms, the time domain wave equation above, can be rewritten in the frequency domain,

$$\underline{\nabla} \wedge \underline{\nabla} \wedge \underline{\tilde{E}}(\underline{r},\omega) = \frac{\omega^2}{c^2}\underline{\tilde{E}}(\underline{r},\omega) + \mu_0 \omega^2 \underline{\tilde{P}}(\underline{r},\omega) \tag{5.20}$$

The Fourier transform of the electric field and its inverse are given by,

$$\underline{E}(\underline{r},t) = \frac{1}{2\pi}\int_{-\infty}^{\infty} \underline{\tilde{E}}(\underline{r},\omega)\, exp[-\imath\omega t]\, d\omega \tag{5.21}$$

$$\underline{\tilde{E}}(\underline{r},\omega) = \int_{-\infty}^{\infty} \underline{E}(\underline{r},t)\, exp[\,\imath\omega t]\, dt \tag{5.22}$$

and similarly the polarization transform pair are,

$$\underline{P}(\underline{r},t) = \frac{1}{2\pi}\int_{-\infty}^{\infty} \underline{\tilde{P}}(\underline{r},\omega)\, exp[-\imath\omega t]\, d\omega \tag{5.23}$$

$$\underline{\tilde{P}}(\underline{r},\omega) = \int_{-\infty}^{\infty} \underline{P}(\underline{r},t)\, exp[\,\imath\omega t]\, dt \tag{5.24}$$

Eqns(5.19, 5.20) fully describe the evolution of a pulse in the time and frequency domains respectively. The next two sections look at the time and frequency domain approaches in more detail, and outline their respective advantages and disadvantages.

5.3.2 Time Domain Analysis

In order to highlight the pulse propagation aspects it will be assumed that the medium is of sufficiently large extent in the directions perpendicular to the propagation direction, that transverse variations of the optical field can be ignored. Further, it will also be assumed that only one E-field component exists, $\underline{E}(\underline{r},t) \rightarrow E_x(z,t)$ and that the medium is both homogeneous and isotropic. These assumptions reduce eqn(5.19), to a scalar equation,

$$\frac{\partial^2}{\partial z^2}E_x(z,t) - \frac{1}{c^2}\frac{\partial^2}{\partial t^2}E_x(z,t) - \mu_0\frac{\partial^2}{\partial t^2}P(z,t) = 0 \tag{5.25}$$

In obtaining the above equation the identity, $\underline{\nabla}\wedge\underline{\nabla}\wedge\underline{E} = \underline{\nabla}(\underline{\nabla}\cdot\underline{E}) - \underline{\nabla}^2\underline{E}$, was used.

The electric field can now to be expressed in terms of a slowly varying envelope and a carrier wave,

$$E_x(z,t) = 1/2\,\hat{\underline{x}}\,[A(z,t)\,exp(\imath(\beta_0 z - \omega_0 t) + c.c] \tag{5.26}$$

where $A(z,t)$ is the slowly varying envelope, ω_0 is the carrier frequency, β_0 is the propagation constant and $c.c$ denotes complex conjugate.

Substituting the above expression into eqn(5.22) gives,

$$\tilde{E}(z,\omega) = \tilde{A}(z,\Omega)exp(-\imath\beta_0 z) \tag{5.27}$$

where $\Omega = \omega - \omega_0$ and,

$$\tilde{A}(z,\Omega) = \int_{-\infty}^{\infty} A(z,t)\,exp[\,\imath\Omega t\,]\,dt \tag{5.28}$$

$$A(z,t) = \frac{1}{2\pi}\int_{-\infty}^{\infty} \tilde{A}(z,\Omega)\,exp[-\imath\Omega t]\,d\Omega \tag{5.29}$$

To make further progress it is now necessary to separate the polarization into linear and nonlinear components,

$$P(z,t) = P_L(z,t) + P_{NL}(z,t) \tag{5.30}$$

Linear Component of the Polarization

The linear polarization accounts for the dispersion of the permittivity, and is most naturally related to the E-field in the frequency domain,

$$\tilde{P}_L(z,\omega) = \epsilon_0 \chi^{(1)}(\omega) \tilde{E}_x(z,\omega) \tag{5.31}$$

$$= \epsilon_0 \chi^{(1)}(\omega) \tilde{A}(z,\Omega) exp(-\imath\beta_0 z) \tag{5.32}$$

By taking the Fourier transform of eqn(5.25), neglecting the nonlinear polarization, and applying the slowly varying envelope approximation, the following expression can be obtained,

$$\imath 2\beta_0 \frac{\partial}{\partial z}\tilde{A}(z,\Omega) + \frac{1}{c^2}(\omega_0+\Omega)^2 \epsilon_r(\omega_0+\Omega) A(z,\Omega) - \beta_0 \tilde{A}(z,\Omega) = 0 \tag{5.33}$$

The slowly varying envelope approximation, SVEA, assumes that,

$$\left|\frac{\partial^2 \tilde{A}}{\partial z^2}\right| \ll \left|\beta \frac{\partial \tilde{A}}{\partial z}\right| \tag{5.34}$$

Interestingly Crosignani and co-workers, [11], have recently shown that SVEA is not an approximation, but in fact only eliminates the spurious solutions that are unavoidably introduced when the first-order Maxwell equations are manipulated to derive the second-order wave equation. This is consistent with the observation made by Shen, [12], that ignoring the higher order derivative amounts to neglecting the backward propagating wave.

Before taking the inverse Fourier transform of eqn(5.33) the dispersion of the permittivity will be approximated by expanding $\epsilon(\omega_0 + \Omega)$ about the carrier frequency, ω_0,

$$\epsilon_r(\omega_0 + \Omega) = \epsilon_0 + \Omega\,\epsilon^{(1)} + \frac{1}{2}\Omega^2\epsilon^{(2)} + \frac{1}{6}\Omega^3\epsilon^{(3)} + ... \tag{5.35}$$

where

$$\epsilon^{(m)} = \left[\frac{d^m\epsilon}{d\Omega^m}\right]_{\Omega=\omega_0} \tag{5.36}$$

The time domain pulse propagation equation can now be obtained by substituted eqn(5.35) back into eqn(5.33) and taking the Inverse Fourier transform of the resultant expression, thus,

$$\frac{\partial A}{\partial z} + \frac{1}{v_g}\frac{\partial A}{\partial t} + \frac{\imath}{2}\beta^{(2)}\frac{\partial^2 A}{\partial t^2} = 0 \tag{5.37}$$

Only the first three terms of eqn(5.35) have been retained. The first-order term, $\epsilon^{(1)}$ accounts for the group velocity, while the second-order term describes the Group Velocity Dispersion, $\beta^{(2)}$. Higher order dispersion effects can be taken into account by retaining more of the terms from the Taylor expansion, eqn(5.35).

Nonlinear Component of the Polarization

In the subsequent analysis it will be assumed that the nonlinear polarization induces a Kerr-type nonlinearity and is thus described by the third order susceptibility. The relationship between the nonlinear polarization and the electric field is again most easily expressed in the frequency domain, and is given by,

$$\tilde{P}_{NL}(z,\omega) = \epsilon_0\,\chi^{(3)}(\omega)\,\tilde{E}(z,\omega)\,\tilde{E}(z,\omega)\,\tilde{E}(z,\omega) \tag{5.38}$$

where $\chi^{(3)}(\omega)$ is the third-order susceptibility.

It will also be assumed that the nonlinearity responds instantaneously and is thus dispersionless. The real part of the third order susceptibility describe two effects; an intensity dependent refractive index and third-harmonic generation. The third-harmonic generation effect is very small, unless special steps have been taken to enhance it, and will be neglected in the following analysis. With these assumptions the term proportional to the nonlinear polarization in the scalar wave equation can be written as,

$$\mu_0 \frac{\partial^2 P_{NL}}{\partial t^2} = \frac{\omega^2}{c^2} n_2 |A|^2 A \tag{5.39}$$

where,

$$n_2 = \frac{3}{8 n_0} \chi^{(3)} \tag{5.40}$$

The equation for the evolution of a pulse in a nonlinear dispersive media is thus,

$$\frac{\partial A}{\partial z} + \frac{1}{v_g} \frac{\partial A}{\partial t} + \frac{\imath}{2} \beta^{(2)} \frac{\partial^2 A}{\partial t^2} = \imath \frac{\omega_0}{c} n_2 |A|^2 A \tag{5.41}$$

This equation is referred to as the Nonlinear Schrodinger Equation, (NLS), and has been found to describe many physical phenomena. In optics it has been used to describe pulse propagation in, eg. nonlinear optical fibres.

The Nonlinear Schrodinger Equation can be solved numerically using the split-step method, [1]. This technique numerically propagates the pulse an incremental distance, Δz, first assuming that the medium is purely dispersive, and then assuming it is purely nonlinear. This implicitly assumes that the nonlinearity and dispersion act independently; this is a good approximation provided, Δz is sufficiently small.

By including higher-order temporal derivatives more detailed dispersion effects can be studied, but the resultant equation is more difficult to solve. Similarly, higher-order nonlinear effects, such as self-steepening, can also be included, but again at the expense of ease of solution. These additional complications generally only become important when ultrashort pulses, ($< 100fs$), are being considered.

If pulse evolution in semiconductor devices is being studied, the short propagation distance, typically $\leq 500\mu m$, and low dispersion of the material, generally make it acceptable to neglect the GVD term. This greatly simplifies the pulse propagation equation.

The formalism that has so far been developed has not addressed the problem of attenuation or gain, both of which are important in semiconductors. Gain or loss can be easily incorporated into the formalism, provided their dispersion can be ignored. However an additional equation is required to describe the effects a pulse has on the gain medium of an active semiconductor. The refractive index changes associated with gain saturation can also be accounted for by using the linewidth enhancement factor.

Agrawal and Olsson, [13], have shown that a time-domain analysis of picosecond pulse evolution, in a semiconductor optical amplifier, gives close agreement with experimental results. Their model included gain saturation and LEF induced phase modulation.

Dienes and co-workers have also shown that it is possible to study sub-picosecond pulse propagation using time domain techniques, and obtained good agreement with experimental results. They used a Taylor series expansion to approximate

the dispersion of the imaginary part of the first-order susceptibility and also included the effects of gain saturation, dynamic carrier heating and LEF, [14, 15].

Summary

The time domain analysis of pulse evolution has successfully been applied to the study of soliton propagation, pulse compression effects and active and passive semiconductors.

Higher-order dispersion and nonlinear effects can all be described, but they result in a significant increase in the complexity of the pulse propagation equation, making solution more difficult.

Time domain analysis can successfully describe the evolution of a pulse in nonlinear dispersive media, provided, the frequency dependence of the nonlinearity is negligible, and the pulse is not so short that higher order dispersion effects need to be considered.

5.3.3 Frequency Domain Analysis

In principle the frequency domain is the most natural regime in which to study the pulse propagation of ultrashort pulses, since chromatic dispersion can only be fully described in this domain. This formalism also has no difficulty in incorporating nonlinear dispersion, and permits the nonlinearity and the chromatic dispersion to be treated simultaneously.

The advantages of the spectral approach have previously been pointed out by Pask and Vatarescu, [16], and recently, Francois has extended the spectral formalism by introducing the idea of a Total Field approach, [17]. Instead of treating pulses with different central frequencies separately, Francois has proposed that all the pulses be considered as one total field in the spectral domain.

Unfortunately, the frequency domain nonlinear wave equation can be difficult to solve, and even if a solution is obtained, a numerical Inverse Fourier Transform calculation still needs to be performed; in order to obtain the final temporal pulse profile. Also, if high temporal resolution is required this numerical routine becomes time consuming.

5.4 Summary

The physical origins of the mechanisms that cause such effects as self phase modulation, cross phase modulation, chirp, saturation and chromatic dispersion have been outlined, and their effects on the temporal and spectral properties of a pulse have also been discussed.

The SPM, XPM and dispersion effects all result in variations in instantaneous frequency; this chirp in turn induces spectral broadening. The interplay between dispersion and phase modulation effects can cause either temporal broadening or narrowing depending on whether the initially chirped pulse is in the normal or anomalous dispersion regime.

As well as the effects mentioned above additional phenomena can occur in active semiconductors. Carrier changes can induce phase modulation and saturation effects which can distort the temporal profile of the pulse.

Pulse evolution can be investigated in either the frequency or time domain. The time domain has been successfully used to study pulse propagation in many situations; these include optical fibres and active/passive semiconductors. However, for the analysis of sub-picosecond pulses the higher-order dispersion terms and the response time of the nonlinearity need to be considered. In this case pulse evolution is most naturally described in the frequency domain, but in practice this approach can be difficult to utilize.

The next Chapter studies the propagation of pump and probe pulses in semiconductors, and uses time domain analysis to study the effects the pulses induce on themselves and each other.

References

[1] G.P.Agrawal,"*Nonlinear Fibre Optics*",(Academic Press:New York),(1989).

[2] C.H.Henry, IEEE J. Quant. Electron., QE-18, 259, (1982).

[3] M.Osinski and J.Buus, IEEE J. Quant. Electron., QE-23, 9, (1987).

[4] G.P.Agrawal and C.M.Bowden, IEEE Photon. Technol. Lett., 5, 640, (1993).

[5] A.Hasegawa and F.Tappert, Appl. Phys. Lett., 23, 142, (1973).

[6] L.F.Mollenauer *et al*, Phys. Rev. Lett., 45, 1095, (1980).

[7] H.Nakatsuka *et al*, Phys. Rev. Lett., 47, 910, (1981).

[8] W.J.Tomlinson *et al*, J. Opt. Soc. Am., 1, 139, (1984).

[9] R.L.Fork *et al*, Opt. Lett., 8, 1, (1983).

[10] D.Mestdagh and M.Haelterman. Opt. Commun. 61, 291, (1987).

[11] B.Crosignani *et al*, Opt. Commun., 78, 237, (1990).

[12] Y.R.Shen, "*The Principles Of Nonlinear Optics*", (Wiley:New York), (1984).

[13] G.P.Agrawal & N.A.Olsson, IEEE J. Quant. Electron., QE-25, 2297, (1989).

[14] A.Dienes *et al*, Opt. Lett., 17, 1602, (1992).

[15] M.Y.Hong *et al*, "Subpicosecond Pulse Amplification in Semiconductor Laser Amplifiers: Theory and Experiment", pre-print.

[16] C.Psak and A.Vatarescu, J. Opt. Soc. Am. B, 3, 1018, (1986).

[17] P.L.Francois, J. Opt. Soc. Am. B, 8, 276, (1991).

Chapter 6

Pulses in Passive Nonlinear Media

6.1 Introduction

The co-propagation of a strong pump pulse and a weak probe pulse has been extensively used to experimentally study the dynamic response of nonlinear media, and the results of such investigations have been discussed in Chapter[3]. This Chapter is also concerned with pump-probe propagation, but the emphasis here in on the effects that the pump induced material nonlinearities have on the probe pulse. The pump-induced material changes distort both the temporal and spectral profiles of the probe pulse. The extent to which the pump pulse effects the probe pulse, in a particular medium, is determined by a number of factors. The most important of these are, the strength of the nonlinearity, the intensity and pulsewidth of the pump pulse, and the extent of any time-delay between the pulses. In this Chapter a semi-analytic model for the propagation of pump-probe pulses in a passive nonlinear medium is derived, and general results presented.

6.2 Coupled Pump-Probe Equations for Passive Media

6.2.1 Introduction

When a weak probe pulse enters a nonlinear medium which has just been subjected to an intense pump pulse, the changes induced in the medium by the pump alter the propagation of the probe pulse. A cross phase modulation, (XPM) is generated as well as self phase modulation, (SPM). The XPM induced by the pump dominates over the probe's SPM. Similarly the pump will feel the presence of the probe through a very small XPM component. However the SPM of the pump dominates the XPM generated by the probe.

6.2.2 Theory

By making the slowly varying envelope approximation it is possible to obtain two coupled equations for the propagation of the pump and probe envelope functions, $\mathcal{A}_p(z,t)$ and $\mathcal{A}_s(z,t)$, [1],

$$\imath\left(\frac{\partial \mathcal{A}_p}{\partial z}+\frac{1}{v_p}\frac{\partial \mathcal{A}_p}{\partial t}\right)+\frac{\omega_p\, n_2}{c}\left[|\mathcal{A}_p|^2\,\mathcal{A}_p+2\,|\mathcal{A}_s|^2\,\mathcal{A}_p\right]+\frac{\imath\alpha_p}{2}\mathcal{A}_p=0 \qquad (6.1)$$

$$\imath\left(\frac{\partial \mathcal{A}_s}{\partial z}+\frac{1}{v_s}\frac{\partial \mathcal{A}_s}{\partial t}\right)+\frac{\omega_s\, n_2}{c}\left[|\mathcal{A}_s|^2\,\mathcal{A}_s+2\,|\mathcal{A}_p|^2\,\mathcal{A}_s\right]+\frac{\imath\alpha_s}{2}\mathcal{A}_s=0 \qquad (6.2)$$

Here β_m, ω_m, α_m and n_2 are the propagation constant, carrier frequency, absorption and nonlinear index respectively. The subscript 'm' takes the value of either 's' or 'p' to signify the signal or pump pulses. In obtaining the above

equations it has been assumed that the 'Kerr-type' nonlinearity responds instantaneously and that sum and difference frequency generation is not occurring. The transverse field of both pulses has been assumed to be completely confined within the nonlinear media.

The eqns(6.1-6.2) are more amenable to solution if the envelope functions of the pulses are written in terms of an amplitude and phase,

$$\mathcal{A}_p(z,t) = a(z,t)\, exp[\imath\phi(z,t)] \tag{6.3}$$

$$\mathcal{A}_s(z,t) = b(z,t)\, exp[\imath\theta(z,t)] \tag{6.4}$$

By substituting the above expression into eqns(6.1-6.2), and invoking the pump-probe approximation, $|\mathcal{A}_s|^2 \ll |\mathcal{A}_p|^2$, (thus neglecting the cross phase modulation term, $2 \mid \mathcal{A}_s \mid^2 \mathcal{A}_p$ in eqn(6.1) and the self phase modulation term $\mid \mathcal{A}_s \mid^2 \mathcal{A}_s$ in eqn(6.2)), the following coupled equations can be obtained,

$$\frac{\partial a}{\partial z} + \frac{1}{v_p}\frac{\partial a}{\partial t} = -\frac{\alpha_a a}{2} \tag{6.5}$$

$$\frac{\partial b}{\partial z} + \frac{1}{v_s}\frac{\partial b}{\partial t} = -\frac{\alpha_b b}{2} \tag{6.6}$$

$$\frac{\partial \phi}{\partial z} + \frac{1}{v_p}\frac{\partial \phi}{\partial t} = \frac{n_2 \omega_p a^2}{c} \tag{6.7}$$

$$\frac{\partial \theta}{\partial z} + \frac{1}{v_s}\frac{\partial \theta}{\partial t} = \frac{2 n_2 \omega_s a^2}{c} \tag{6.8}$$

If the initial conditions at z=0 are taken to be,

$$a(0,t) = a_0\, F[(t - t_0)/\tau] \tag{6.9}$$

$$b(0,t) = b_0\, G[t/\tau] \tag{6.10}$$

$$\phi(0,t) = \theta(0,t) = 0 \tag{6.11}$$

where τ is the pulsewidth and t_0 is the initial time displacement, then the solutions to eqns(6.5-6.7) are,

$$a(z,t) = a_0\, F[(t - t_0 - z/v_p)/\tau]\, exp(-\alpha_p z/2) \tag{6.12}$$

$$b(z,t) = b_0\, G[(t - z/v_s)/\tau]\, exp(-\alpha_s z/2) \tag{6.13}$$

$$\phi(z,t) = \frac{\omega_p\, n_2\, a_0^2}{c}\, L_{eff}(z)\, F^2[(t - t_0 - z/v_p)/\tau] \tag{6.14}$$

where

$$L_{eff}(z) = \frac{1 - exp(-\alpha_p z)}{\alpha_p} \tag{6.15}$$

and $F[t,z]$ and $G[t,z]$ are the initial pulse profiles.

Substituting eqn(6.12) into eqn(6.8) gives,

$$\frac{\partial\theta}{\partial z} + \frac{1}{v_s}\frac{\partial\theta}{\partial t} = \frac{2\, n_2\, \omega_s\, a_0^2}{c}\, F^2[(t - t_0 - z/v_p)/\tau]\, exp(-\alpha_p z) \tag{6.16}$$

Now if new variables $U = t - z/v_s$ and $Z = z$ are defined, then eqn(6.12) becomes,

$$a(U,Z) = a_0\, F[\,(U - t_0)/\tau - \eta Z\,]\, exp(-\alpha_p Z/2) \tag{6.17}$$

where $\eta = (1/v_p - 1/v_s)/\tau$, and if use is made of,

$$\frac{\partial}{\partial Z} = \frac{\partial}{\partial z} + \frac{1}{v_s}\frac{\partial}{\partial t} \tag{6.18}$$

then eqn(6.16) becomes,

$$\frac{\partial\theta}{\partial Z} = \frac{2\, n_2\, \omega_s\, a_0^2}{c}\, F^2[\,(U - t_0)/\tau - \eta Z\,]\, exp(-\alpha_p Z) \tag{6.19}$$

and thus,

$$\theta(z,t) = \frac{2\omega_s\, n_2\, a_0^2}{c} \int_0^z exp(-\alpha_p z')\, F^2[(\,t - t_0 - z/v_s - z'(1/v_p - 1/v_s)\,)/\tau]\; dz' \tag{6.20}$$

6.3 Induced Temporal Effects

Eqns(6.12-6.14) and eqn(6.20) describe the co-propagation of a strong pump and a weak probe pulse in the same waveguide. The temporal overlap between the two pulses and the intensity of the pump, induces a significant alteration in the phase of the probe signal. The probe experiences a phase variation across its pulse profile which is no longer proportional to its own intensity or centred about its peak value. The maximum phase change now occurs at a position that is dependent on both the initial time delay between the pulses and the difference in their group velocities. The changes induced in the pump by the probe are small and can be neglected.

Any changes in the phase will, in turn, alter the chirp, $\delta\omega$, induced across the pulse.

$$\delta\omega = -\frac{\partial\theta(z,t)}{\partial t} \tag{6.21}$$

The minus sign in eqn(6.21) occurs because the harmonic time variation of the pulse has been assumed to be of the form $exp(-\imath\omega t)$.

Both the magnitude and profile of the phase and chirp of the probe pulse can be controlled by the pump pulse, as can be seen in figures(6.1-6.2). In calculating these figures the initial pulse profiles were assumed to be Gaussian.

Two parameters can be used to describe the relationship between the pump and the probe's phase, $\eta z = (1/v_p - 1/v_s)z/\tau$ and $T_0 = t_0/\tau$. Here τ denotes the pulse width. The value of ηz influences both the maximum magnitude and width of the phase variation across the probe. Higher values result in a lower and broader phase profile. ηz is a measure of the walk-off between the two pulses

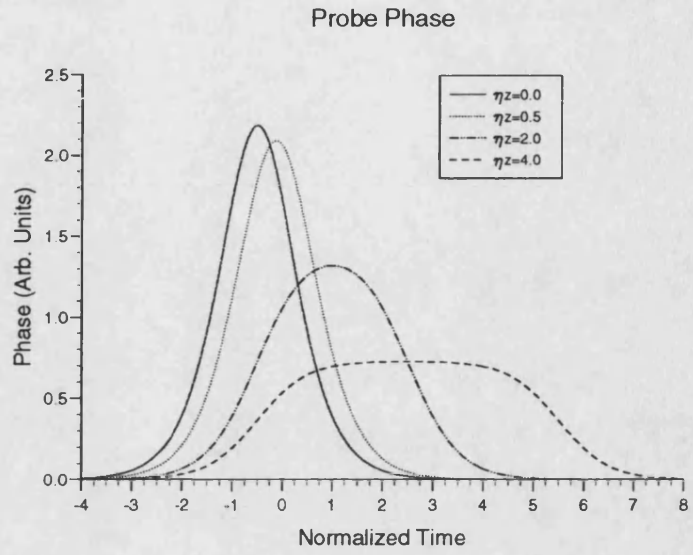

Figure 6.1: The Phase across the probe calculated for various ηz values assuming a $T_0 = -1.0$ and $(\omega_s\, n_2\, a_0^2)/c = 2\pi$.

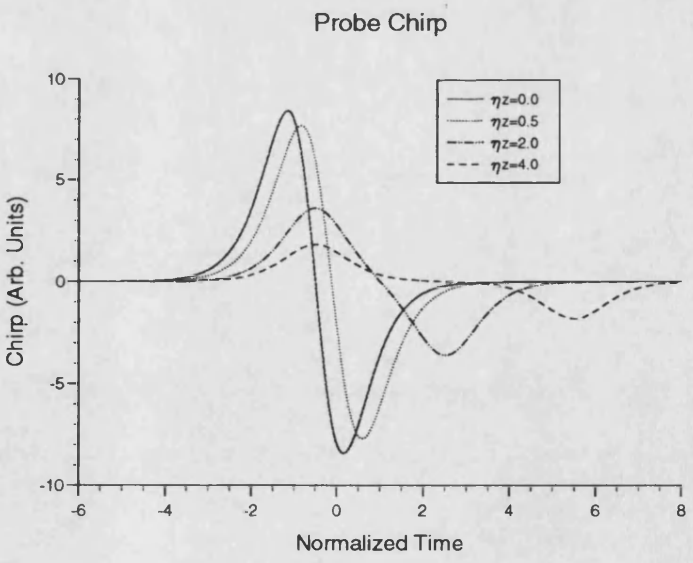

Figure 6.2: The Chirp profiles associated with the phase profiles shown in figure(6.1).

as they propagate down the guide, and the normalized time delay, T_0, causes a displacement of the phase profile, [2].

6.4 Induced Spectral Effects

Any large distortion in the temporal profile of a pulse, results in a considerable change in the frequency spectrum of the pulse. The spectral profile of the propagated probe pulse can be obtained by taking the Fast Fourier Transform of the amplitude and phase, obtained from eqns(6.12-6.14) and eqn(6.20). The XPM induced phase change results in a broadened spectrum and also induces some additional oscillatory structure into the trace. In general, the spectrum consists of many peaks, with the outermost being the most intense. The number of peaks increases linearly with the maximum induced phase.

The origin of the oscillatory structure can be understood by considering how the time dependent chirp affects the spectrum. In general the same chirp occurs at two temporal positions along the probe pulse; these points represent two waves of the same frequency but different phases. Hence they can interfere constructively or destructively depending on their relative phase, resulting in the multi-peaked structure observed.

In the following sub-sections the effects induced on the spectrum of the probe pulse by a time delay, a loss, a group velocity mismatch and an initial chirp, will be investigated. The initial profiles of both the pump and probe will be taken to be Gaussian, with the same pulse width. The pulse widths need not be the same, but have been chosen to be so for convenience. No additional effects are introduced if the pulses have different pulse widths.

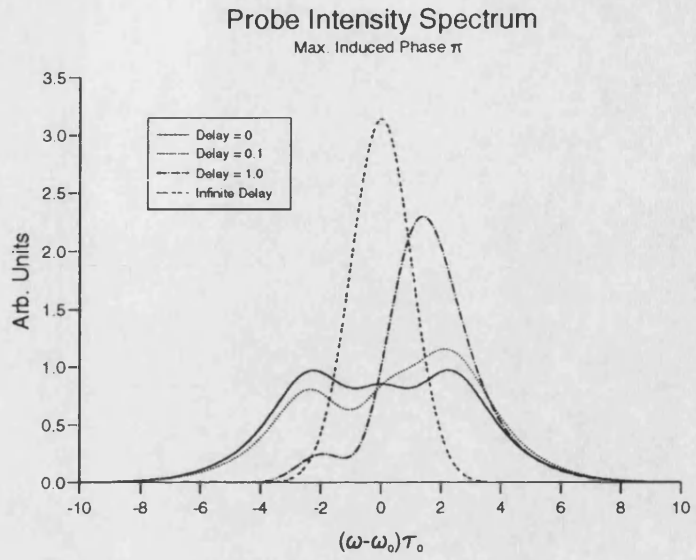

Figure 6.3: Time Delay normalised with respect to the pulse width.

6.4.1 Time Delay

If the time delay, loss and velocity mismatch are all set to zero then the maximum induced cross phase modulation will occur. If there is a time delay between the pump and the probe then the overlap between the pulses will no longer be complete. One edge of the probe pulse will experience a reduced cumulative XPM induced phase change, as the pulse propagates in the medium, and hence the spectrum will become asymmetric. This is shown in figure(6.3), where the effect of different time delays can be seen; the maximum phase change possible was π. As the time delay tends towards infinity, so the spectrum tends towards that of a Gaussian i.e the spectrum of the initial probe profile is obtained. A Gaussian spectral profile is obtained at infinite time delay, because SPM of the probe has not been included.

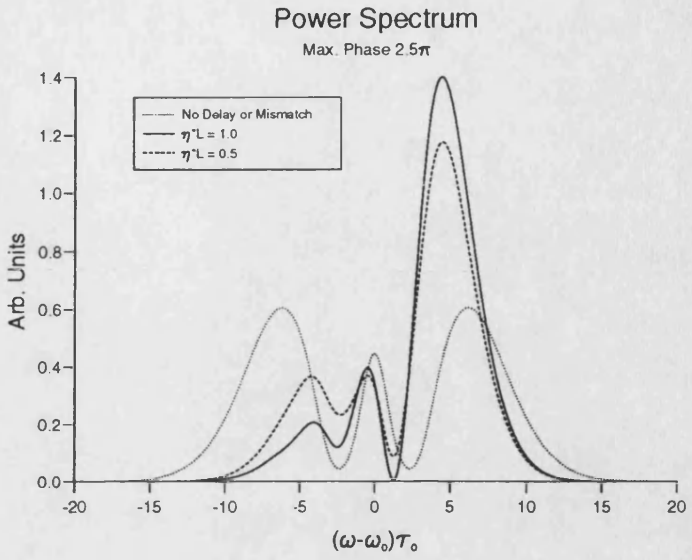

Figure 6.4: Walk-off only. The two Group Velocity Mismatches used were $\eta L = 0.5$ and $\eta L = 1.0$

6.4.2 Group Velocity Mismatch

If the time delay and the loss are both set to zero and only the group velocity mismatch is varied, the probe pulse spectrum is again found to be asymmetric, since one edge of the probe pulse experiences a greater XPM. Also the presence of a velocity mismatch sets a limit on the maximum phase attainable before walk-off occurs. At some point down the guide the pulses will have walked through each other, and will no longer be temporally overlapped. The walk-off sets a maximum effective distance over which the pump and probe are temporally overlapped. The group velocity mismatch destroys the linear dependence of the nonlinear phase on the distance. This is shown in figure(6.4).

At some distance down the guide, l_{max}, the pulses will no longer be temporally overlapped, and hence XPM will no longer influence the probe phase. The distance l_{max} is given, when there is no time delay, by

$$l_{max} = 2\tau(v_s - v_p) \tag{6.22}$$

In general the optical properties and physical dimensions of semiconductor devices are such that co-propagating pump-probe pulses in a semiconductor do not suffer walk-off.

6.4.3 Absorption

If now the time delay and mismatch are nullified and the absorption coefficient is increased the resultant spectra exhibit reduced oscillatory features, since the maximum induced phase attainable is diminished. The loss acts to saturate the XPM, by reducing the intensity of both pulses. The loss can be thought of as introducing another effective propagation distance,

$$z \rightarrow \left(\frac{1 - e^{-\alpha z}}{\alpha}\right) \tag{6.23}$$

From figure(6.5) it can be seen that both the amplitude and the number of peaks reduces as the attenuation increases. In a lossless medium the probe would have experienced a peak nonlinear phase of 2.5π.

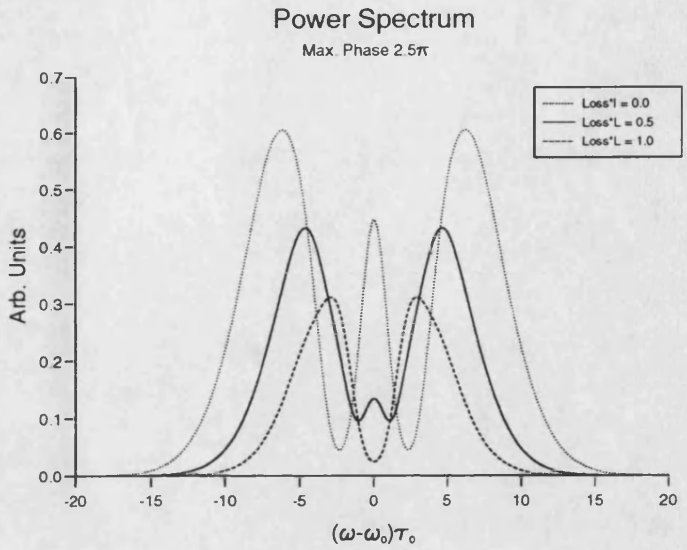

Figure 6.5: Attenuation only. The two losses used were: $\alpha L = 0.5$ and $\alpha L = 1.0$

6.4.4 Combined Effects

Since the sign of t_0 and ηL can be either positive or negative; four combination of the time delay and mismatch are possible,

1. Pump leads the Probe pulse, $t_0 > 0$
   (a) Probe faster than Pump, $\eta > 0$
   (b) Probe slower than Pump, $\eta < 0$
2. Pump behind the Probe pulse, $t_0 < 0$
   (a) Probe faster than Pump, $\eta > 0$
   (b) Probe slower than Pump, $\eta < 0$

In cases 1(a) and 2(b) the pulse that is initial time delayed also has a larger group velocity. Hence the faster pulse will, provided the propagation distance is

great enough, catch up and eventually pass the slower pulse. If the conditions are such that the faster pulse has completely walked through the slower pulse, then the probe spectrum will be symmetric and the maximum XPM will have been induced. If however, the conditions are such that the two pulses are still temporally overlapping after propagating through to the end, then the final spectrum will be asymmetric, since the induced XPM will not be the same on both sides of the probe pulse.

In cases 1(b) and 2(a) the temporally delayed pulse is also the slower of the two. If the pulses are not temporally overlapped initially, then no XPM will be induced and only SPM will contribute to the probe's spectrum. If the pulses are initially slightly temporally overlapped, then some XPM will be induced before the pulses separate, and the resultant probe spectrum will be asymmetric. However, the spectra from cases 1(b) and 2(a) will be different because the pump will have induced XPM on different sides of the probe pulse.

The effect of introducing some attenuation not only reduces the overall intensity of the spectra but also reduces the maximum phase attained and hence changes the spectral profile.

In cases 1(a) and 2(b) the absorption will cause the probe spectrum to become asymmetric, even if the pulses completely walk through each other. The attenuation of the pump results in one side of the probe pulse experiencing less XPM from the attenuated pump, and hence differences in the probe spectra will occur depending on whether the pump walks through the pump or vice versa.

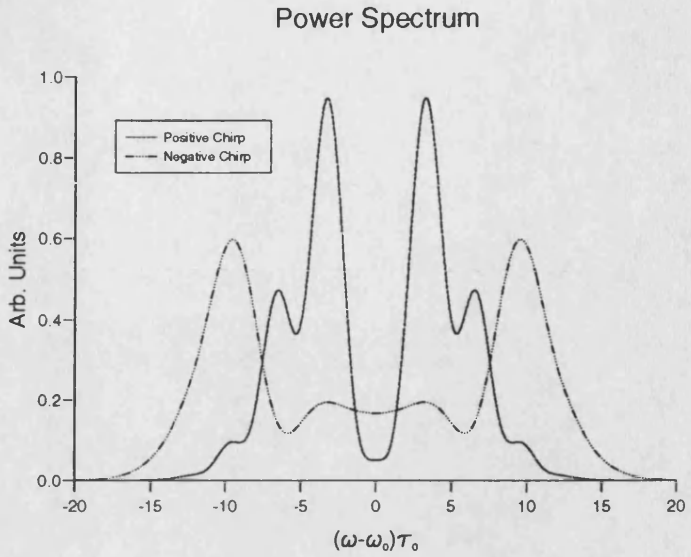

Figure 6.6: Positive and Negative Initial Chirp Only. The Chirp parameter used was $C = \pm 0.5$.

In cases 2(b) and 2(a) the attenuation enhances the spectral asymmetry by effectively causing the pulses to separate more quickly. As the magnitude of XPM is dependent on the intensity of the pump, the attenuation results in less XPM being induced as the pulses separate.

6.4.5 Initial Chirp

The addition of some initial linear chirp markedly affects the spectrum. The chirp is expressed using the following initial condition,

$$\theta(t,0) = -\frac{C}{2}\frac{t^2}{\tau^2} \tag{6.24}$$

Here the chirp parameter is denoted by C and can be either positive or negative. If it is positive it adds to the phase at the centre of the pulse and hence increases the oscillatory nature of the spectrum.

If the chirp parameter is negative the wings of spectrum are enhanced and the phase in the central region is reduced. The phase introduced by a negative initial chirp, is of opposite sign to that induced by the pump, except near the wings of the probe pulse.

The effects of both a positive and negative initial chirp, when there is no loss, mismatch or time delay, can be seen in figure(6.6). Gaussian initial pulse profiles were used and the maximum phase that could possibly be induced by the pump was set to be 2.5π.

The positive initial chirp produces a spectrum which has most of the power confined around the central frequency, ω_0. It also has more peaks and a narrower spectrum than when C is negative. The negative initial chirp concentrates most of the power in the outer most peaks.

If now loss, group velocity mismatch and both positive and negative time delays are included, the resultant spectra, for both negative and positive initial chirp, are shown in figures(6.7-6.8), respectively.

The negative chirp has a devastating effect on the spectrum. For a positive time delay almost all the power is confined in one peak. The negative chirp has all but destroyed the oscillatory features and reduced the width of the spectrum. The positive time delay has combined with the chirp to lump virtually all the power into one peak. When the time delay is negative the spectrum is broadened considerably, and has a flat profile over most of the frequency range. Only at the wings of the spectrum do the phases add constructively to produce two weak peaks.

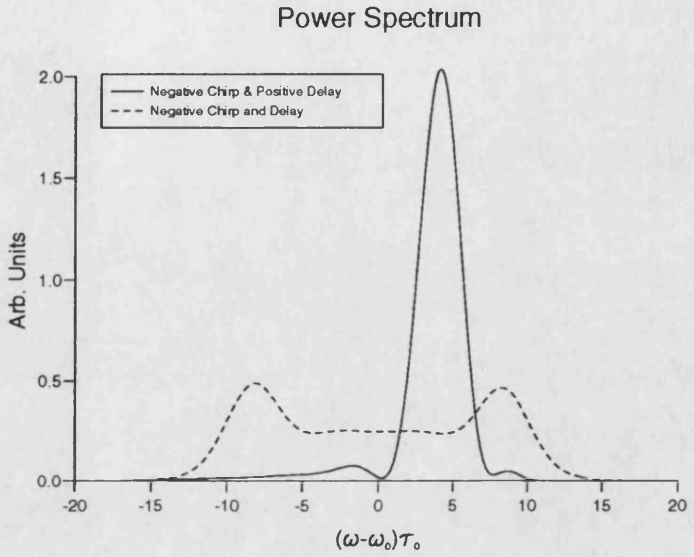

Figure 6.7: Negative Chirp with all the other effects. Values used where: $C = 0.5$, $t_0 = \pm 0.5$, $\eta L = 1.0$ and $\alpha L = 0.1$

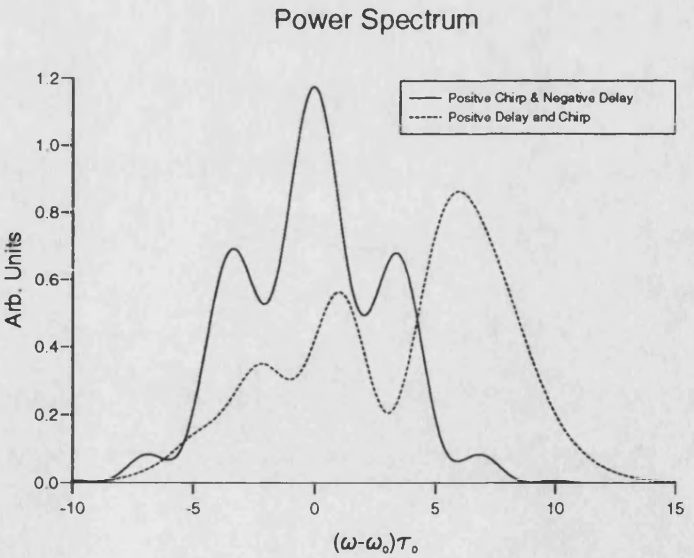

Figure 6.8: Positive Chirp with all the other effects. Values used where: $C = -0.5$, $t_0 = \pm 0.5$, $\eta L = 1.0$ and $\alpha L = 0.1$

Positive chirp increases the phase at the centre of the spectrum, and thus increases the number of peaks. The positive time delay and the mismatch both force most of the power into one side of the spectrum. When the delay is negative some of the power is pulled back into the side of the spectrum where the mismatch has reduced the amount of XPM induced phase.

The sign of the initial chirp is determined by the source generating the optical field. Pulses generated by semiconductor lasers are usually negatively chirped. This is because the amplification process in semiconductors causes a reduction in the carriers which in turn causes an increase in the refractive index.

6.4.6 Weak Self Phase Modulation

In the previous sections the probe self phase modulation was neglected. This was a valid approximation because the XPM of an intense pump pulse was much larger than the SPM, but at lower pump intensities the SPM starts to become important. The SPM can easily be accounted for in this model, as it simply adds an additional term to the phase. Also, only one of the features analysed in the previous sections, the loss, affects the SPM. The attenuation again gives rise to an effective distance, given by eqn(6.23). The probe induced SPM is given by,

$$\theta_{SPM}(U,z) = \frac{n_2\,\omega_s\,b_0^2}{c}\left(\frac{1-e^{-\alpha_s z}}{\alpha_s}\right)G^2[U,z] \tag{6.25}$$

The effect of this term becomes most apparent when either the time delay or the mismatch is very large, or when the XPM is relatively small.

6.4.7 Counter-Propagating Pulses

An analogous situation to the co-propagation effect of walk-off occurs when counter-propagating pulses are launched into a medium. In this case the pump and probe pulses are propagating in opposite directions, and thus they 'walk-through' each other. The formalism derived in this Chapter can also model counter-propagating pulses.

If the probe is assumed to be propagating in the forward direction then $v_p \rightarrow -v_p$, and thus eqn(6.20) becomes,

$$\theta(z,t) = \frac{2\omega_s n_2 a_0^2}{c} \int_0^z exp(-\alpha_p z') F^2[(t - z/v_s - z_0/v_s + z'(1/v_p + 1/v_s))/\tau]\, dz' \tag{6.26}$$

where z_0 is the initial displacement of pump pulse.

The spectral effects induced in the counter-propagating case are similar to those obtained in the co-propagating regime when ηz is large. This is because the counter-propagating pulses are only overlapped for a very short time and thus little cross phase modulation can be induced. The initial spatial displacement z_0 has the same effect as the initial time delay t_0 associated with the co-propagating case.

6.5 Summary

The effects induced by time delayed pulses, which have different group velocities, propagating in a nonlinear medium, fall into two categories,

(a) Pulses initially approaching

(b) Pulses initially separating

Case(a): when the conditions are such that the time delayed pulse is also the faster of the two, then, provided a sufficient distance has been propagated, the faster pulse will have walked through and passed the slower pulse. The resultant probe spectrum will be symmetric, and the maximum cross phase modulation, (XPM), will have been induced.

Case(b) If the time delayed pulse is the slower of the two, then cross phase modulation, induced by the pump, will only have occurred on one side of the probe pulse. The strength of the XPM is dependent on the extent of initial temporal overlap between the pulses and the magnitude of the group velocity mismatch. The edge of the pulse on which the XPM is induced is dependent on whether the pump leads the probe or the probe leads the pump. The resultant probe spectrum will thus be asymmetric.

In a lossy medium the attenuation of both pulses results in less nonlinear phase being accumulated, compared to the lossless case. The attenuation also causes the probe spectrum to become asymmetric.

Depending on the sign of the initial chirp either the phase at the centre or at the wings will be increased. A positive initial chirp concentrates the power in the centre of the spectrum and increases the number of peaks. If the initial chirp is negative the power is spread over all of the spectrum with slightly greater power confined in the wings. The number of peaks is also reduced.

When all four features, (ie. a time delay, a group velocity mismatch, a absorption and a chirp), occur at the same time the power spectrum can become very complicated, and in general the probe spectrum will be broadened and asymmetric.

If the self phase modulation, SPM, of the probe pulse is included, its effect only becomes fully apparent when the time delay or the mismatch is large, ie in a regime in which the XPM is small. The SPM otherwise simply adds a small additional component to the phase induced by the pump pulse.

Counter-propagating pulses induce effects that are similar to those experienced by co-propagating pulses experiencing walk-off.

References

[1] J.T.Manassah, Appl. Optics, 26, 3747, (1987).

[2] P.S.Spencer and K.A.Shore, NATO MIDIT ASI Meeting,'*Future Directions of Nonlinear Dynamics in Physical and Biological Systems*',Lyngby, Denmark, 1992.

Chapter 7

Pulses in Nonlinear Directional Couplers.

7.1 Introduction

The recent interest in optical pulse processing for telecommunications and optical computing applications, has highlighted the need for an all-optical switch. For telecommunication purposes such a switch should also have a fast response.

One of the most promising candidates in the field of all-optical switching is the Nonlinear Directional Coupler, (NLDC). The first published theoretical analysis of the transmission characteristics of a nonlinear directional coupler, by Jensen, [1], indicated that such a device could act as an all-optical switch. A directional coupler consists of two parallel waveguides in close proximity to one another. The transmission characteristics of a linear directional coupler are such that, light launched into one of the waveguides will, provided the appropriate device length has been chosen, emerge from the adjacent waveguide. Jensen showed

that by introducing a nonlinear layer into the structure this switching could be inhibited at certain optical powers, thereby producing a directional coupler that had intensity dependent transmission characteristics:- a NLDC.

Fast pulse operation of nonlinear directional couplers has not yet been totally successfully realized using semiconductor devices. This is because a semiconductor that has both a fast, large nonlinearity and a small absorption has not yet been identified. However, the recent discovery of a large, fast nonlinear refraction in semiconductor optical amplifiers has opened the possibility of realizing a fast all-optical switch. By using two semiconductor optical amplifiers, biased to transparency, in a nonlinear directional coupler configuration, it may be possible to produce a lossless fast all-optical switch. The essentially lossless nature of such devices offers the possibility of cascading large numbers of the devices in optical switching networks. In fact, depending on the bias current applied, an optical amplifier NLDC can be made to have either, a net gain, a net loss, or to be lossless.

The continuous wave, (CW), or steady state operation of nonlinear directional couplers has been analysed using a variety of techniques:

- Standard coupled mode theory, [1].
- Linear supermode analysis, [2].
- Nonlinear supermode analysis, [3].
- Self-consistent numerical modelling, [4].

However, only a limited amount of work has been published on the pulsed operation of such devices, [5].

This Chapter outlines a model for pulse propagation in coupled semiconductor optical amplifiers that uses linear supermode analysis, and includes the effects of gain saturation, the linewidth enhancement factor, chirp, two-photon absorption, and an instantaneous nonlinear index. In Section[7.2] the theoretical framework of the analysis technique is outlined. Section[7.3] describes the numerical approach used to solve the relevant coupled nonlinear equations. In the last section the model is used to predict the transmission characteristic of an actual NLDC. The experimentally measured characteristics of the device and those predicted by the model are compared.

7.2 Analysis of Pulse Propagation in NLDC.

7.2.1 Introduction

Modal distributions of Linear Waveguide Structures

The spatial distribution of an optical field, transverse to the propagation direction, in a linear dielectric waveguide is constrained to specific profiles or modes, which maintain their shape as the field propagates down the waveguide. In planar structures of isotropic media two types of modes can be supported, and these are designated as TE or TM modes, depending on the orientation of the electric field, [6].

In general, linear twin waveguide structures can support more than one mode, and thus the transverse distribution of the total field will consist of a superposition of several modes. The waveguides of directional couplers are usually designed so

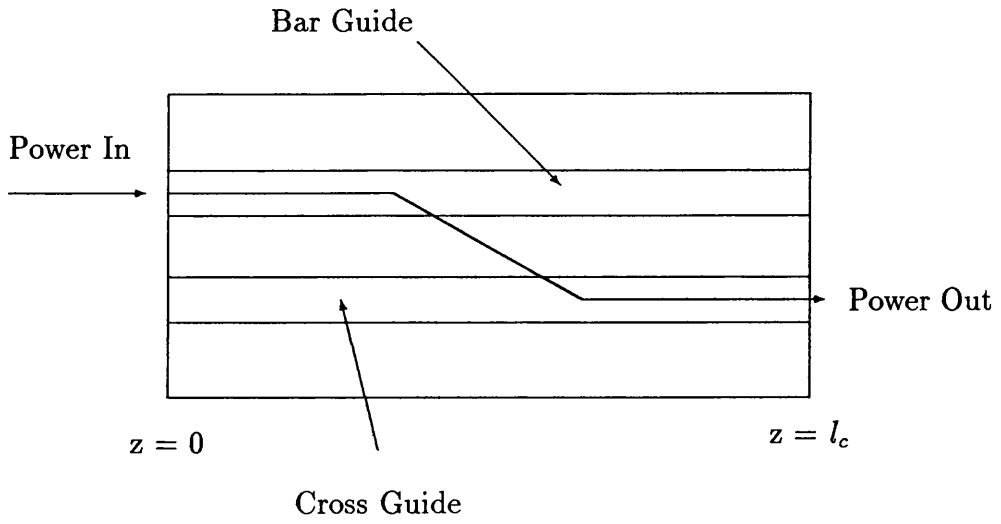

Figure 7.1: Schematic of switching in a directional coupler.

that the coupler only supports two modes. The difference in the propagation constants of these two modes results in phase differences developing between them, which in turn causes periodic changes in optical power distribution in the waveguides with propagation distance. The phase differences cause constructive or destructive interference between the modes, and it is this beating effect that causes the switching observed in such devices, [figure(7.1)]. In a linear coupler there is no power transfer between the modes; their amplitudes remain constant, and the optical switching is caused solely by the beating of the modes.

The coupling length of the waveguides is the distance over which the two modes have to propagate to ensure that a beam launched into waveguide exits from the adjacent guide. The coupling length is given by $l_c = \pi/(\beta_1 - \beta_2)$, where β_1 and β_2 are the propagation constants of the two modes of the directional coupler. The guide into which the optical field is launched is often referred to as the Bar guide, and the adjacent one as the Cross guide.

One of the main formalisms that has been developed to analyse linear multiple waveguide devices is Coupled Mode Theory, (CMT), [6]. In coupled mode theory a twin-waveguide structure is viewed as two individual guides in close proximity. The interaction between the two waveguides is represented as a dielectric perturbation. This approach uses the modes that the individual waveguides support to approximate the modes of the whole structure. Generally an analytic expression for the modal profiles of the complete structure can be found using this method.

Alternatively, the transverse modes of a multiple waveguide structure can be calculated directly. This so-called "supermode" approach is more general than coupled mode theory, [7]. In the case of twin guide structures supermode theory yields, in one limit, the operational characteristics of a directional coupler, and in the other, describes the interaction of the two lowest order modes of a single waveguide. This approach generally requires the modes to be calculated numerically.

A modified form of the supermode approach is used in this Chapter to approximate the modes of a nonlinear directional coupler. A supermode analysis of a NLDC has several advantages over an equivalent CMT investigation of such devices. In CMT the nonlinearity is viewed as a second-order approximation, since the modes of the linear directional coupler are first approximated using the modes of the individual waveguides of the coupler. Also, the possibility that the nonlinearity is confined to only specific areas of the coupler is more easily handled using supermode theory. In addition, supermode theory has the advantage of being able to describe both nonlinear multi-mode single waveguides and nonlinear couplers.

7.2.2 Nonlinear Twin Waveguide Structures

The exact electric field distribution and the propagation constants in any nonlinear waveguide and hence in a NLDC are, in general, power dependent, [10, 11]. In the following analysis it will be assumed that the magnitude of the induced nonlinear index is sufficiently small, (in comparison to the background refractive index), to allow the power dependence of the transverse mode shapes to be neglected, but sufficiently large to induce power dependent propagation constants. For simplicity, the optical field will be assumed to be TE polarized and consideration will be given to the total transverse electric field, ($\underline{E} = [0, E_{NL}, 0]$).

The electric field, E_{NL}, in a nonlinear directional coupler satisfies the following time domain wave equation,

$$\nabla^2 E_{NL} - \mu_0\epsilon_0\frac{\partial^2 E_{NL}}{\partial t^2} - \mu_0\frac{\partial^2 P_L}{\partial t^2} - \mu_0\frac{\partial^2 P_{NL}}{\partial t^2} = 0 \tag{7.1}$$

where P_L and P_{NL} are the linear and nonlinear polarizations respectively. The linear and nonlinear polarizations are related to the electric field by the following expressions, (Appendix[B]),

$$P_L(r,t) = \epsilon_0\frac{1}{2\pi}\int_{-\infty}^{\infty}\chi^{(1)}(\omega)\,\tilde{E}_{NL}(r,\omega)\,e^{-\imath\omega t}\,d\omega \tag{7.2}$$

and,

$$P_{NL}(r,t) = \epsilon_0\frac{3}{4}\chi^{(3)}E_{NL}(r,t)E_{NL}(r,t)E_{NL}(r,t) \tag{7.3}$$

where $\tilde{E}_{NL}(r,\omega)$ is the Fourier Transform of the applied optical field. The first-order susceptibility is complex and thus $\chi^{(1)} = \chi_R^{(1)} + \imath\chi_I^{(1)}$. Eqn(7.3) assumes that the nonlinearity responds instantaneously and is therefore dispersionless.

In the subsequent analysis eqn(7.1) will be solved using a perturbation technique, which uses the orthogonal modes of an equivalent linear directional coupler. The transverse modes of the linear coupler are obtained from the electric field, E_L, in a linear directional coupler, which satisfies the following wave equation,

$$\nabla^2 E_L - \mu_0 \epsilon_0 \frac{\partial^2 E_L}{\partial t^2} - \mu_0 \frac{\partial^2 P_L}{\partial t^2} = 0 \tag{7.4}$$

The modal profile, F_m, and propagation constant, β_m, of mode m are related to the electric field by,

$$E_L(r,t) = \sum_m \frac{1}{2} F_m(x,y) e^{i(\beta_m z - \omega_0 t)} \tag{7.5}$$

By substituting eqn(7.5) into eqn(7.4) and using eqn(7.2), it can be seen that F_m and β_m must satisfy,

$$\frac{\partial^2 F_m}{\partial x^2} + \frac{\partial^2 F_m}{\partial y^2} + \left(\frac{\epsilon_r \omega_0^2}{c^2} - \beta_m^2 \right) F_m = 0 \tag{7.6}$$

where the relationship $\epsilon_r(\omega_0) = (1+\chi^{(1)}(\omega_0))$ has been used, along with $\mu_0 \epsilon_0 = 1/c^2$.

It will now be assumed that a good approximation to the transverse modal profiles of the NLDC can be obtained by using only the first two supermodes of the composite linear structure. This is justified provided the nonlinearity can be considered as a small perturbation, hence,

$$E_{NL}(r,t) = \frac{1}{2} A_1(z,t) F_1(x,y)\, e^{i(\beta_1 z - \omega_0 t)} + \frac{1}{2} A_2(z,t) F_2(x,y)\, e^{i(\beta_2 z - \omega_0 t)} \tag{7.7}$$

where $A_1(z,t)$ and $A_2(z,t)$ are the slowly varying envelopes of the two modes. The functions $A_1(z,t)$ and $A_2(z,t)$ describe the temporal profiles of the modes and account for the small correction arising from the power dependence of the propagation constants.

By substituting eqn(7.2) into eqn(7.1) the following expression can be obtained,

$$\nabla^2 E_{NL} - \mu_0 \frac{\partial^2 P_{NL}}{\partial t^2} = -\frac{\mu_0 \epsilon_0}{2\pi} \int_{-\infty}^{\infty} \omega^2 \epsilon_r(\omega)\, \tilde{E}_{NL}(r,\omega)\, e^{-\imath\omega t}\, d\omega \qquad (7.8)$$

By using eqn(7.7) and eqns(5.27-5.29) the term on the right hand side of eqn(7.8) can be expanded to give,

$$\sum_{m=1,2} \left[\frac{1}{2} F_m(x,y)\, e^{\imath(\beta_m z - \omega_0 t)} \left(\int_{-\infty}^{\infty} (\omega_0 + \Omega)^2\, \epsilon_r(\omega_0 + \Omega)\, \tilde{A}_m(z,\Omega)\, e^{-\imath\Omega t}\, d\Omega \right) \right] \qquad (7.9)$$

By following the same procedure as that outlined in section[5.3.2], (ie. expanded the permittivity about ω_0), the above equation can be simplified to give,

$$\sum_{m=1,2} \left[\frac{1}{2} F_m(x,y)\, e^{\imath(\beta_m z - \omega_0 t)} \left(k_0^2\, \epsilon_r(\omega_0)\, A_m(z,t) + \frac{\imath 2\beta_m}{v_g} \frac{\partial A_m(z,t)}{\partial t} \right) \right] \qquad (7.10)$$

where $\mu_0 \epsilon_0 = 1/c^2$, and $k_0 = \omega_0/c$

In obtaining the above expression it has been assumed that the spectral width of the optical pulse is much less than ω_0, and thus only the first two terms of the expansion have been retained. This assumption is easily satisfied by the picosecond pulses being studied here, and in fact would be valid for pulses as short as 100 fs. Higher order dispersion effects can be included if more of the terms of the Taylor expansion of $\epsilon_r(\omega_0 + \Omega)$ are retained.

The permittivity in the above analysis has also been assumed to be purely real, ie. $\chi_I^{(1)} = 0$, and thus $\epsilon_r(\omega_0) = 1 + \chi_R^{(1)}(\omega_0)$.

In obtaining eqn(7.10) it has been assumed that both the envelope functions are travelling at the same group velocity. This is a valid first approximation because in typical semiconductor devices the distance propagated, ($\sim 1mm$),

and the difference between the group velocities, (Group Velocity dispersion $<$ $10fs/nm$, [12]), are such that no appreciable pulse separation occurs.

By substituting eqn(7.3) and eqn(7.10) into eqn(7.8) and then applying the slowly varying envelope approximation in conjunction with eqn(7.6); the following equation for the slowly varying envelope function is obtained,

$$\begin{aligned} &F_1(x,y)e^{\imath(\beta_1 z-\omega_0 t)}\left[\imath 2\beta_1\frac{\partial A_1(z,t)}{\partial z}+\frac{\imath 2\beta_1}{v_g}\frac{\partial A_1(z,t)}{\partial t}+k_0^2\Delta_1(r,t)A_1(z,t)\right]+ \\ &F_2(x,y)e^{\imath(\beta_2 z-\omega_0 t)}\left[\imath 2\beta_2\frac{\partial A_2(z,t)}{\partial z}+\frac{\imath 2\beta_2}{v_g}\frac{\partial A_2(z,t)}{\partial t}+k_0^2\Delta_2(r,t)A_2(z,t)\right] \\ &=0 \end{aligned} \tag{7.11}$$

where $\Delta_m(r,t)=A_m^{-1}\chi_R^{(3)}(x,y)\Psi_m$, (Appendix[B]).

$$\Psi_1(r,t)=\frac{3}{4}\left(F_1^2|A_1|^2A_1+2F_2^2|A_2|^2A_1+2F_2^2A_2^2A_1^*e^{-2\imath(\beta_1-\beta_2)z}\right) \tag{7.12}$$

$$\Psi_2(r,t)=\frac{3}{4}\left(F_2^2|A_2|^2A_2+2F_1^2|A_1|^2A_2+2F_1^2A_1^2A_2^*e^{2\imath(\beta_1-\beta_2)z}\right) \tag{7.13}$$

At present the third-order susceptibility is assumed to be purely real.

Eqn(7.11) can be separated into two coupled equations by making use of the fact that the linear modes are orthogonal, ie,

$$\frac{2\omega_0\mu_0}{\beta_m}\int\int_{-\infty}^{+\infty}F_mF_j^*\,dxdy=\delta_{ij} \tag{7.14}$$

The modal profiles have been normalised to carry unit power. Multiplying eqn(7.11) by F_m^* and integrating over all space, gives the following two coupled equations,

$$\frac{\partial A_1(z,t)}{\partial z}+\frac{1}{v_g}\frac{\partial A_1(z,t)}{\partial t}=Q_1(z)A_1(z,t)+Q_2A_2(z,t)e^{\imath(\beta_2-\beta_1)z} \tag{7.15}$$

$$\frac{\partial A_2(z,t)}{\partial z}+\frac{1}{v_g}\frac{\partial A_2(z,t)}{\partial t}=Q_3(z)A_2(z,t)+Q_4A_1(z,t)e^{-\imath(\beta_2-\beta_1)z} \tag{7.16}$$

where

$$Q_1(z) = \frac{\imath k_0^2}{2\beta_1} \int\int_{-\infty}^{+\infty} F_1 \Delta_1 F_1^* \, dxdy \tag{7.17}$$

$$Q_2(z) = \frac{\imath k_0^2}{2\beta_1} \int\int_{-\infty}^{+\infty} F_2 \Delta_1 F_1^* \, dxdy \tag{7.18}$$

$$Q_3(z) = \frac{\imath k_0^2}{2\beta_2} \int\int_{-\infty}^{+\infty} F_2 \Delta_2 F_2^* \, dxdy \tag{7.19}$$

$$Q_4(z) = \frac{\imath k_0^2}{2\beta_2} \int\int_{-\infty}^{+\infty} F_1 \Delta_2 F_2^* \, dxdy \tag{7.20}$$

The general supermode formalism for pulse propagation in a NLDC is given by the above set of equations, and at this point it is worth re-stating the assumptions which have been made in obtaining eqns(7.15-7.20),

1. The nonlinearity reacts instantaneously and is assumed to cause a perturbation of the propagation constant. The modal profiles are assumed to be unchanged.

2. It is assumed that the modes of a linear directional coupler can be used to approximate the E-field of a nonlinear directional coupler.

3. The optical field is assumed to be TE polarised, and the radiation modes have been ignored.

4. The slowly varying envelope approximation has been applied.

5. The coupler is assumed to be passive and lossless.

6. Group velocity dispersion has been neglected.

The assumptions in points [1-4] are central to the present approach. The remaining points can be relaxed without invalidating this method and have been used to simplify the initial analysis.

The effects of linear absorption and two-photon absorption can be incorporated by including the imaginary parts of the first and third order susceptibilities respectively.

Active devices can be modelled by taking account of the interaction between the optical field and the carriers of the gain medium. The effect of group velocity dispersion can be included if the second-order term of the Taylor expansion of the real part of the permittivity is retained.

In subsequent sections the complexity of the problem is gradually increased until a set of coupled equations that describes pulse propagation in an active NLDC, in which two-photon absorption is present, are obtained.

7.2.3 Lossless Symmetric NLDC

It will now be assumed that the coupler being investigated consists of two identical passive waveguides that are parallel to one another. The modes of the device, $F_1(x,y)$ and $F_2(x,y)$, may then be taken to represent the symmetric and anti-symmetric modes of the structure. From symmetry considerations the integrals Q_2 and Q_4 are then found to be zero.

In the passive case the transverse mode function $F_1(x,y)$ and $F_2(x,y)$ are purely real. Substituting for Ψ_m in the remaining two integral expressions, Q_1 and Q_3, gives the following expressions,

$$A_1(z,t)Q_1(z) = \imath\left[C_1|A_1|^2A_1 + 2C_2|A_2|^2A_1 + 2C_2A_2^2A_1^* e^{-2\imath\Delta\beta z}\right] \quad (7.21)$$

$$A_2(z,t)Q_3(z) = \imath\left[C_3|A_2|^2A_2 + 2C_2|A_1|^2A_2 + 2C_2A_1^2A_2^* e^{+2\imath\Delta\beta z}\right] \quad (7.22)$$

and $\Delta\beta = \beta_1 - \beta_2$,

$$C_1 = \int\int_{-\infty}^{+\infty} F_1^2(x,y)\,\chi^{(3)}(x,y)\,F_1^2(x,y)\,dxdy \quad (7.23)$$

$$C_2 = \int\int_{-\infty}^{+\infty} F_1^2(x,y)\,\chi^{(3)}(x,y)\,F_2^2(x,y)\,dxdy \quad (7.24)$$

$$C_3 = \int\int_{-\infty}^{+\infty} F_2^2(x,y)\,\chi^{(3)}(x,y)\,F_2^2(x,y)\,dxdy \quad (7.25)$$

and

$$\Lambda = \frac{3k_0^2}{8\beta_1} \quad (7.26)$$

The overlap integrals C_1, C_2 and C_3, determine the strength of the nonlinear interaction. In obtaining eqn(7.26) it has been assumed that $\beta_2 \simeq \beta_1$. By changing to the retarded reference frame, $T = t - z/v_g$, the two partial differentials in eqn(7.15) reduce to,

$$\frac{\partial}{\partial z} + \frac{1}{v_g}\frac{\partial}{\partial t} = \frac{\partial}{\partial z} \quad (7.27)$$

Using the new reference frame it can be shown that the following two equations can be obtained,

$$\frac{\partial A_1}{\partial z} = \imath\Lambda\left[C_1 \mid A_1 \mid^2 A_1 + 2C_2 \mid A_2 \mid^2 A_1 + C_2A_2^2A_1^* e^{-2\imath\Delta\beta z}\right] \quad (7.28)$$

$$\frac{\partial A_2}{\partial z} = \imath\Lambda\left[C_3 \mid A_2 \mid^2 A_2 + 2C_2 \mid A_1 \mid^2 A_2 + C_2A_1^2A_2^* e^{+2\imath\Delta\beta z}\right] \quad (7.29)$$

By defining the complex amplitude function in terms of an amplitude and phase, $A_m(z,T) = \sqrt{P_m(z,T)}\,exp(\imath\phi_m(z,T))$, the coupled equations can be separated into four real equations.

$$\frac{\partial P_1}{\partial z} = 2\Lambda C_2 P_1 P_2 \, sin(2\Theta) \tag{7.30}$$

$$\frac{\partial P_2}{\partial z} = -2\Lambda C_2 P_1 P_2 \, sin(2\Theta) \tag{7.31}$$

$$\frac{\partial \phi_1}{\partial z} = 2\Lambda C_1 P_1 + \Lambda C_2 P_2 \, [2 + cos(2\Theta)] \tag{7.32}$$

$$\frac{\partial \phi_2}{\partial z} = 2\Lambda C_3 P_2 + \Lambda C_2 P_1 \, [2 + cos(2\Theta)] \tag{7.33}$$

where $\Theta = \Delta\beta z + (\phi_1 - \phi_2)$

An analytic solution to the coupled equations(7.30-7.33), in terms of Jacobian elliptic functions, has previously been reported. By expressing the differential equations for the slowly varying envelope function in the retarded reference frame and neglecting higher order dispersion, the resultant equations for pulse evolution in a passive NLDC, have been shown here to have the same functional form as those that describe the CW operation of a NLDC, [2].

7.2.4 A Lossy Passive NLDC

In order to model the transmission characteristics of a lossy NLDC, the previously neglected imaginary part of the linear permittivity must be re-incorporated in the model. The loss can be accounted for in eqns(7.15-7.20) by adding a non-zero imaginary part to Δ_m,

$$\Delta_m = A_m^{-1} \chi_R^{(3)} \Psi_m + \imath \chi_I^{(1)} \tag{7.34}$$

It is still assumed that the transverse profiles, (F_1, F_2), can be represented by the, (real), supermodes of the lossless structure.

The imaginary part of the linear susceptibility is related to the absorption coefficient, α_0, by the following expression,

$$\alpha_0 = \frac{\omega_0}{cn_0}\chi_I^{(1)} \tag{7.35}$$

where n_0 is the background refractive index, c is the velocity of light in free space, and ω_0 is the frequency of the incident optical field. Thus,

$$\Delta_m = A_m^{-1}\chi_R^{(3)}\Psi_m + i\frac{\alpha_0 cn_0}{\omega_0} \tag{7.36}$$

When the complex Δ_m is substituted into eqns(7.17-7.20) the imaginary part of Δ_m gives rise to the following additional terms in eqn(7.21)

$$-\left(q_1A_1 + q_2A_2\, e^{-i(\beta_1-\beta_2)z}\right) \tag{7.37}$$

and in eqn(7.22):

$$-\left(q_3A_2 + q_2A_1\, e^{+i(\beta_1-\beta_2)z}\right) \tag{7.38}$$

where the integrals q_1, q_2 and q_3 are given by,

$$q_1 = 1/2\int_{-\infty}^{\infty} F_1(x,y)\alpha(x,y)F_1(x,y)\; dxdy \tag{7.39}$$

$$q_2 = 1/2\int_{-\infty}^{\infty} F_1(x,y)\alpha(x,y)F_2(x,y)\; dxdy \tag{7.40}$$

$$q_3 = 1/2\int_{-\infty}^{\infty} F_2(x,y)\alpha(x,y)F_2(x,y)\; dxdy \tag{7.41}$$

If $\alpha(x,y)$ is a constant in the transverse direction, it may be taken outside the integral, and then modal orthogonality reduces q_2 to zero. If $\alpha(x,y)$ is not constant then the cross integral is no longer zero. The integrals q_1 & q_3 exist regardless of whether the loss/gain is uniform. The factor q_2 accounts for the influence of one of the supermodes on the other supermode, controlled by the imaginary part of the permittivity whilst q_1&q_3 account for the effect of the imaginary part of the permittivity on each individual mode separately.

Following the same procedure as the previous section and separating the additional terms from $\chi^{(1)}$, into their real and imaginary parts, results in the following four coupled amplitude and phase equations,

$$\frac{\partial P_1}{\partial z} = 2\Lambda C_2 P_1 P_2 \, sin(2\Theta) - 2q_1 P_1 - 2q_2\sqrt{P_1 P_2}cos(\Theta) \tag{7.42}$$

$$\frac{\partial P_2}{\partial z} = -2\Lambda C_2 P_1 P_2 \, sin(2\Theta) - 2q_1 P_2 - 2q_2\sqrt{P_1 P_2}cos(\Theta) \tag{7.43}$$

$$\frac{\partial \phi_1}{\partial z} = 2\Lambda C_1 P_1 + \Lambda C_2 P_2 \, [2 + cos(2\Theta)] + q_2\sqrt{\frac{P_2}{P_1}}sin(\Theta) \tag{7.44}$$

$$\frac{\partial \phi_2}{\partial z} = 2\Lambda C_3 P_2 + \Lambda C_2 P_1 \, [2 + cos(2\Theta)] - q_2\sqrt{\frac{P_1}{P_2}}sin(\Theta) \tag{7.45}$$

The cross terms that emanate from $\chi_I^{(1)}$ have a similar functional form to those that are associated with the nonlinear index. In the amplitude differential equations the terms that arise from the nonlinearity contain $sin(\Theta)$ terms, while those that describe loss contain $cos(\Theta)$ terms. This difference arises from the fact that the nonlinear index comes from the real part of the susceptibility, $\chi_r^{(3)}$, while the absorption comes from the imaginary part, $\chi_I^{(1)}$. The integral expressions for absorption are dependent on transverse fields and not on the square of the modes, because unlike the nonlinear index, the absorption arises from the first order susceptibility.

7.2.5 Active NLDC

Introduction

An active NLDC can be obtained using two parallel identical optical amplifiers, figure(7.2a). An added complication arises when consideration is given to active devices, whose gain is determined by a carrier density. In this case account must be taken of the effect the pulse has on the carrier density. When a pulse propagates through a semiconductor active medium two significant effects occur; the pulse is amplified and its phase altered via the Linewidth Enhancement Factor, (LEF), [Chapter(5)]. The pulse also affects the gain of the medium. If the pulse is sufficiently intense gain saturation occurs.

Gain Saturation

When an optical pulse propagates through an active semiconductor it causes fluctuations in the carrier density, and thus variations in the gain. Therefore there is a need for a carrier rate equation, to relate the carrier density to the gain and the optical field. An appropriate equation is [13]:

$$\frac{\partial N}{\partial t} = \frac{I}{qV} - \frac{N}{\tau_c} - \frac{g(N) \mid E \mid^2}{\hbar\omega} \tag{7.46}$$

Here N is the carrier density, I is the injected current, q is the electronic charge, V is the volume, $\hbar\omega$ is the photon energy, τ_c is the carrier recombination time, $g(N)$ is the gain and E is the optical field amplitude. The first term on the right hand side, (RHS), of eqn(7.46) describes the rate at which the electrical pumping increases the active region carrier density. The last term is the stimulated emission term which represents the rate at which carriers are removed from the

conduction band as the optical pulse is being amplified.

If both of the identical optical amplifiers of the NLDC are assumed to be biased to transparency they will have identical carrier distributions. In the following analysis it will be assumed that the carrier concentration profile of the coupler, is only non-zero under the waveguides, figure(7.2b), and has the same constant value under each guide. (The possibility of a non-symmetric carrier density profile can also be included in this formalism.)

By integrating over the transverse direction and assuming a linear dependence between the gain and the carriers, $g_l(N) = a(N - N_0) = g_{l0}\Delta N$, eqn(7.46) simplifies to give,

$$\frac{\partial g_l}{\partial t} = \frac{g_0 - g_l}{\tau_c} - \frac{g_{l0}}{E_{sat}}[\Gamma_1 P_1 + \Gamma_2 P_2] \tag{7.47}$$

where g_{l0} is the unsaturated gain of the device

$$\Gamma_1 = \int\int_{-\infty}^{+\infty} F_1 \Delta N(x,y) F_1 \, dxdy \tag{7.48}$$

$$\Gamma_2 = \int\int_{-\infty}^{+\infty} F_2 \Delta N(x,y) F_2 \, dxdy \tag{7.49}$$

and the small signal gain is given by,

$$g_0 = aN_0(I/I_0 - 1) \tag{7.50}$$

$I_0 = qvN_0/\tau_c$ and E_{sat} is the saturation energy.

In obtaining eqn(7.47) the retarded reference frame has been used. The power of the symmetric and anti-symmetric modes are denoted by P_1 and P_2, respectively.

The first term on the RHS of eqn(7.47) can be neglected because the picosecond pulses being considered in this Chapter are much shorter than the carrier

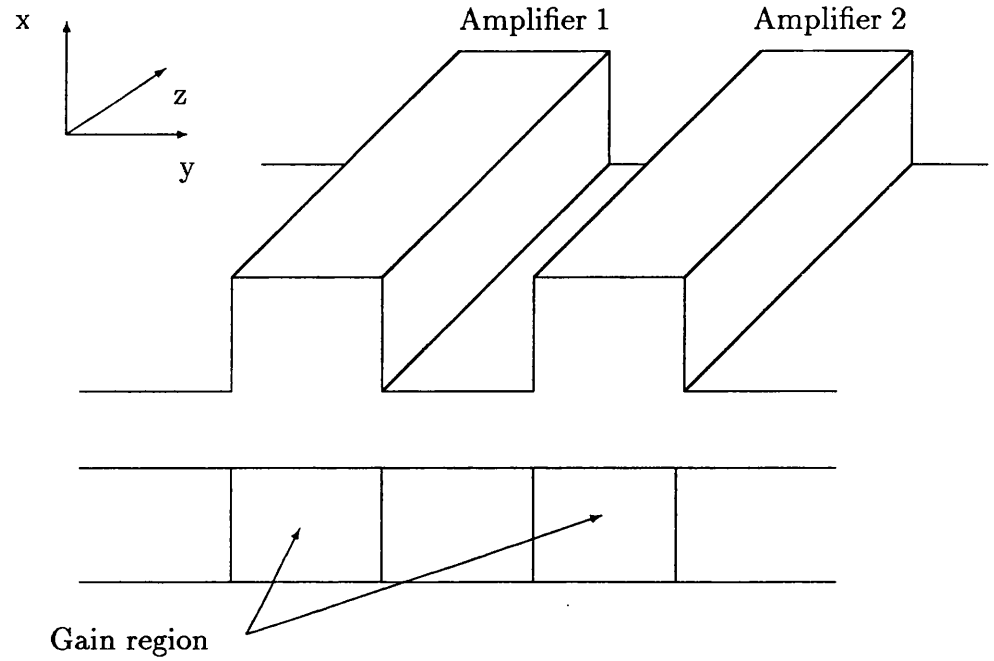

(a)

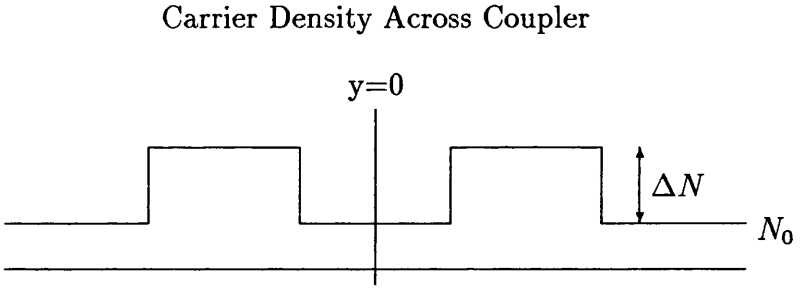

(b)

Figure 7.2: (a) Schematic of active nonlinear directional coupler, (b) Carrier distribution across the coupler. N_0 is the transparency carrier density and ΔN is net carrier density above N_0.

recombination time, $\tau_c \sim 1ns$. Physically this means that the pulse is so short that the gain has no time to recover, thus,

$$\frac{\partial g_l}{\partial t} = -\frac{g_{l0}}{E_{sat}}[\Gamma_1 P_1 + \Gamma_2 P_2] \tag{7.51}$$

which can be integrated to give the gain at time t:

$$g_l(t) = g_{l0}\, e^{-\frac{U_{in}(t)}{E_{sat}}} \tag{7.52}$$

where,

$$U_{in}(t) = \int_{-\infty}^{t} \Gamma_1 P_1(z,\acute{t}) + \Gamma_2 P_2(z,\acute{t})\; d\acute{t} \tag{7.53}$$

and g_{l0} is the small signal single pass gain of the device.

Eqn(7.52) indicates that the modal gain at time t is dependent on the fraction of the pulse that has already been amplified. Eqn(7.53) shows that the saturation is also dependent on the proportion of each mode within the gain medium. This is because the magnitude of the saturation is determined by the extent to which stimulated emission has reduced the carrier density. The amount of stimulated emission is in turn dependent on the field intensity within the gain medium.

Pulse propagation in an active medium

As well as causing gain fluctuations, the pulse induced carrier changes also cause refractive index fluctuations. In laser amplifier theory these refractive index changes are usually taken into account using the linewidth enhancement factor, α, [14]. This relates the carrier induced changes in the gain, to fluctuations in the refractive index.

The effect of the gain and the linewidth enhancement factor, must be included in the pulse evolution equation. This is achieved by adding additional terms to eqn(7.36), such that,

$$\Delta_m = A_m^{-1}\chi_R^{(3)}\Psi_m + \imath\frac{\alpha_0 c n_0}{\omega_0} - \frac{c n_0}{\omega_0}(\imath+\alpha)g(N) \tag{7.54}$$

Using the same procedure as in Section[7.2.3] and substituting Δ_m into eqns(7.17 - 7.20), results in the following additional terms appearing in eqn(7.21),

$$\left(\frac{1-\imath\alpha}{2}\right) g_l\Gamma_1 A_1 \tag{7.55}$$

and in eqn(7.22),

$$\left(\frac{1-\imath\alpha}{2}\right) g_l\Gamma_2 A_2 \tag{7.56}$$

No cross terms are present because the carrier density is symmetric about the centre of the NLDC, figure(7.2b). If now the complex envelope functions, A_1, A_2, are separated into their real and imaginary parts, then the following coupled equations for the amplitude and phase are obtained,

$$\frac{\partial P_1}{\partial z} = 2\Lambda C_2 P_1 P_2\, sin(2\Theta) - 2q_1 P_1 - 2q_2\sqrt{P_1 P_2}cos(\Theta) + g_l\Gamma_1 P_1 \tag{7.57}$$

$$\frac{\partial P_2}{\partial z} = -2\Lambda C_2 P_1 P_2\, sin(2\Theta) - 2q_1 P_2 - 2q_2\sqrt{P_1 P_2}cos(\Theta) + g_l\Gamma_2 P_2 \tag{7.58}$$

$$\frac{\partial \phi_1}{\partial z} = 2\Lambda C_1 P_1 + \Lambda C_2 P_2\,[2+cos(2\Theta)] + q_2\sqrt{\frac{P_2}{P_1}}sin(\Theta) - \frac{g_l\Gamma_1\alpha}{2} \tag{7.59}$$

$$\frac{\partial \phi_2}{\partial z} = 2\Lambda C_3 P_2 + \Lambda C_2 P_1\,[2+cos(2\Theta)] - q_2\sqrt{\frac{P_1}{P_2}}sin(\Theta) - \frac{g_l\Gamma_2\alpha}{2} \tag{7.60}$$

7.2.6 Two Photon Absorption in a NLDC

The analysis so far has not considered the imaginary part of the third-order susceptibility, $\chi_I^{(3)}$. This term, like its first-order equivalent, $\chi_I^{(1)}$, represents an attenuation process. In fact $\chi_I^{(3)}$ describes two-photon absorption, (TPA). This nonlinear absorption process is intensity dependent, and thus the peak of the pulse will experience a larger total absorption than the rest of the pulse.

TPA can be incorporated into the present formalism by including the imaginary part of the third-order susceptibility in the equation for Δ_m, i.e,

$$\Delta_m = A_m^{-1}(\chi_R^{(3)} + \imath\chi_I^{(3)})\Psi_m + \imath\frac{\alpha_0 c n_0}{\omega_0} - \frac{c n_0}{\omega_0}(\imath + \alpha)g(N) \qquad (7.61)$$

Substituting this new Δ_m into eqns(7.17-7.20), and then using the same procedure as Section[7.2.3], results in the following coupled equations for the amplitude and phase of the symmetric and anti-symmetric modes,

$$\begin{aligned}\frac{\partial P_1}{\partial z} = {} & 2\Lambda C_2 P_1 P_2\, sin(\,2\Theta\,) - 2q_1 P_1 - 2q_2\sqrt{P_1 P_2}cos(\Theta) + g_l\Gamma_1 P_1 \\ & -2\Lambda\tilde{C}_1 P_1^2 - 2\Lambda\tilde{C}_2 P_1 P_2\,[2 + cos(\,2\Theta)\,]\end{aligned} \qquad (7.62)$$

$$\begin{aligned}\frac{\partial P_2}{\partial z} = {} & -2\Lambda C_2 P_1 P_2\, sin(\,2\Theta\,) - 2q_1 P_2 - 2q_2\sqrt{P_1 P_2}cos(\Theta) + g_l\Gamma_2 P_2 \\ & -2\Lambda\tilde{C}_3 P_2^2 - 2\Lambda\tilde{C}_2 P_1 P_2\,[2 + cos(\,2\Theta)\,]\end{aligned} \qquad (7.63)$$

$$\begin{aligned}\frac{\partial \phi_1}{\partial z} = {} & 2\Lambda C_1 P_1 + \Lambda C_2 P_2\,[2 + cos(\,2\Theta)\,] + q_2\sqrt{\frac{P_2}{P_1}}sin(\Theta) - \frac{g_l\Gamma_1\alpha}{2} \\ & +\Lambda\tilde{C}_2 P_2\, sin(\,2\Theta\,)\end{aligned} \qquad (7.64)$$

$$\begin{aligned}\frac{\partial \phi_2}{\partial z} = {} & 2\Lambda C_3 P_2 + \Lambda C_2 P_1\,[2 + cos(\,2\Theta)\,] - q_2\sqrt{\frac{P_1}{P_2}}sin(\Theta) - \frac{g_l\Gamma_2\alpha}{2} \\ & -\Lambda\tilde{C}_2 P_1\, sin(\,2\Theta\,)\end{aligned} \qquad (7.65)$$

where

$$\tilde{C}_1 = \int\int_{-\infty}^{+\infty} F_1^2(x,y)\,\chi_I^{(3)}(x,y)\,F_1^2(x,y)\;dxdy \tag{7.66}$$

$$\tilde{C}_2 = \int\int_{-\infty}^{+\infty} F_1^2(x,y)\,\chi_I^{(3)}(x,y)\,F_2^2(x,y)\;dxdy \tag{7.67}$$

$$\tilde{C}_3 = \int\int_{-\infty}^{+\infty} F_2^2(x,y)\,\chi_I^{(3)}(x,y)\,F_2^2(x,y)\;dxdy \tag{7.68}$$

The propagation of a pulse in an active NLDC is described by the four coupled equations shown above, and the carrier rate equation, eqn(7.51). These equations include the effects of gain saturation, LEF, free carrier absorption and two-photon absorption.

7.3 Numerical Analysis Technique

7.3.1 Introduction

The supermode analysis of the pulsed operational characteristics of a nonlinear directional coupler, derived in the previous section, is based on the composite modes of a linear coupler of equivalent dimensions, and it was implicitly assumed that these modes were known. The numerical technique used to calculate these modes is outlined in this section. This section also describes the method used to solve the coupled equations eqns(7.63-7.66) and eqn(7.51), and the tests that have been undertaken to validate the approach used. In subsection[7.3.3] the coupled equations that describe the operational characteristics of a passive nonlinear directional coupler are solved in the CW limit, and the results compared with published work. In subsection[7.3.4] the technique used to calculate pulsed operational characteristics is outlined. Subsection[7.3.5] describes the tests used to check that the model calculates linear absorption and TPA correctly. Subsection[7.3.6] explains the split-step technique used to treat active devices and also outlines the tests undertaken to check that gain saturation has been modelled correctly. The last subsection explains the technique used to calculate the spectral profiles of the pulse emerging from both guides.

7.3.2 Linear Modes of the Composite structure

The modal field pattern in a linear directional coupler have been calculated using the equivalent transmission line technique, [9]. In this method a transmission matrix for the whole structure is obtained by representing each dielectric layer

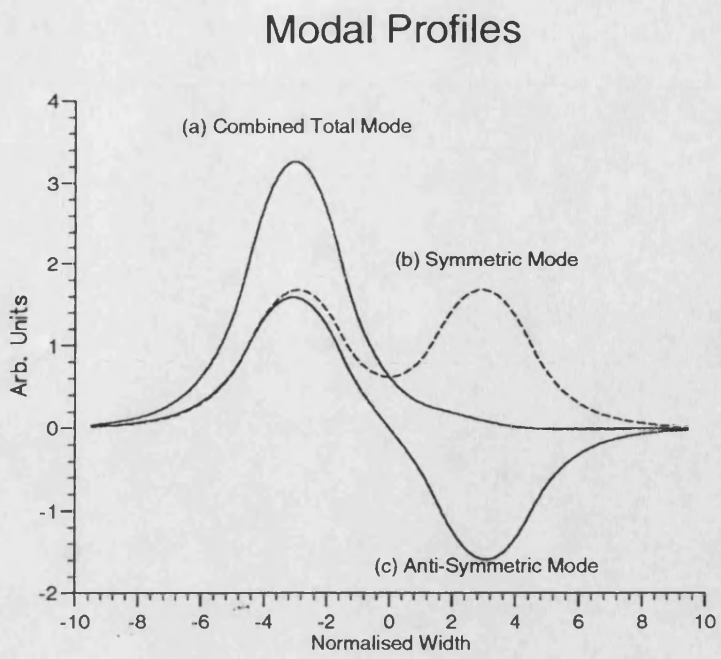

Figure 7.3: Modal Profiles in an equivalent passive media.

by a transmission line element. The modes shown in figure(7.3) were calculated for a waveguide structure consisting of two parallel $3\mu m$ wide guides, which are $3\mu m$ apart. The permittivities of the guide region was taken to be 11.28 and that of the surrounding area was taken to be 11.22. As the two guides are identical, symmetric and anti-symmetric modes are supported. These results were calculated assuming the wavelength of the incident light was $1.55\mu m$.

The overlap integrals, used in the formalism developed in section[7.2], are calculated by numerically integrating the modal profiles obtained from the equivalent transmission line theory. It is assumed that the majority of the field profile in the other orthogonal transverse direction is contained within the nonlinear region. In other words the dimensions and permittivities of the layers that make up the NLDC are such that essentially all the field is propagating within the non-

$P_1 = P_2$
$\theta = 0$
$z_{end} = 2\pi$
$K = 1$
$\Delta\beta = 1$
$C_1 = C_2 = C_3 = 1$

Table 7.1: Data used in CW evaluation of the numerical technique used to solve the coupled equations that describe the operational characteristics of a passive lossless NLDC.

linear layer. Thus the confinement factor is approximately unity and the overlap integrals are simply the reciprocal of the thickness of the nonlinear region.

7.3.3 CW Operational Characteristics of Passive NLDC

The coupled first order differential pulse amplitude and phase equations, eqns(7.30 - 7.33), were solved using the Runge - Kutta - Merson routine taken from NAG. In the CW limit the pulse propagation equations for a NLDC reduce to those derived in [2], hence this limit can be used to test the validity of the numerical solutions. The CW limit is obtained by neglecting the time dependence of the amplitude and phase functions.

In order to validate the numerical technique the initial conditions shown in Table(7.1) were chosen to simplify the solution of the coupled differential equations. It is assumed that the two guides are identical and weakly coupled, so that the overlap integrals, eqns(7.23 - 7.25) can be taken to have the same values. The initial conditions shown in Table(7.1) are the same as those used in [2].

Using the initial data shown in Table(7.1), the fraction of the power in one of the modes of the coupler, (for various total powers), is shown in figure(7.4). The

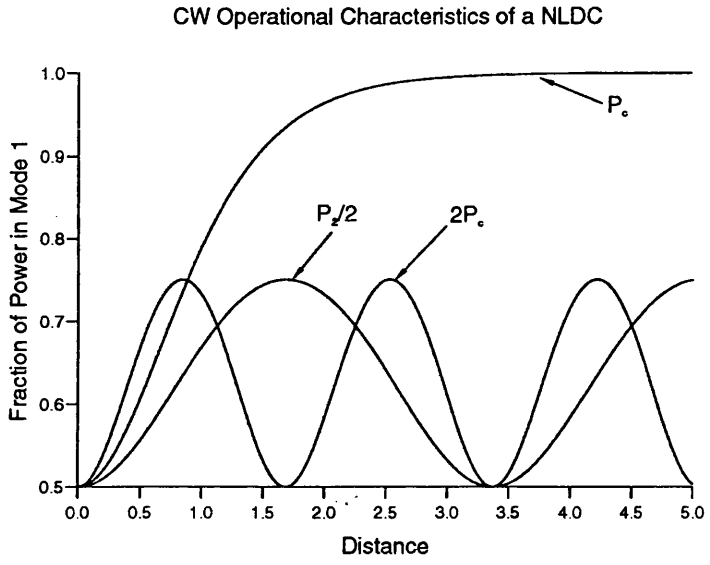

Figure 7.4: Fraction of power in mode 1 for various total powers

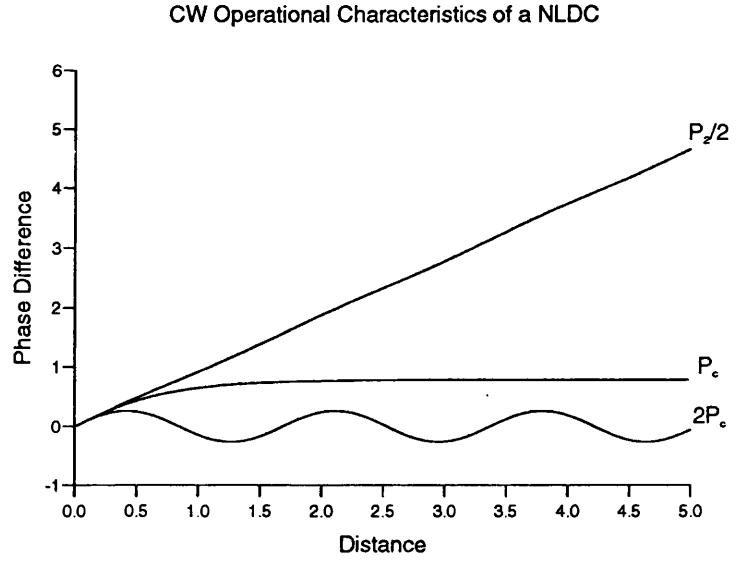

Figure 7.5: Phase difference, $(\theta - \Delta\beta z)$, between the two modes for various total powers

associated phase is shown in figure(7.5). These results agree with those in [2]. From figure(7.4) it is clear that there is a critical power, P_c, at which one mode decays asymptotically. Above or below P_c the power is exchanged periodically between the two modes.

For $P << P_c$ the nonlinear shift is small and the coupler is essentially linear, and thus there is minimal power transfer between the guides. The operational characteristics are characterised by the linear coupling length of the device. Both modes carry approximately the same power.

As P increases towards P_c, the additional phase associated with the nonlinearity results in increased power transfer between the two modes and lengthens the oscillation period. The frequency of oscillation is now power dependent. At the critical power the nonlinear contribution is such that complete power transfer between the modes occurs. Strictly speaking complete transfer does not occur, because the mode power asymptotically approaches unity. If the nonlinearity is defocussing the power is transferred to the antisymmetric mode, and if it is focussing the power is transferred to the symmetric mode.

For $P >> P_c$ large power transfer occurs between the modes in each period, and again the frequency of the power transfer is power dependent. The power that a particular mode carries various significantly within each period.

7.3.4 Pulsed Operational Characteristics of a Passive NLDC

A simplified case of pulse propagation in a NLDC can be analysed, by sweeping the power to account for the initial time dependence of the amplitude profiles, and then using same numerical routine as section[7.3.3] to solve the equations(7.30 - 7.33).

The functions P_m and ϕ_m, (where m = 1 or 2), obtained from eqns(7.42-7.45) represent the amplitude and phase of the symmetric and anti-symmetric modes. By substituting these into eqn(7.7) the temporal profile of the optical field for the whole of the NLDC is found. However, experimentally the temporal profile of the optical field is only usually measured over a restricted section of the NLDC - generally only the field emerging from one of the waveguides is recorded.

The instantaneous power of the pulse emerging from either of the guides can be obtained from the following expression,

$$P_j(t) = P_1 \int_{Rj} F_1^2(x,y)\, dxdy + P_2 \int_{Rj} F_2^2(x,y)\, dxdy + 2\sqrt{P_1 P_2}\, cos(\Delta\beta z + \Delta\phi) \int_{Rj} F_1(x,y) F_2(x,y)\, dxdy \qquad (7.69)$$

where P_j is the instantaneous pulse power in region Rj, and $\Delta\phi = \phi_1 - \phi_2$.

The temporal profiles of the pulses emerging from both guides, for three different input peak powers, ($2P_c$, P_c, and $P_c/2$), are shown in figures(7.6-7.7). The length of the NLDC was taken to be that of the coupling length of a linear coupler and the index nonlinearity was assumed to be only induced in the guide regions of the NLDC. The initial pulse profile was taken to be Gaussian.

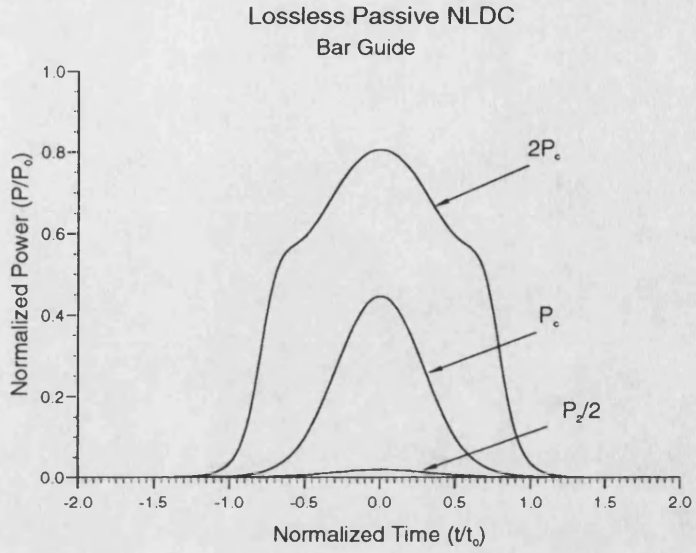

Figure 7.6: Pulse profile at the end of the Bar waveguide for three input powers, P_0, $2P_2$, P_c, and $P_2/2$. Where P_c is the critical power, and t_0 is the pulsewidth.

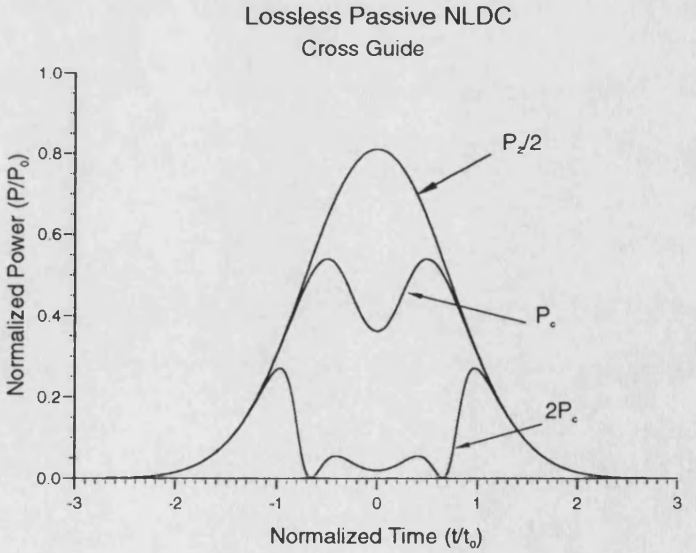

Figure 7.7: Pulse profile of the pulse emerging from the cross waveguide.

Case 1. When the peak pulse power is greater than the critical power significant pulse distortion occurs. Above the critical power a considerable amount of power oscillates between the two modes, and the period of this oscillation is dependent on the power. This results in different amounts of the high power sections of the pulse appearing in the cross and bar guides.

Case 2. When the peak pulse power is equal to the critical power it is only the central section of the pulse that can induce sufficient power transfer between the modes to inhibit their complete transfer to the cross guide. The low power wings switch to the cross guide, just as they would in a linear coupler, since they are unable to induce power transfer between the modes.

Case 3. When the peak pulse input power is less than P_c, the NLDC essentially acts like a linear coupler, and virtually all the pulse is in the cross guide at the end of the NLDC.

7.3.5 Pulse in Lossy Passive NLDC

Linear Absorption

To ensure that the linear absorption routine had been implemented correctly eqns(7.42 - 7.43) were solved using the same Runge-Kutta-Merson as before, and the resultant data used to calculate the total average output power versus the total input power, figure(7.8). As expected the linear absorption gives rise to a linear plot, the gradient of which represents the total loss, L. The total loss can

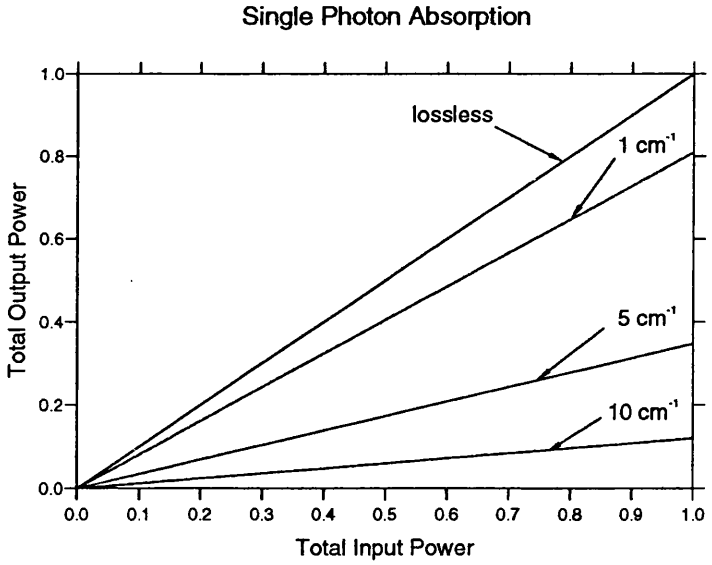

Figure 7.8: Output power for various input power obtained assuming three different absorption coefficients.

be related to the linear absorption coefficient by,

$$P_{out} = LP_{in} \qquad where \;\; L = e^{-\alpha_0 z} \tag{7.70}$$

The absorption coefficients obtained from the data in figure(7.8) and the initial value used in the calculations were found to be the same.

The total powers shown in figure(7.8) are time averaged values obtained from the instantaneous pulse power using,

$$p_T = E_T\, R \tag{7.71}$$

where p_T is the total average power, R is the pulse repetition rate, and E_T is the energy of the pulse,

$$E_{Rj} = 1/2\tau \int_{-\tau}^{\tau} P_T(t)\, dt \tag{7.72}$$

τ is the pulses temporal width and P_T is the instantaneous power.

Two-Photon Absorption

The rate at which the intensity of a CW optical beam decreases as it propagates in a medium, in which both linear absorption, α_0, and two-photon absorption, β_{TPA}, are present, is given by,

$$\frac{dI}{dz} = -(\alpha_0 + \beta_{TPA} I)I \tag{7.73}$$

where α_0 and β_{TPA} are the linear and two-photon absorption, (TPA), coefficients respectively. The solution of eqn(7.73) is

$$I = \frac{I_0\, e^{-\alpha_0 z}}{1 + \beta_{TPA} I_0 l_{eff}} \tag{7.74}$$

where I_0 is the input power, and,

$$l_{eff} = \frac{1 - e^{-\alpha_0 z}}{\alpha_0} \tag{7.75}$$

By assuming that there is no linear absorption, and rearranging the reduced eqn(7.74), the following expression can be obtained,

$$\frac{1}{T} = \frac{I_0}{I} = 1 + \beta_{tpa} z I_0 \tag{7.76}$$

where T is the transmission.

To check that the TPA had been incorporated correctly, eqns(7.63 - 7.66) were solved using the Runge-Kutta-Merson method, assuming that the TPA was the only phenomenon present. The gradient of the line obtained by plotting $1/T - 1$ against I_0 can be used to calculate β_{TPA}. This value was checked and was found to be in agreement with the β_{TPA} entered as an initial parameter.

7.3.6 Evaluation of Gain Saturation Model

When active NLDCs are considered the carrier rate equation and the coupled amplitude and phase equations have to be solved simultaneously. The effect of adding another differential equation to the model necessitates an alteration to the method of solution. A split step approach has been utilized, whereby the device is separated into sections, or cells, of length ΔZ. Within each cell, a three step approach to finding the solution at ΔZ, has been used. This consist of a nonlinear half step, a saturation step, and another nonlinear step, figure(7.9a).

Initially gain saturation is ignored and the coupled nonlinear power and phase equations are solved as in section[7.3.4]. Intermediate pulse profiles, (found at split step point, $\Delta z/2$), are then used as the input for the saturation step. In this step it is assumed that only saturation is present and eqns(7.63 - 7.66) and eqn(7.51) are solved at Δz. The resultant amplified profiles are then used as the initial values for the next nonlinear step, figure(7.9b).

This process is repeated for a number of sections. The width of the sections was gradually reduced until subsequent reductions in Δz produced no discernible change in the final output of the device. The order in which the nonlinear and gain saturation steps were carried out was found to be unimportant. The same results were obtained regardless of whether the nonlinear effects or the saturation effects were considered in the initial half step.

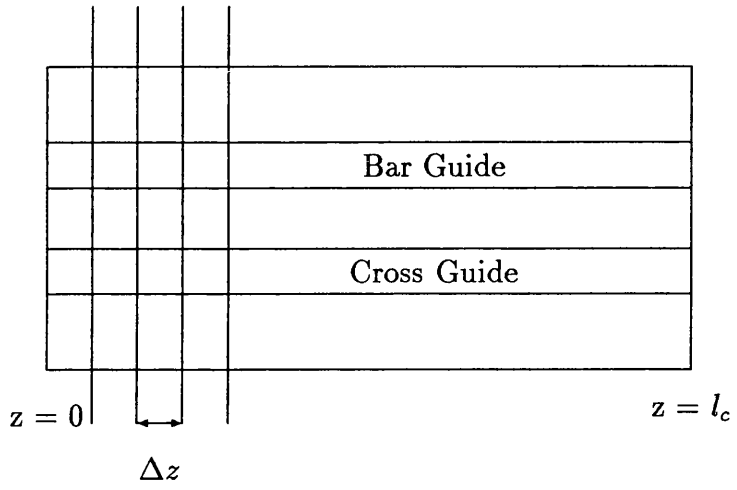

(a)

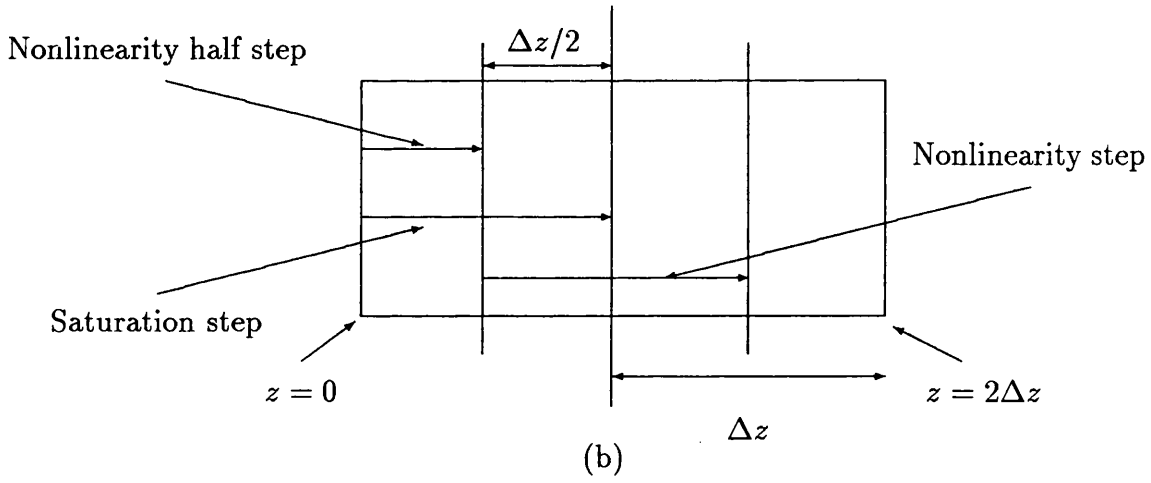

(b)

Figure 7.9: Schematic of numerical solution technique.
(a) The coupler is sub-divided into small sections Δz, and (b) split step approach is used to solve the coupled pulse envelope and saturation equations.

In the saturation step the nonlinear terms are ignored and hence eqns(7.63 - 7.64) reduce to,

$$\frac{\partial P_1}{\partial z} = g_l \Gamma_1 P_1 \tag{7.77}$$

$$\frac{\partial P_2}{\partial z} = g_l \Gamma_2 P_2 \tag{7.78}$$

and the solution to these equations is,

$$P_1 = P_{01}\, e^{g_l \Gamma_1 \Delta z} \tag{7.79}$$

$$P_2 = P_{02}\, e^{g_l \Gamma_2 \Delta z} \tag{7.80}$$

where P_{01} and P_{02} are the powers in the two mode at z=0.

This split step approach assumes that the gain saturation and nonlinearity act independently, Hong *et al*, [15] have also used this approach to analyse ultra-short pulse propagation in optical amplifiers.

In the limit $\Gamma_1 \sim \Gamma_2$ it has been shown that an analytic solution to eqn(7.51), [13], exists. Good agreement was obtained when the results calculated using numerical technique outlined above, (obtained assuming $\Gamma_1 \sim \Gamma_2$), were compared to those obtained using the analytic expression in [13].

7.3.7 Spectral Profiles

The power spectrum of a general pulse is obtained by using the following expression,

$$S(\omega) = \left| \int_{-\infty}^{\infty} U(z,t)\, exp[\imath(\,\theta(z,t) + (\omega - \omega_0)t\,)]\; dt \right|^2 \tag{7.81}$$

where U(z,t) is the envelope function of the pulse, $\theta(z,t)$ is its phase and ω_0 is the carrier frequency.

In single waveguide structures the total optical field of the whole device is used in calculating the spectrum. However, in multiple waveguide structures only the spectrum of the optical field emerging from individual waveguides of the multiguide structure is usually measured, ie, the spectrum of the whole structure is not recorded.

The section of the total field that couples into the experimental equipment used to measure the spectrum, can be found theoretically using an overlap integral. The required sections of the total field is obtained by weighting the total optical field of the device, by a function, Ω, that represents the part of the device that is being spectrally investigated. Strictly speaking the function Ω should be the modal profile of the sampling equipment. Thus,

$$U(z,t)\, e^{\theta(z,t)} = \Gamma_1' \sqrt{P_1(z,t)}\, e^{\phi_1(z,t)} + \Gamma_2' \sqrt{P_2(z,t)}\, e^{\phi_2(z,t)}\; dx\, dy \tag{7.82}$$

where,

$$\Gamma_1' = \int\int_{-\infty}^{\infty} \Omega(x,y)\, F_1(x,y)\; dx\, dy \tag{7.83}$$

$$\Gamma_2' = \int\int_{-\infty}^{\infty} \Omega(x,y)\, F_2(x,y)\; dx\, dy \tag{7.84}$$

The spectrum of the pulse emerging from the individual guides of the NLDC being considered in this Chapter, were calculated assuming that Ω was zero over the half of the coupler that did not contain the guide being investigated, and was unity over the half of NLDC that did contain the guide being investigated.

The spectra of the pulses shown in figures(7.6, 7.7) are shown in figures(7.10, 7.11). The Fourier Transforms were carried out numerically using a Fast Fourier Transform routine from the NAG Fortran Library. To test the routine a low power Gaussian pulse was used as the initial pulse profile, the spectrum of the pulse emerging from the cross guide was checked to ensure that it had a Gaussian profile of the correct spectral width.

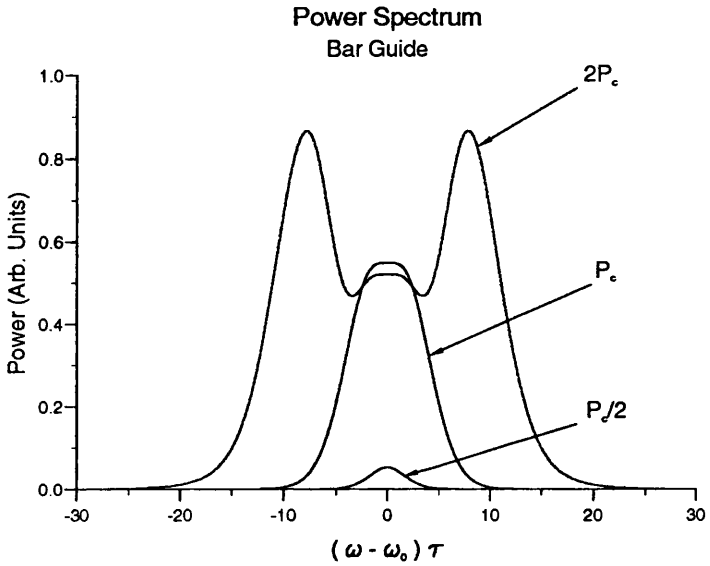

Figure 7.10: Power spectrum of the pulse emerging from the bar guide for three peak powers: $2P_c$, P_c, and $P_c/2$.

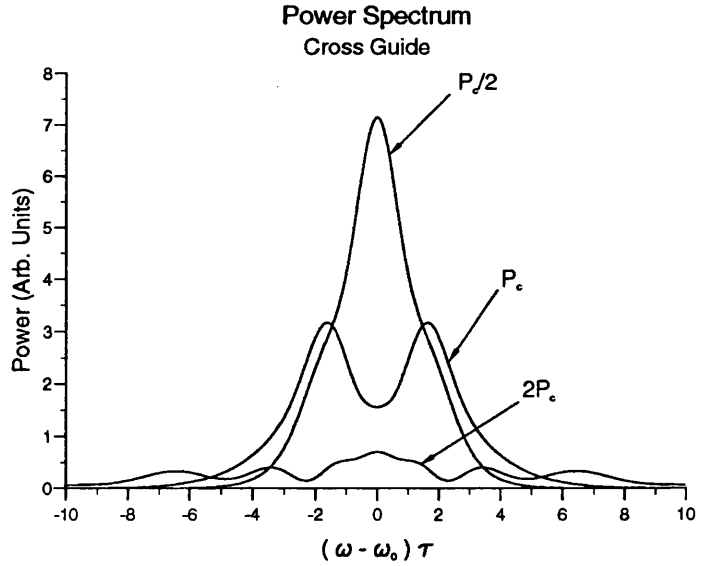

Figure 7.11: Corresponding power spectrum of the pulse emerging from the cross guide.

7.4 Results

7.4.1 Introduction

This section is separated into three parts, the first considers the effects that attenuation, gain saturation, and the linewidth enhancement factor individually have on the transmission characteristics of a NLDC.

The second part considers pulse propagation in a NLDC constructed from two coupled semiconductor optical amplifiers, and compares the results to those obtained experimentally for such devices. The switching in these devices is induced by Kerr-type instantaneous nonlinear refraction.

The last sections considers the possibility of gain switching in coupled semiconductor amplifiers, in this case the switching is being induced by the linewidth enhancement factor. Trillo and Wabnitz, [5] have previously analysed these devices using coupled mode theory.

7.4.2 Switching Characteristics of Pulsed NLDC

Before comparing the experimentally measured operational characteristics of an active NLDC, (fabricated using two coupled semiconductor optical amplifiers), with those predicted by the model derived in this chapter; the effects that each of the physical phenomena, incorporated in the model, have on a pulse, will be outlined.

In order to highlight the effects that the individual physical phenomena have on the NLDC, the switching characteristic of a lossless passive NLDC will initially be investigated. The subsequent results will then be compared against these results to assess the effects that, linear absorption, two-photon absorption, gain saturation and the linewidth enhancement factor, individually induce.

Switching Characteristics of a Passive Lossless NLDC

The fraction of the output power in the bar and cross guides against average input power of a Gaussian pulse launched into the bar guide is shown in figure(7.12) for a NLDC consisting of two parallel $3\mu m$ guides, which are $3\mu m$ apart. The waveguides have an effective permittivity of 11.28, while that of the surrounding is 11.22. Only the waveguides have a nonlinear refractive index, and the device length was assumed to be the same as the linear coupling length, ie $l_c = 2.1179\ mm$. The central wavelength of the 14ps input pulse used in the following calculations is taken to be $1.55\mu m$, and the repetition rate is assumed to be 82 MHz.

At low power the coupler acts linearly and the majority of the power emerges from the cross guide. The remainder of the power is spread over the rest of the coupler. As the power increases more of the power starts to emerge from the bar guide, and at the critical power, P_c, the power in both guides is the same. Above P_c more power is in the bar guide.

The difference between the CW, (Dotted line), and pulsed operations, (Continuous line), of a NLDC can be seen in figure(7.12). The contrast ratio between

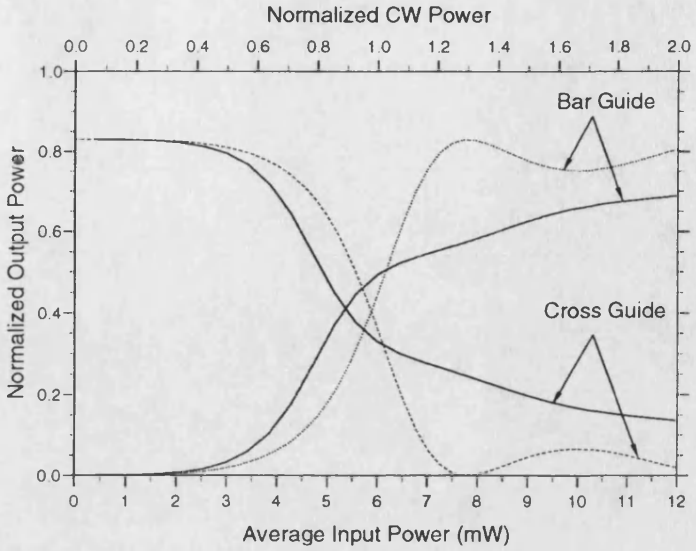

Figure 7.12: Switching characteristics of Gaussian pulses, (Continuous line), and a CW beams, (Dotted line), in a passive lossless NLDC

the power in each of the guides is not as good in the pulse case, this is because the nonlinearity causes only the central sections of the pulse to switch back to the guide, leaving the wings still in the cross guide.

Switching Characteristics of a Lossy Passive NLDC

The effect that loss has on the transmission characteristics can be seen in figure(7.13). The linear absorption causes a marked increase in the magnitude of the critical power, and results in drastic reduction in the contrast ratio above P_c. The introduction of Two-Photon Absorption (TPA) results in a further deterioration in the operational characteristics, in fact the combined absorption is sufficient to inhibit power dependent switching. This is because TPA has a disproportionately greater effect on the high power sections of the pulse, and it is these sections that

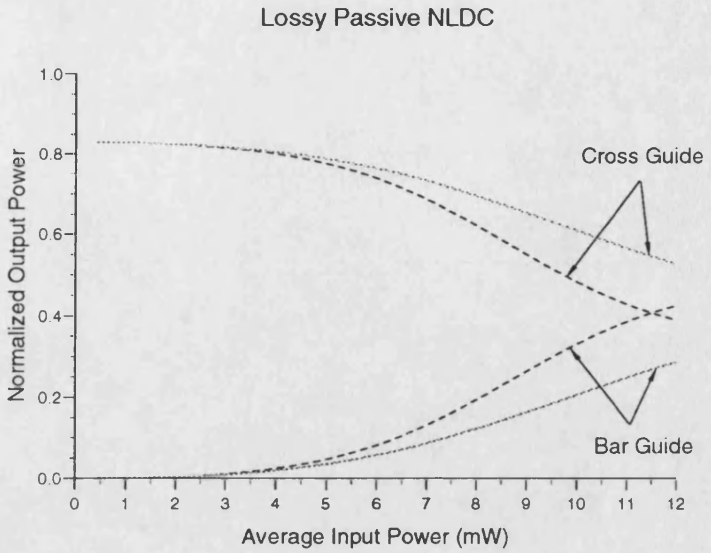

Figure 7.13: Switching characteristics of Gaussian pulses in a lossy passive NLDC (a) The dashed line was calculated assuming only linear loss of $\alpha_0 = 10\ cm^{-1}$ was present. (b) The solid line assumes that two-photon absorption is also present $\beta_{TPA} = 10$ cm/GW.

are normally switched back into the launch guide.

The effect that TPA has on the temporal profile of a pulse can be seen in figure(7.14). Two-photon absorption primarily affects the high intensity section of the pulse, resulting in significant pulse distortion. The results shown in figure(7.14) were calculated assuming that TPA was the only absorption process present.

The TPA also affects the spectral profile, as can be seen in figure(7.15). The reduced intensity profiles of the pulse result in smaller phase changes being induced, and hence less structure is apparent in the spectra.

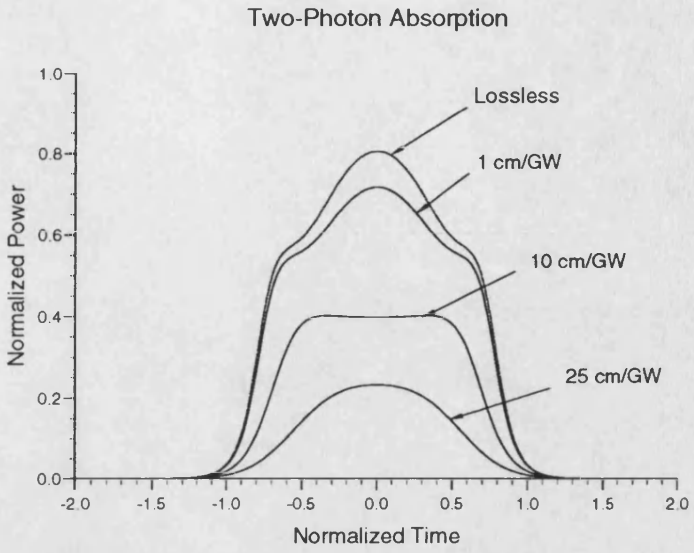

Figure 7.14: Effect of Two-Photon Absorption on the temporal profile of a pulse emerging from the bar guide. The peak power of input pulse is twice that of the critical power of a lossless passive NLDC.

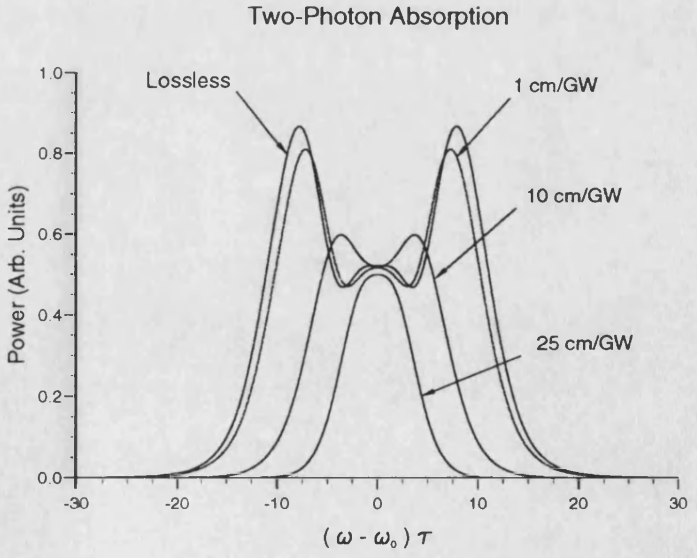

Figure 7.15: The corresponding spectral profile of the pulses shown in figure(7.14).

Switching Characteristics of an Active NLDC

The introduction of amplification causes changes in the transmission characteristics and distorts the output spectral and temporal profiles. These changes are induced by the additional amplitude and phase effects caused by the amplification and the linewidth enhancement factor (LEF) respectively.

The results shown in figures(7.16 - 7.18) were calculated assuming there was no absorption, ie $\alpha_0 = 0$, and $\beta_{TPA} = 0$, and the linewidth enhancement factor was assumed to be 6. The saturation energy was set at 30 pJ and the unsaturated single pass gain $G_0 = exp(g_{lo}l_c) = 2$.

The critical power of an active NLDC is lower than that of a passive NLDC of the same dimensions. The amplification increases the amplitude of the pulse thus inducing a larger nonlinear index, which in turn increases the magnitude of the induced phase. The linewidth enhancement factor also induces an additional phase component, and these two phase factors can either add constructively, figure(7.16a) or destructively, figure(7.16b), depending on the relative signs of the LEF and nonlinearity. In either case the effect of the amplification is greater than that of the linewidth enhancement factor, and thus in both case the critical power is lower than that of a passive NLDC.

The effect of gain saturation on the temporal profile of the pulse emerging from the bar guide is shown in figure(7.17). Gain saturation causes the leading edge of the pulse to steepen with increased amplification. This in turn causes the peak of the pulse to be shifted forward in time. The saturation also broadens the pulse. All these features are induced because the leading edge of the pulse experiences

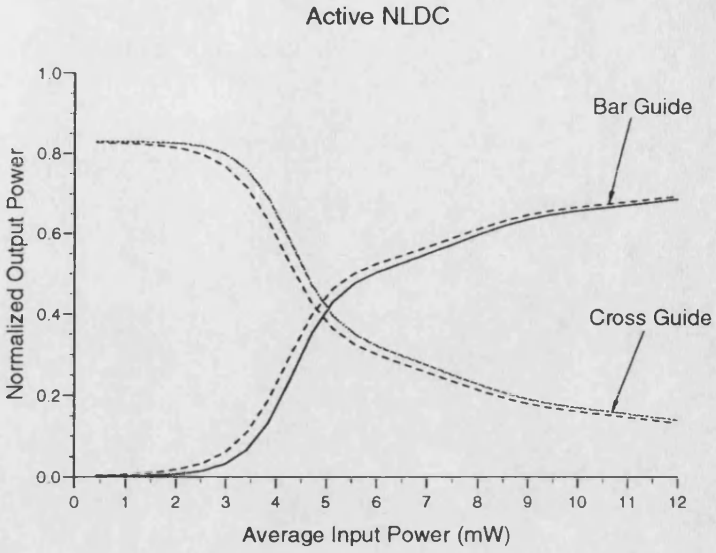

Figure 7.16: Switching characteristics of an active NLDC, (a) Dashed line: the phase induced by the nonlinearity and the LEF are of the same sign, (b) Solid line: the phase induced by the two effects are of opposite sign.

greater amplification than the rest of the pulse. The asymmetry in the temporal profile is also reflected in the spectral profile, figure(7.17). Both figures(7.17, 7.18) were calculated assuming that the initial peak power was twice that of the critical power of a lossless passive NLDC.

7.4.3 Comparison between Theoretical and Experimental Results

Recently Davies *et al*, [16], have published experimentally measured operational characteristics of an active NLDC. The devices tested consists of two parallel $2\mu m$ wide active guides separated by $2\mu m$. An effective index step of 0.02 was used to define the 1.4 mm long waveguides. The device was estimated to have a linear loss of 35 to 40 cm^{-1} and a two photon coefficient of $\beta_{TPA} \sim 30cm/GW$.

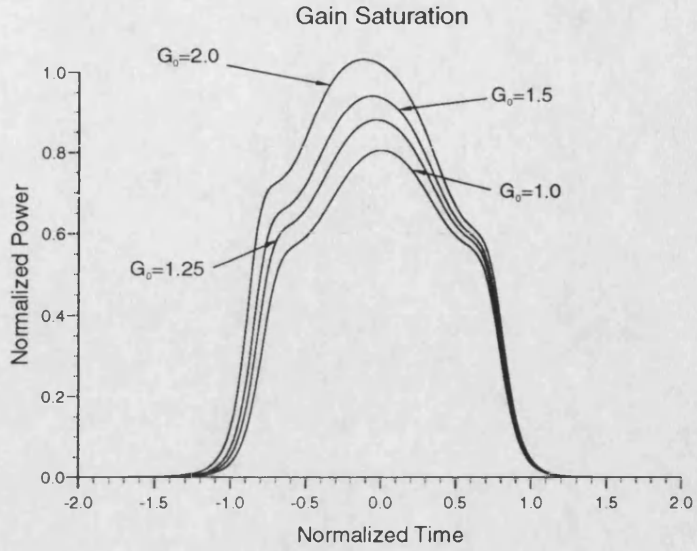

Figure 7.17: Effect of Gain saturation on the temporal profile of a pulse emerging from the bar guide. The peak power of the pulse launched in the NLDC is twice that of the critical power of a lossless passive NLDC.

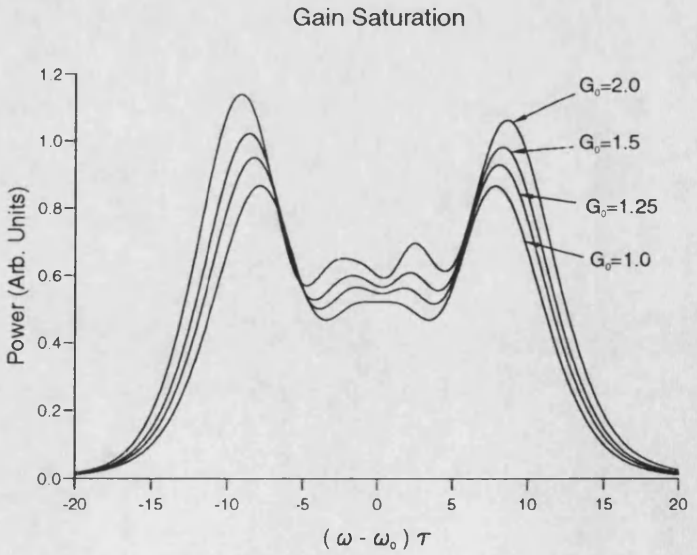

Figure 7.18: The corresponding spectral profile of a the pulse shown in figure(7.17).

The nonlinear index of the device was estimated to be of the order of $10^{-11} - 10^{-12}\ cm^2/W$, and the same bias current was applied to both guides. The device was probed using a colour centre laser operating at 1540 nm, which produced 14ps pulses at a repetition rate of 82 MHz.

The NLDC transmission characteristics were measured under three different operating conditions, ie in gain, transparency and loss regimes. The results Davies *et al* obtained are shown in figure(7.19),

To model these devices the coupled pulse equations(7.63 - 7.66) and eqn(7.52) were solved using the following values, $\alpha_0 = 40\ cm^{-1}$, $\beta_{TPA} = 40\ cm/GW$, $E_{sat} = 20\ pJ$, $\alpha = 6$, and $n_2 = -5.0 \times 10^{-11}\ cm^2/W$. The loss mechanisms were assumed to be present across the whole of the NLDC. However, the nonlinear refraction was assumed to be induced only in the waveguides. The initial pulse profile was taken to be Gaussian with a pulse width of 14 ps and central wavelength of $1.55\mu m$. The pulse repetition rate was assumed to be 82 MHz. The symmetric and anti-symmetric modes for the structure outlined in [16] were calculated and their propagation constants used to obtain the linear coupling length, which was found to be $l_c = 0.714\ mm$. To maintain agreement with reference[16] the device length used in the model was taken to be 1.4 mm, (ie, twice the linear coupling length).

The calculated transmission characteristics, figures(7.20 - 7.21) show the same general trends as those obtained experimentally. In the loss regime the phase contribution from the linewidth enhancement factor works with the nonlinearity to enhance the switching, but is accompanied by increased absorption. Conversely, in the gain regime the phase induced by the LEF works against the nonlinearity

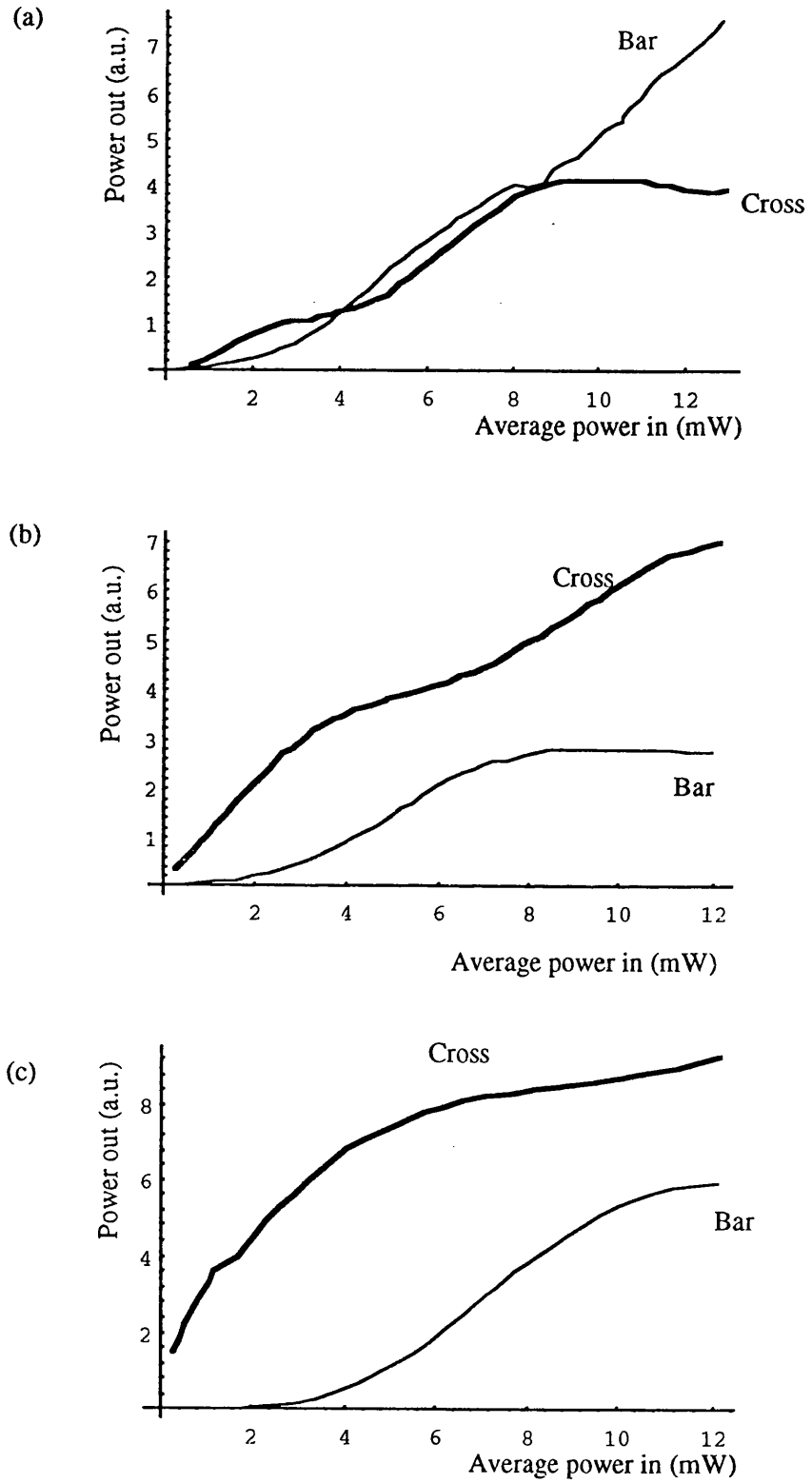

Figure 7.19: Experimentally measured transmission characteristics of an active NLDC in the (a) loss regime, (b) transparency point, and (c) gain regime, taken from [16].

reducing the switching, but the total output power has been increased. At the transparency point the intrinsic loss and two-photon absorption are sufficient to inhibit switching.

Figure(7.20) was calculated assuming an absorption loss of $L = 0.5$, where $P_{out} = LP_{in}$, and P_{in} total input power and P_{out} is the total output power. The experimental measured results in this regime show a double crossing of the bar and cross lines. This features is not observed in the theoretical results. However, the uncertainty in the physical parameters probably accounts for this discrepancy. Better agreement between the theoretical and experimental results would be achieved, if the external optics used in the experimental measurements were accounted for in the model. The external optics can be accounted for by using overlap integrals to calculate the coupling between the modes of the NLDC and those of the external optics. The model also assumes that the initial pulse is not chirped.

The magnitude of the nonlinear index used in the calculations is probably an underestimate of the true value. This is because in the calculations it has been assumed that all the field is fully contained within the nonlinear region in one of the transverse directions.

The switching characteristics under all bias conditions can be improved by assuming a smaller value for the background loss. The transmission characteristics at the transparency point have been re-calculated assuming that $\alpha_0 = 20\ cm^{-1}$, and are shown in figure(7.23). It would appear that a significant improvement in the transmission characteristics of these devices would be obtained if the background loss was reduced.

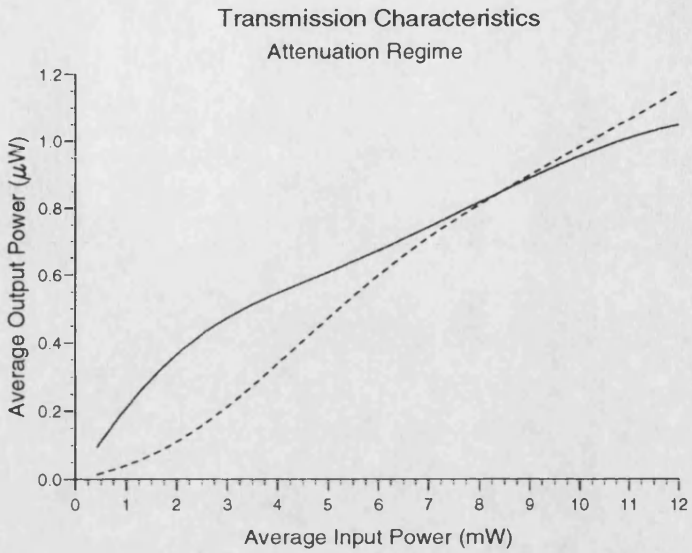

Figure 7.20: Transmission Characteristics in loss regime (a) Bar Guide - Continuous line (b) Cross Guide - Dashed line. Calculated using $L_0 = 0.5$, where $P = L_0 P_0$.

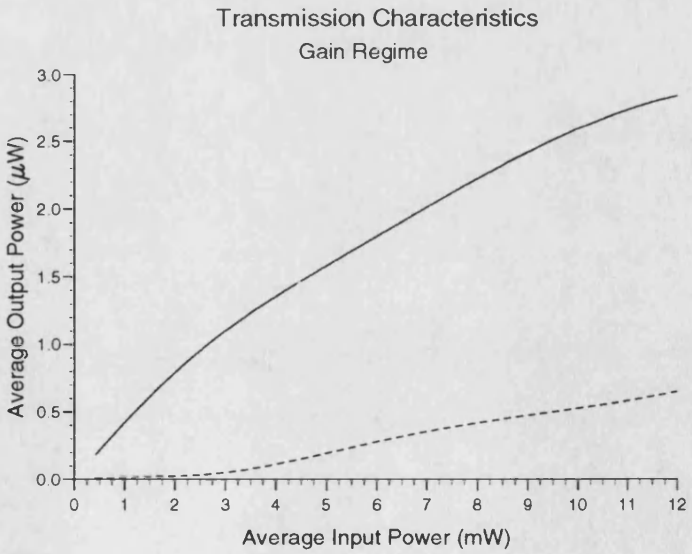

Figure 7.21: Transmission Characteristics in gain regime (a) Bar Guide - Continuous line (b) Cross Guide - Dashed line. Calculated using $G_0 = 2$, where $P = G_0 P_0$.

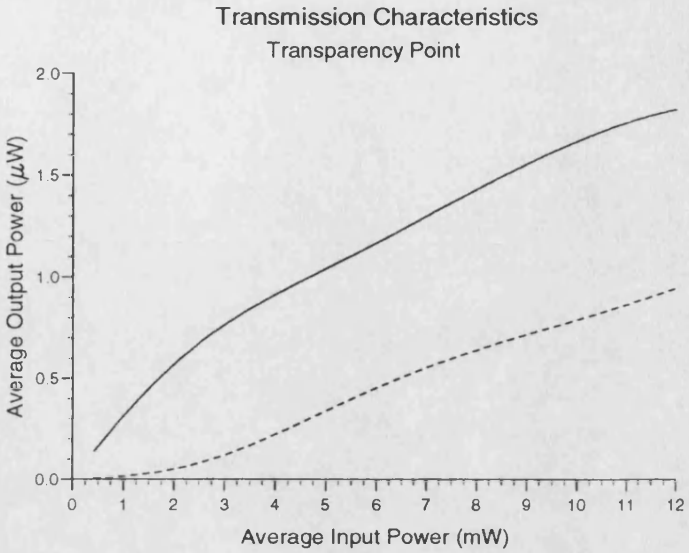

Figure 7.22: Transmission Characteristics at transparency point (a) Bar Guide - Continuous line (b) Cross Guide - Dashed line.

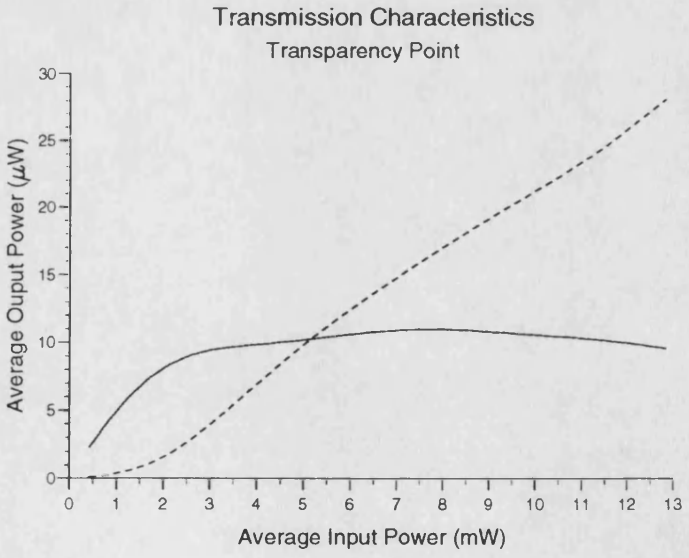

Figure 7.23: Transmission Characteristics at transparency point calculated assuming all the parameters as those used in figure(7.22) except that here the linear loss was taken to be $\alpha_0 = 20\ cm^{-1}$ (a) Bar Guide - Continuous line (b) Cross Guide - Dashed line.

7.4.4 Gain switching in Coupled Optical Amplifiers

Trillo and Wabnitz, [5], have investigated the possibility of saturation induced self-switching in active NLDCs. In this case the NLDC is assumed to have no Kerr-type nonlinearity. The switching is induced by phase changes caused by the interplay between the Linewidth Enhancement Factor, (LEF), and gain saturation. During amplification the carrier density in the gain medium drops, causing a reduction in the gain and an increase in the refractive index. The amplification of an intense pulse causes significant changes in both the gain and the index. However in the case of weak pulses these changes can be ignored.

Trillo and Wabnitz used coupled mode theory to analyse this type of saturation induced switching. The NLDC they analysed was assumed to have identical waveguides biased under the same conditions. Hence at low powers the modal gain and the phase induced by the LEF are the same in both guides. Partial switching begins to occur when the gain of one of the guides starts to saturate. The waveguides saturate at different rates and hence the modal gains are no longer the same. The difference in the modal gains induces a phase mismatch between the guides thus causing switching. Saturation needs to occur before a phase mismatch can develop, and thus only the rear of the pulse can be switched. The numerical calculation undertaken by Trillo and Wabnitz showed that partial self-switching was possible. This type of saturation induced switching cannot easily be studied using the formalism derived in this Chapter. This is because the formalism at present does not allow the waveguides to saturate at different rates.

The present formalism can be used to investigate another type of switching that exploits the fact that the modal gains of symmetric and anti-symmetric modes of the NLDC are slightly different. At low powers a small phase difference, induced by the LEF, exists between the modes. The magnitude of this phase difference is directly proportional to the gain, g_l, and thus high gains may be able to induce switching. Gain saturation causes a reduction in the gain and thus has an adverse affect on the switching. In this case the leading edge of the pulse is switched. The saturation induced reduction in the gain inhibits the transfer of the rear of the pulse.

To model this 'modal gain' switching the terms associated with nonlinear refraction in equations(7.63 - 7.66) have to be neglected. In order to simplify the analysis the terms associated with the two loss mechanisms will also be neglected, hence the model reduces to,

$$\frac{\partial P_1}{\partial z} = g_l \Gamma_1 P_1 \tag{7.85}$$

$$\frac{\partial P_2}{\partial z} = g_l \Gamma_2 P_2 \tag{7.86}$$

$$\frac{\partial \phi_1}{\partial z} = -\frac{g_l \Gamma_1 \alpha}{2} \tag{7.87}$$

$$\frac{\partial \phi_2}{\partial z} = -\frac{g_l \Gamma_2 \alpha}{2} \tag{7.88}$$

$$\frac{\partial g_l}{\partial t} = -\frac{g_{l0}}{E_{sat}} [\Gamma_1 P_1 + \Gamma_2 P_2] \tag{7.89}$$

where Γ_1 and Γ_2 represent the fraction of each mode within in the gain medium.

If gain saturation is ignored an analytic solution to eqns(7.85 - 7.88) can be obtained, and from these it can be shown that the LEF induced phase difference, $\Delta\phi$, between the two modes is given by,

$$\Delta\phi = \frac{\alpha}{2} \Delta\Gamma \, g_l \, l_c \tag{7.90}$$

where $\Delta\Gamma$ is the difference between the confinement factors of the two modes, and l_c is the linear coupling length of the device.

Using typical values of $\alpha = 6$ and $\Delta\gamma = 0.1$ eqn(7.90) predicts that a massive gain of $G_0 = exp(g_l l_c) = 35 \times 10^3 = 45\ dB$, is required to produce a π phase difference. This simple calculation clearly indicates that self-switching using this mechanism is not feasible, even under the most favourable conditions. Including gain saturation only further reduces the switching performance by causing a reduction in the gain.

Numerical calculation were carried out assuming a saturation energy of $E_{sat} = 30pJ$. It was found that the coupler acted linearly unless unrealistically large initial gain values were assumed. The NLDC was taken to have the same dimensions and dielectric step as the device analysed in section[7.3.2].

The two switching mechanisms outlined in this section are very different. In the Trillo and Wabnitz case the switching is caused by a saturation induced phase mismatch which caused the rear of the pulse to switch. However, in the modal gain case saturation reduces the switching. Also the leading edge of the pulse is switched in this case.

Neither of these approaches fully models the situation that occurs in real devices. The coupled mode analysis models the saturation effects correctly, but does not fully account for the multi-mode aspects of a directional coupler. Coupled mode analysis neglects the fact that the eigenmodes of the device will have different modal gains. The supermode based formalism derived in this chapter, correctly accounts for the multi-mode aspects but not the saturation effects. It

may be possible to identify structures where modal switching can be more effectively achieved. The present analysis, however, gives little encouragement for investigating further this technique, and hence a more sophisticated model has not been considered.

Comparison between Kerr and Saturation induced Switching

The transmission characteristics of both of the gain switching mechanisms outlined in section[7.4.4] differ considerably from those of section[7.4.3]. The Kerr nonlinearity responsible for the switching in section[7.4.3] improves with pulse power, but the converse is true of gain switching mechanism outlined in this section.

In the gain switching case the two output pulse spectra are similar, but in the Kerr case they are very different. This is because gain switching cuts the input pulses smoothly into two parts. Hence the output pulse profiles are similar. However, a Kerr - type nonlinearity causes only the high power section of the pulse to switch and thus output profiles are very different. This in turn causes the two output spectra to be very different.

References

[1] S.M.Jensen , IEEE J. Quantum Electron., QE-18, 1580, (1982).

[2] Y.Silberberg and G.I.Stegeman, Appl. Phys. Lett., 50, 801, (1987).

[3] F.Dios, X.Nogues, and F.Canal, Opt. Quant. Electron., 24, 1191, (1992).

[4] M.Cada and J.D.Begin, IEEE J. Quantum Electron., QE-26, 361, (1990).

[5] S.Trillo *et al*, IEEE J. Quantum Electron., QE-27, 401, (1991).

[6] D.Marcuse, "*Theory of Dielectric Optical Waveguides*", (Academic Press: New York), (1974).

[7] A.Yariv,"*Optical Electronics*", (Holt, Rinehart and Winston: New York), (1985).

[8] P.N.Butcher and D.Cotter, "*The Elements of Nonlinear Optics*", (Cambridge Uni. Press: Cambridge), (1990).

[9] S.Ramo, J.R.Whinnery and T. Van Duzer, "*Fields and Waves in Communication Electronics*", (Wiley: New York), (1984).

[10] A.D.Boardman and P.Egan, IEEE J. Quantum Electron., QE-22, 319, (1986).

[11] P.M.Lambkin and K.A.Shore, J. Opt. Soc. Am. B, 6,669, (1989).

[12] K.L.Hall *et al*, Appl. Phys. Lett., 56, 1740, (1990).

[13] A.E.Siegman, "*Lasers*", (University Science: Mill Valley, CA), (1986).

[14] C.H.Henry, IEEE J. Quant. Electron., QE-18, 259, (1982).

[15] M.Y.Hong *et al*, "Subpicosecond Pulse Amplification in Semiconductor Laser Amplifiers: Theory and Experiment", pre-print.

[16] D.O.Davies *et al*, Electron. Lett., 29, 1710, (1993).

[17] Y. Chen, A.W Snyder, and D.N. Payne., J. Quant. Elect., QE-28, 239, (1992).

Chapter 8

Conclusions

8.1 Introduction

This thesis has been concerned with the nonlinear optical properties of semiconductors and the dynamic response of semiconductor nonlinear waveguides. The origins of semiconductor optical nonlinearities have been highlighted, and particular attention has been paid too mechanisms that can induce fast large nonlinear index changes. Measurements of quantum well intersubband absorption have been presented and a model for the optical properties of intersubband transitions has also been derived. A formalism has been developed that can describe the fast refractive index nonlinearity recently observed in semiconductor optical amplifiers.

The latter half of the thesis was concerned with pulse propagation in semiconductors. The temporal and spectral distortion a pulse experiences when propagating in a dispersive or nonlinear medium have been outlined, and a model for the co-propagation of a strong pump pulse and a weak probe pulse in a dispersive

nonlinear medium has been derived. A formalism to describe pulse propagation in a nonlinear directional coupler has also been derived and the results obtained compared with experimental data.

8.2 Optical Properties of Intersubband Transitions

The intersubband absorption in InGaAs/InAlAs quantum wells, of various well widths and doping concentrations, have been presented. These results were then used to calculated various physical parameters. The matrix element of the intersubband transition between the ground state and first excited state was found to be larger than that previously reported for this material system, at $\sim 25\mathring{A}$, for a $50\mathring{A}$ well. However, matrix elements as large as this have been measured in GaAs/AlGaAs quantum wells. The dephasing time for the InGaAs/InAlAs system was estimated to be $\sim 55\ fs$, and is consistent with the reported values. The anticipated variation of the resonant wavelength with doping and incident beam angle was obtained. The value of the nonparabolicity factor calculated from the resonant wavelength variation with well width was also found to be in good agreement with previously reported values.

A model for the optical properties of intersubband transitions, that includes the frequency dependence of the dephasing time has been derived, and the predicted value of the nonlinear index was found to be in good agreement with the experimentally measured values of $n_{NL} \sim 10^{-7}\ cm^2/W$. The magnitude of the linear and nonlinear absorption coefficients was also found to agree with published values. The frequency dependence of the dephasing time caused an increase in the

spectral asymmetry of the linear and nonlinear refractive index and absorption.

Intersubband transitions have several potential practical uses, and a number of groups are looking at ways of using these transitions to produce both sources and detectors that operate in the far infra-red. It may also be possible to use the large nonlinear refraction associated with these transitions in an all-optical switch. However, for this purpose a means of reducing the large absorption that accompanies these transitions needs to be found; fortunately a number of schemes have recently been proposed that could reduce the absorption significantly.

8.3 Nonlinear Refraction in Semiconductor Optical Amplifiers

The mechanisms that cause the optical properties of an active semiconductor to become nonlinear, when perturbed by an ultra-short pulse, have been outlined, and their dependence on the risetime of the optical pulse has been indicated - the faster the risetime, the smaller the induced nonlinearity. The nonlinear index observed in semiconductor amplifiers is known to consist of several components, and a model for the instantaneous component of nonlinear refraction has been derived in this thesis. The values predicted by the model for the nonlinear index were found to be in good agreement with those obtained experimentally. The Optical Stark effect was identified as the mechanism responsible for inducing the fast component of the nonlinear index.

The nonlinear Kramers-Kronig relationship has previously been used to obtain the nonlinear index from the nonlinear absorption. The expression derived for the nonlinear absorption in this thesis cannot be used in this manner because it invalidates the Kramers-Kronig relationship - since the perturbation that induces the nonlinearity does not remain constant over the Kramers-Kronig integral.

The prospects of utilizing this instantaneous nonlinear refraction to produce a fast all-optical switch appear to be good, provided the effects of the slower components of the nonlinear refraction can be removed. This however, would appear to be possible if the optical amplifier is operated at transparency.

8.4 Pulse Propagation in Nonlinear Dispersive Medium

The effects induced in a dispersive nonlinear medium have been outlined, and a formalism for the co-propagation of a strong pump pulse and a weak probe pulse has been derived. This model was then used to investigate how a group velocity mismatch and a time delay between the pulses can induce walk-off. The effects that chirp, attenuation, and walk-off have on the spectrum of the probe pulse were also analysed.

When this formalism was used to model pump-probe propagation in semiconductors it was found that typical material and device parameters are such that the effects of walk-off can be ignored.

The formalism has the potential to be extended to include active media. This could be achieved by using a split step approach, (similar to that employed in Chapter[7]), to incorporating the necessary carrier rate equation needed to describe active media.

8.5 Pulse Propagation in a Nonlinear Directional Coupler

A directional coupler consists of two parallel waveguides in close proximity to one another, and the transmission characteristics of this structure are such that light launched into one waveguide may emerge from the adjacent waveguide. A nonlinear directional coupler, (NLDC), is formed by introducing a nonlinear layer into the structure of a coupler. This causes the operational characteristics to become power dependent - the intensity of the incident light determines which guide the light exits.

In this thesis a formalism has been derived that can model the pulsed operational characteristics of a nonlinear directional coupler. The model assumes that the magnitude of the induced nonlinear index is sufficiently small, (in comparison to the background refractive index), to allow the power dependence of the transverse modes to be neglected, but is sufficiently large to induce power dependent propagation constants. The electric field of a NLDC is approximated using the symmetric and anti-symmetric modes of an equivalently dimensioned linear coupler, and the nonlinearity is assumed to respond instantaneously. It was assumed that because picosecond pulses were being considered, group velocity dispersion and other higher-order dispersion effects could be neglected. The

model can describe pulse propagation in passive and active NLDCs, and includes the effects of linear absorption, two-photon absorption, gain saturation, and the linewidth enhancement factor.

If the magnitude of the induced nonlinearity is larger and/or the pulses shorter then a different approach from that used in this thesis needs to be employed to model the transmission characteristics of a NLDC. If the nonlinearity significantly perturbs the modal profile then the actual nonlinear modes need to be found. If shorter pulses are being considered then higher dispersion effects need to be considered and it may no longer be valid to assume that the nonlinearity responds instantaneously.

The model was used to investigate gain switching in active directional couplers, and it was found that coupler structures are unsuitable for this type of switching. Trillo and Wabnitz also came to the same conclusion using a different approach.

Recent experiments have indicated that it may be possible to realise a NLDC by using two semiconductor optical amplifiers, biased to transparency, in a coupler configuration. The transmission characteristics calculated using the model were found to be in good agreement with those obtained experimentally. Closer agreement with the experimental results could be achieved by better modelling the carrier profile of the NLDC.

The model has also predicted that much improved switching would be obtained, in semiconductor optical amplifier based NLDC, if the losses were reduced. If such reductions are achievable then these devices should be capable of operating as an all-optical switch. Recently other configurations have been pro-

posed that use a single semiconductor optical amplifier as the nonlinear element in an optical fibre loop, and these devices have been shown to have the potential to realise an actual all-optical switch. Therefore the prospects of producing a commercially viable all-optical switch in the near future look encouraging.

Appendix A

Energy Levels in Quantum Wells

A.1 Nonparabolicity in Quantum wells

Several different methods of incorporating nonparabolicity into the calculation of quantum well energy levels have been proposed [1, 4]. The method adopted here assumes that the effective mass is energy dependent, [4]. It recasts the envelope function approximation, derived by [5], into an energy dependent effective mass form in which the interface boundary conditions are obtained in a manner consistent with the nonparabolicity of the well and the barrier material. The energy levels are calculated by solving the well and barrier dispersion relationships in conjunction with the boundary condition in a consistent manner. The dispersion relationship in the well is,

$$E = \frac{\hbar^2 k_w^2}{2m_w^*(E)} \tag{A.1}$$

the dispersion relation in the barrier is

$$E = V - \frac{\hbar^2 k_b^2}{2m_b^*(E)} \tag{A.2}$$

and the boundary condition is

$$\left[\frac{k_w m_b^*(E)}{k_b m_w^*(E)} - \frac{k_b m_w^*(E)}{k_w m_b^*(E)}\right] tan(k_w l) = 2 \tag{A.3}$$

Here the subscripts w and b denote well and barrier, k the wavenumber, V is the energy barrier height and l is the well width. The energy dependent effective masses are given by

$$m_w^*(E) = m_w^*(1 + E/E_w) \tag{A.4}$$

$$m_b^*(E) = m_b^*(1 - (V - E)/E_b) \tag{A.5}$$

where E_w and E_b are the energy gaps in the well and the barrier. The non-parabolicity parameter is related to the energy gap and the effective mass by

$$\gamma_i = \frac{\hbar^2}{2m_i^* E_i} \quad (i = w, b) \tag{A.6}$$

The model also relates the following properties on the two sides of the interface,

$$m_w^*/m_b^* = E_w/E_b \tag{A.7}$$

$$(m_b^*/m_w^*)^2 = \gamma_w/\gamma_b \tag{A.8}$$

The energy levels of the samples were calculated by using the above formalism and the following material parameters, $\gamma_w = 9 \times 10^{-19} m^2$, $m_w^* = 0.42 m_0$, $m_b^* = 0.075 m_0$, and V=500meV.

References

[1] D.F.Nelson, R.C.Miller, and D.A.Kleinman, Phys, Rev. B, 35, 7770, (1987)

[2] T.Hiroshima and R.Lang, Appl. Phys. Lett., 49, 456, (1986)

[3] M.Zachau, Semicond. Sci. Technol., 3, 879, (1988)

[4] G.Bastard, Phys, Rev. B, 25, 7584, (1982)

[5] E.B.Dupont et al, Appl. Phys. Lett., 60, 2121, (1992)

Appendix B

Nonlinear Polarization in Twin-Mode Structures

B.1 Nonlinear Polarization

When an electric field, $\underline{E}(\underline{r},t)$, is applied to a medium, a polarization, $\underline{P}(\underline{r},t)$, is induced. This polarization can be described in terms of a power series,

$$\underline{P}(\underline{r},t) = \underline{P}^{(0)}(\underline{r},t) + \underline{P}^{(1)}(\underline{r},t) + \underline{P}^{(2)}(\underline{r},t) + \cdots + \underline{P}^{(n)}(\underline{r},t) \qquad \text{(B.1)}$$

where $P^{(0)}$ is the dc polarization, $P^{(1)}$ is the linear polarization, $P^{(2)}$ is the first nonlinear term, and $P^{(n)}$ is the $(n-1)$th order nonlinear term of the polarization.

In the most general case the relationship between the nth order polarization and the applied electric field is given by, [1],

$$\underline{P}^{(n)}(\underline{r},t) = \epsilon_0 \int_{-\infty}^{\infty} d\omega_1 \cdots \int_{-\infty}^{\infty} d\omega_n \, \chi^{(n)}(\omega_\sigma;\omega_1,...,\omega_n) \,|\, \tilde{E}(\underline{r},\omega_1)\cdots\tilde{E}(\underline{r},\omega_n) \qquad \text{(B.2)}$$

where the frequency label ω_σ satisfies $\omega_\sigma = \omega_1 + \omega_2 + \omega_3 + \ .....$ and $\chi^{(n)}(\omega_\sigma)$ denotes the nth order susceptibility. The electric field in the frequency domain

is given by,

$$\tilde{E}(\underline{r},\omega) = \int_{-\infty}^{\infty} \underline{E}(\underline{r},t)\, e^{\imath\omega t}\, dt \tag{B.3}$$

Eqn(B.2) can be greatly simplified if the amplitude fluctuations of the applied electric fields are much slower than the relaxation time of the polarization. In that case the nonlinear response depends only on the instantaneous values of the field envelopes, and thus eqn(B.2) reduces to, [1],

$$\underline{P}^{(n)}(\underline{r},t) = \epsilon K\, \chi^{(n)}(\omega_\sigma;\omega_1,...,\omega_n) \mid E_{\omega_1}(\underline{r},t)\cdots E_{\omega_n}(\underline{r},t) \tag{B.4}$$

K is a scalar factor that is dependent on the order of the polarization.

When an electric field is applied to a material with a centro-symmetric crystal structure, the first three significant terms of eqn(B.1) are given by,

$$\underline{P}(\underline{r},t) = \underline{P}^{(0)}(\underline{r},t) + \underline{P}^{(1)}(\underline{r},t) + \underline{P}^{(3)}(\underline{r},t) \tag{B.5}$$

The second-order polarization reflects any asymmetry in the response of the medium to positive and negative applied fields and therefore is only non-zero in materials lacking inversion symmetry. Thus $P^{(2)} = 0$ is zero in centro-symmetric materials.

Interestingly most semiconductor have a centro-symmetric crystal structure and thus the first non-zero nonlinear polarization term is $P^{(3)}$. Therefore if a sufficiently long optical pulse is applied to a semiconductor the first nonlinear polarization term will be given by,

$$\underline{P}^{(3)}(\underline{r},t) = \epsilon K\, \chi^{(3)}(\omega_\sigma;\omega_1,...,\omega_n) \mid E_{\omega_1}(\underline{r},t)E_{\omega_2}(\underline{r},t)E_{\omega_2}(\underline{r},t) \tag{B.6}$$

B.2 Twin-Waveguide Structures

The optical field of a pulse in a semiconductor waveguide structure that supports two modes, can be represented by,

$$\underline{E}(\underline{r},t) = 1/2\,\left(\underline{E}_0(\underline{r},t)e^{\imath\omega_0 t} + \underline{E}_0(\underline{r}\,t)e^{-\imath\omega_0 t}\right) \tag{B.7}$$

where

$$\underline{E}_0(\underline{r},t) = A_1(z,t)F_1(x,y)\,e^{\imath\beta_1 z} + A_2(z,t)F_2(x,y)\,e^{\imath\beta_2 z} \tag{B.8}$$

Here F_m and β_m are the modal profile and propagation constant of mode m, (where m = 1 or 2). A_m is the slowly varying envelope of mode m.

The nonlinear polarization ($\underline{P}^{(3)}$) induced by such a pulse will be triply resonant, since $E = E_{\omega_1} = E_{\omega_2} = E_{\omega_3}$, and will have terms oscillating around $\pm\omega_0$ and $\pm 3\omega_0$. If it is assumed that the waveguide structure inhibits third harmonic generation, then the nonlinear polarization field will only have terms oscillating around $\pm\omega_0$, ie,

$$\underline{P}^{(n)}(\underline{r},t) = 1/2\,\left(\underline{P}^{(3)}_{\omega_\sigma}(\underline{r})\,e^{\imath\omega_\sigma t} + \underline{P}^{(3)*}_{\omega_\sigma}(\underline{r})\,e^{-\imath\omega_\sigma t}\right) \tag{B.9}$$

where $\underline{P}^{(3)*}_{\omega_\sigma} = \underline{P}^{(3)}_{-\omega_\sigma}$, and $\omega_\sigma = \omega_0$

By substituting eqn(B.7) into eqn(B.6) and only retaining terms oscillating at $\pm\omega_0$, the following expression can be obtained,

$$\underline{P}^{(3)}_{\omega_\sigma} = \chi^{(3)}(x,y)\left(F_1\Psi_1(r,t)\,e^{-\imath\beta_1 z} + F_2\Psi_2(r,t)\,e^{-\imath\beta_2 z}\right) \tag{B.10}$$

where

$$\Psi_1(r,t) = \frac{3}{4}\left(F_1^2|A_1|^2A_1 + 2F_2^2|A_2|^2A_1 + 2F_2^2A_2^2A_1^*\,e^{-2\imath(\beta_1-\beta_2)z}\right) \tag{B.11}$$

$$\Psi_2(r,t) = \frac{3}{4}\left(F_2^2|A_2|^2A_2 + 2F_1^2|A_1|^2A_2 + 2F_1^2A_1^2A_2^*\,e^{+2\imath(\beta_1-\beta_2)z}\right) \tag{B.12}$$

In general $\chi^{(3)}$ is complex and thus $\chi^{(3)} = \chi_R^{(3)} + i\chi_I^{(3)}$. The real part describes a Kerr-type index nonlinearity and the imaginary part denotes two-photon absorption.

References

[1] P.N.Butcher and D.Cotter, "*The Elements Of Nonlinear Optics*", (Cambridge Uni. Press: Cambridge), 1990.